

~~CONFIDENTIAL~~

Copy 252  
RM L57J11  
13673

TECH LIBRARY KAFB, NM



NACARM L57J11

13 DEC 1973  
13 DEC 1973  
0144741



# RESEARCH MEMORANDUM

6087

AERODYNAMIC LOAD DISTRIBUTION OVER A 45° SWEPT WING  
HAVING A SPOILER-SLOT-DEFLECTOR AILERON AND  
OTHER SPOILER AILERONS FOR MACH NUMBERS  
FROM 0.60 TO 1.03

By F. E. West, Jr., Charles F. Whitcomb,  
and James W. Schmeer

Langley Aeronautical Laboratory  
Langley Field, Va.

CLASSIFIED DOCUMENT

This material contains information affecting the National Defense of the United States within the meaning of the espionage laws, Title 18, U.S.C., Secs. 793 and 794, the transmission or revelation of which in any manner to an unauthorized person is prohibited by law.

**NATIONAL ADVISORY COMMITTEE  
FOR AERONAUTICS**

WASHINGTON

December 5, 1957

~~CONFIDENTIAL~~

## NATIONAL ADVISORY COMMITTEE FOR AERONAUTICS

## RESEARCH MEMORANDUM

AERODYNAMIC LOAD DISTRIBUTION OVER A 45° SWEPT WING  
HAVING A SPOILER-SLOT-DEFLECTOR AILERON AND  
OTHER SPOILER AILERONS FOR MACH NUMBERS  
FROM 0.60 TO 1.03

By F. E. West, Jr., Charles F. Whitcomb,  
and James W. Schmeer

## SUMMARY

A loads investigation was made with flap spoiler ailerons, deflector ailerons, and a spoiler-slot-deflector aileron on a 45° swept-wing-body combination. These controls were located in the vicinity of the 70-percent wing chord line and extended outboard to 87 percent of the wing semispan. Control projection was varied only for the deflector ailerons. The wing had an aspect ratio of 4, a taper ratio of 0.60, and NACA 65A006 airfoil sections parallel to the plane of symmetry. Static pressures were measured on the wing and some of the controls at several spanwise stations for Mach numbers from 0.60 to 1.03, Reynolds numbers from  $5.05 \times 10^6$  to  $6 \times 10^6$ , and an angle-of-attack range of about 0° to 20°.

This investigation is a closely related extension of a pressure study (see NACA RM L54C17a) of retractable spoiler ailerons. The results of these two investigations indicate that the effects of flap spoiler ailerons and retractable spoiler ailerons on the wing pressures are generally similar. Adding a slot deflector to a spoiler-aileron configuration creates low pressures on the deflector rear surface and the subsequent wing lower surface which have a favorable effect on rolling moment, particularly at high angles of attack. At low angles of attack the low pressures associated with a slot deflector have their largest effects on the spanwise and chordwise loadings for a swept wing at the inboard stations. These low pressures tend to be of the same magnitude as the upper-surface pressures behind a spoiler which are lowest at the inboard stations. At high angles of attack where a spoiler has a rather small effect on wing loading, the low pressures associated with a

slot deflector affect the loading over most of the wing span. The control spanwise load distributions were similar in shape for the spoiler aileron and the spoiler and deflector components of the spoiler-slot-deflector aileron at low angles of attack.

## INTRODUCTION

Very few pressure data for spoiler-aileron configurations have been available at transonic speeds for use in load calculations or in studying the effects of spoiler ailerons on the flow about wings. A test program was, therefore, initiated in the Langley 16-foot transonic tunnel to provide static-pressure data for various spoiler-aileron configurations in the transonic speed range for a large angle-of-attack range.

The initial results of this test program (see ref. 1) were for a  $45^{\circ}$  swept-wing-body combination having retractable and plug spoiler ailerons. The most recent phase of this test program, reported herein, was primarily the investigation at  $0^{\circ}$  yaw of spoiler-slot-deflector ailerons and flap spoiler ailerons on essentially the same model used in the initial phase. These controls were located in the vicinity of the 70-percent wing chord line and extended from the vicinity of the body to 87 percent of the wing semispan (same as the spoiler ailerons used in the initial phase of the investigation).

In this paper the wing normal-force characteristics, centers of load, and span-load and chordwise pressure distributions for one of the spoiler-slot-deflector aileron configurations and one of the flap spoiler-aileron configurations are compared with those for the basic model. Tabulated wing pressure coefficients and spoiler and deflector loading characteristics are also given for these two control configurations. The effects of wing leading-edge chord-extensions on the spoiler-slot-deflector loads are also included. There are shown, in addition, the effects of varying projection of a deflector aileron and of removing inboard segments of the flap spoiler aileron on the wing chordwise pressure distributions. Except for the configurations having only a deflector aileron, control projection was not varied.

A few of these pressure data results have been presented in reference 2 and six-component force balance data obtained simultaneously with the present pressure data have been presented in reference 3.

CONFIDENTIAL

## SYMBOLS

All chords are parallel to the vertical plane of symmetry. Wing coefficients include contribution of controls.

$b$	wing span
$b_i$	inboard-end location of various controls
$c$	local basic wing chord
$\bar{c}$	average basic wing chord
$c'$	basic wing mean aerodynamic chord
$c_d$	local chord of deflector rear face
$\bar{c}_d$	average chord of deflector rear face
$c_s$	local chord of spoiler front face
$\bar{c}_s$	average chord of spoiler front face
$c_n$	wing section normal-force coefficient, <u>Wing section normal force</u> $qc$
$c_{n_d}$	deflector section normal-force coefficient, <u>Deflector section normal force</u> $qc_d$
$c_{n_s}$	spoiler section normal-force coefficient, <u>Spoiler section normal force</u> $qc_s$
$C_N$	wing-panel normal-force coefficient, $\int_{0.135}^{1.0} c_n \frac{c}{c} d\left(\frac{y}{b/2}\right)$
$C_p$	pressure coefficient, $\frac{p_1 - p}{q}$

d distance along  $c_d$  measured from deflector leading edge

$d_{cp}$  distance along  $c_d$  measured from deflector leading edge to deflector section center of load

M free-stream Mach number

p free-stream static pressure

$p_l$  local static pressure

q free-stream dynamic pressure

s distance along  $c_s$  measured from spoiler hinge line

$s_{cp}$  distance along  $c_s$  measured from spoiler hinge line to spoiler section center of load

S total wing area

x distance along c measured from wing leading edge, positive downstream

$x_{cp}$  longitudinal location of wing section center of load measured from wing leading edge, positive downstream

$X_{cp}$  longitudinal location of wing panel center of load measured from leading edge along  $c'$ , positive downstream

y lateral distance from plane of symmetry

$Y_{cp}$  lateral location of wing panel center of load measured from plane of symmetry

$\alpha$  angle of attack

$\delta_d$  projection of deflector into airstream, fraction of c, measured from wing surface perpendicular to wing chord line

$\delta_s$  projection of spoiler into airstream, fraction of c, measured from wing surface perpendicular to wing chord line

~~CONFIDENTIAL~~  
APPARATUS

## Tunnel and Model

The investigation was conducted in the Langley 16-foot transonic tunnel, the airflow and power characteristics of which are presented in reference 4. Figure 1 presents the geometric details of the sting-supported model. The steel wing had a quarter-chord line sweep of  $45^{\circ}$ , a taper ratio of 0.60, an aspect ratio of 4.0, and NACA 65A006 airfoil sections parallel to the plane of symmetry. The wing had no geometric incidence, dihedral, or twist, and was mounted in a midwing position on the fuselage. The steel fuselage was a body of revolution with a fineness ratio of 10. (See ref. 1 for fuselage ordinates.) The quarter-chord point of the wing mean aerodynamic chord was located at the longitudinal position of the maximum fuselage diameter.

## Lateral-Control and Chord-Extension Configurations

Figure 2 shows some of the geometry of the lateral-control and chord-extension configurations used in the test program. More extensive geometric sectional details for the spoiler-slot-deflector aileron and one of the deflector ailerons are shown in figure 1. All the control devices were made of steel and were mounted on the left wing.

Except for modifications involving the removal of small inboard segments, the same spoiler was used for all configurations that included a spoiler. It was projected 7.8 percent of the wing local chord above the wing upper surface and was hinged at the 68.1-percent wing chord line. (See fig. 1(b).) In the undeflected position, this spoiler would extend over 12 percent of the wing chord. When the inboard end of the spoiler extended to the fuselage ( $b_1 \approx 0.14 \frac{b}{2}$ ), the fuselage-spoiler juncture was sealed. The wing slot (3.8 percent of the local wing chord) extended from 15 to 87 percent of the semispan. Ribs, which had a height of 2.4 percent of the local wing chord and a width of 0.25 inch, were located in the wing slot parallel to the plane of symmetry at the 20-, 30-, 39-, 48-, 57-, 66-, 75-, and 83-percent-semispan stations. Braces for the flap-type spoiler were mounted on top of these ribs. (See fig. 1(b).)

The deflector of the spoiler-slot-deflector aileron projected 5.5 percent of the local wing chord below the wing lower surface with the inboard end located at the fuselage. In its undeflected position, this deflector would extend over 8.6 percent of the wing chord. The deflector was hinged at the 73.8-percent wing chord line and was fastened to the wing by seven braces. (See fig. 1(b).)

~~CONFIDENTIAL~~

The configurations having only a deflector utilized a deflector that had a chord length of about 7.8 percent of the local wing chord when in the undeflected position. Although this deflector extended inboard to the fuselage, it was not contoured to fit the fuselage closely. For the deflector configurations having a gap between the deflector and wing surface, spacers with a height of 2 percent of the local wing chord and a width of 5/16 inch were located at seven semispan stations. (See fig. 1(c).)

The leading-edge chord-extensions, which are similar to those discussed in references 5 and 6, extended forward 15 percent of the local wing chord from the 65-percent-semispan station to the wing tip. The chord extensions had the same section ordinates back to their maximum thickness as did the basic airfoil sections at corresponding spanwise stations. The airfoil contour paralleled the wing chord line between the maximum thickness of the chord extensions and the maximum thickness of the wing.

#### Pressure Instrumentation

Static-pressure orifices were distributed parallel to the vertical plane of symmetry at the 13.5- (average), 25-, 40-, 55-, 70-, 85-, and 95-percent-semispan stations on the left wing panel. A total of 45 orifices were located on the upper and lower wing surfaces at each spanwise station. The orifices at the wing-fuselage juncture (average 0.135 semispan station) were actually located on the fuselage 0.1 inch from the wing surface. Orifices located on the front and rear faces of the spoiler (with and without the slot deflector) and the deflector used in the spoiler-slot-deflector combination were only utilized for pressure measurements when the controls extended inboard to the fuselage. These orifices were distributed parallel to the vertical plane of symmetry at the 14-, 25-, 40-, 55-, 70-, and 85-percent-wing semispan stations. Eight orifices and six orifices were located on the spoiler and deflector, respectively, at each spanwise station. (See fig. 1(b).) The pressures were transmitted by means of small tubing through the model and its support system to mercury manometer boards.

#### TESTS

The configurations shown in figure 2 were generally tested through an angle-of-attack range from  $0^\circ$  to approximately  $21.5^\circ$  for Mach numbers from 0.60 to 0.94 and up to angles of  $19.4^\circ$ ,  $15.4^\circ$ , and  $13.2^\circ$  for Mach numbers of 0.98, 1.00, and 1.03, respectively. These maximum angles were not attained for all of the configurations because of model stress

or tunnel power limitations. The variation of Reynolds number (based on wing mean aerodynamic chord) with Mach number is presented in figure 3.

#### DATA REDUCTION

The pressure data were generally reduced by the methods described in reference 1. For some conditions, however, the normally used rectangular-step integration did not provide sufficiently accurate section pitching-moment coefficients for the spoiler or deflector. Hence, for these conditions the moments were obtained by manually integrating the faired pressure distributions for the controls.

No corrections have been applied to the data. Sting interference effects on the flow over the relatively remote wing and lateral controls are believed to be negligible. Also tunnel wall effects are small for the present test Mach number range. (See ref. 7.) Angle-of-attack accuracy is estimated to be within  $\pm 0.1^\circ$ .

#### RESULTS

Wing static-pressure coefficients are given for the configuration with the spoiler aileron extending to the fuselage in table I and for the spoiler-slot-deflector aileron configuration in table II. Tabulated basic wing pressure coefficients are available in reference 1.

Wing chordwise pressure distributions showing the effects of lateral control projection or the effects of changes in lateral control configuration are shown in figures 4 to 10. In figure 4 the upper-surface pressure coefficients for the spoiler-aileron configuration are based on both wing pressures and the pressures obtained on the front surface of the spoiler aileron. The pressures on the spoiler aileron rear surface and on the portion of the wing surface over which the spoiler aileron extends were not utilized in obtaining the pressure distributions. These latter spoiler aileron and wing pressures tend to be equal. They have, therefore, been omitted to simplify the pressure distributions. Their values were approximately equal to the upper-surface wing pressures obtained immediately downstream of the spoiler.

For the spoiler-slot-deflector aileron configuration in figure 7, the pressures on the front surface of the spoiler and on the rear surface of the deflector have been utilized in the chordwise pressure distributions. In this case the pressures between the wing and controls have been omitted.

Since control pressures were obtained only for the two configurations where the lateral controls extended into the body, control pressures are not available for the chordwise pressure distributions shown for the remaining control configurations in figures 5, 6, 8, 9, and 10. For these configurations the pressure distributions have not been extended over the control portion of the wing.

Wing spanwise load distributions and wing section center-of-pressure locations are presented in figures 11 and 12, respectively, for the basic model, for the spoiler-slot-deflector configuration, and for the configuration with the spoiler aileron extending to the fuselage. Wing-panel normal-force characteristics, lateral center-of-pressure locations, and longitudinal center-of-pressure locations for these three configurations are presented in figures 13 to 15, respectively.

Control load characteristics are shown in figures 16 to 21 for the spoiler-slot-deflector aileron. These characteristics are with and without the leading-edge chord-extensions added to the model. Figures 16, 18, and 19 also include the control load characteristics for the spoiler aileron that extended to the fuselage.

In figures which show comparisons at one angle of attack, the angle given is an average for the compared configurations. The maximum deviation from this angle is  $\pm 0.1^\circ$ .

## DISCUSSION

### Wing Chordwise Pressure Distributions

Spoiler ailerons.- At  $M = 0.60$ , figure 4(a) shows that at low angles of attack the addition of the spoiler aileron to the model caused an increase in the upper-surface pressures ahead of the spoiler, a decrease in the upper-surface pressures behind the spoiler, and a decrease in the lower-surface pressures. The effects were about the same as those shown in reference 1 with retractable spoilers deflected  $0.04c$ . In both cases the flow was separated ahead of and behind the spoilers. The primary difference was that, behind the retractable spoiler aileron, complete recovery of the flow generally occurred before the flow reached the wing trailing edge at  $\frac{y}{b/2} = 0.135$  and  $0.25$ . In the present case similar flow recovery was not obtained probably because of the higher deflection of the spoiler aileron above the wing surface.

The region of fairly large pressure rise ahead of the spoiler aileron extended forward of the spoiler in approximately the shape of a

spanwise wedge with the apex and the highest pressure occurring at  $\frac{y}{b/2} = 0.135$ . The peculiar shape of the pressure distribution upstream of the spoiler-aileron top edge at  $\frac{y}{b/2} = 0.25$  was a result of the pressures near the leading-edge front surface of the spoiler aileron being less than either the immediately preceding wing pressures or the following spoiler-aileron pressures. This pressure pattern is believed to be associated with a vortex-type flow lying in the separated region ahead of the spoiler-aileron trailing edge. (See ref. 1.)

As the angle of attack was increased for  $M = 0.60$ , the effect of the spoiler aileron on the wing pressures did not change appreciably until angles of attack were reached where flow separation on the basic wing began to progress inboard from the wing tip. (See fig. 4(a).) At these angles of attack the spoiler-aileron influence was reduced, as would be expected, since the spoiler aileron was in a separated flow region where the local flow was predominantly spanwise. (A discussion pertaining to flow separation and other flow phenomena over the basic wing may be found in ref. 6.)

Figure 4 shows that, as the Mach number was increased from 0.60 to 1.03, the influence of the spoiler aileron on the lower-surface pressures became confined to the trailing-edge region. This confinement probably occurred because shocks on the lower surface opposed the upstream transmission of pressure changes. On the upper surface, the forward extent of the spoiler-aileron influence became more confined at the inboard stations, and at  $\frac{y}{b/2} = 0.135$  some pressure recovery occurred behind the spoiler aileron at the higher Mach numbers. The confinement on the upper surface was probably caused by the presence of a shock wave associated with the separation point ahead of the spoiler aileron. The presence of this shock would have opposed the upstream transmission of the spoiler pressure field except outboard where the boundary layer was thickened.

Figure 4 also shows some unexplained effects of increasing Mach number from 0.60 at angles of attack of about  $8.5^\circ$  and  $13^\circ$ . At an angle of attack of about  $8.5^\circ$  and Mach numbers of 0.80 and 0.90, the spoiler aileron has much less effect on the upper-surface pressures for a short distance upstream of its trailing edge at  $\frac{y}{b/2} = 0.55$  than at  $\frac{y}{b/2} = 0.40$  or 0.70. A similar effect occurs at  $\frac{y}{b/2} = 0.70$  for the higher Mach numbers. At an angle of attack of about  $13^\circ$  and some of the higher Mach numbers, the addition of the spoiler aileron to the model caused an increase in normal force at the two outboard stations where flow

separation existed on the basic model. With increasing Mach number this normal-force increase reached a maximum at a Mach number of about 0.94 and then decreased to a very low value at a Mach number of 1.00. Although the reasons for the normal-force increase are not known, the relative-projection of the spoiler to the boundary-layer thickness must certainly be a factor.

Since inboard lateral controls do not usually extend into the fuselage on actual aircraft, inboard portions of the spoiler aileron were removed to determine the fuselage end-plate effect on the wing pressures. The results for the inboard stations are presented without discussion in figures 5 and 6 for two representative Mach numbers. Since moving the inboard end location to  $0.16b/2$  or  $0.22b/2$  had negligible effects on the wing pressures at the outboard stations, these pressures are not shown. The effects of inboard end location on the rolling moments were small, as shown in reference 3.

The qualitative effects on rolling-moment effectiveness of the usual pressure changes due to the spoiler ailerons were as follows: The pressure rise on the upper surface ahead of the spoiler-aileron trailing edge and the pressure reduction on the lower surface decreased normal force and thus contributed to a favorable rolling moment. The pressure reduction on the upper surface behind the spoiler aileron, however, was adverse. At higher angles of attack rolling-moment effectiveness decreased because of wing flow separation. The actual rolling-moment coefficients resulting from the pressure changes are available in reference 3.

Spoiler-slot-deflector aileron. - In figure 7 the compression region on the lower surface, which is due to deflector projection, is shown as terminating at about the 70-percent chord line. This chordwise position corresponds to the deflector leading edge. The compression region on the upper surface, which is due to spoiler projection, is shown as terminating at about the 74-percent chord line. This position corresponds to the spoiler trailing edge.

Comparison of figures 4 and 7 shows that adding the slot deflector to the spoiler generally had negligible effects on the upper-surface pressures ahead of the spoiler. Behind the spoiler at the  $0.135b/2$  station, the addition generally resulted in more upper-surface pressure recovery for the lower Mach numbers. In many cases, for stations outboard of  $0.25b/2$ , the effect of the addition was also to reduce slightly the upper-surface pressures behind the spoiler.

The unexplained effects on the pressures which were discussed for a spoiler-aileron configuration at angles of attack of about  $8.5^\circ$  and  $13^\circ$  also occurred for the spoiler-slot-deflector aileron configuration.

~~CONFIDENTIAL~~

As shown in figure 7(a), the lower-surface pressures ahead of the deflector became more positive. Figure 7(a) also shows for a Mach number of 0.60 that on the lower surface behind the deflector there was considerable pressure recovery at the 0.135b/2 station for all angles of attack and at the 0.25b/2 station for the higher angles of attack. At the other spanwise stations flow separation apparently existed over the deflector rear surface and the following wing surface for all angles of attack. In the outboard portion of this separated region, the pressures approached those existing on the upper surface behind the spoiler.

The unusual shape of the pressure pattern existing over the deflector rear surface and the downstream wing surface at the 0.25b/2 station may be associated with a separated vortex-type flow such as that believed to occur ahead of the spoiler and also discussed in reference 1. Increasing angle of attack or Mach number generally had very little effect on the type of flow existing on the lower surface of the spoiler-slot-deflector configuration. (See fig. 7.)

With respect to rolling-moment effectiveness, the most important pressure changes due to the addition of the slot deflector to the spoiler-aileron configuration were on the wing lower surface. The pressure rise on the wing surface ahead of the deflector was detrimental; whereas, the pressure reduction on the deflector rear surface and the following wing surface was beneficial. Unpublished results show that the magnitude of the pressure rise, which corresponded to an increase in normal force, was reduced appreciably by decreasing the deflector chord so that its deflection was 0.04c instead of 0.055c. If the deflector chord is decreased so that its leading edge is at the slot leading edge for the unprojected case, then the pressure rise can probably be eliminated. (See ref. 8.)

At low angles of attack the pressure reduction on the deflector rear surface and the subsequent wing lower surface resulted in increased rolling moment as it caused the normal-force load over the wing trailing-edge region to decrease from a positive to an almost negligible value. The magnitude of the pressure reduction was largest at the inboard stations. At high angles of attack the pressure reduction resulted in the wing trailing-edge loading decreasing considerably over the entire span of the aileron.

Deflector ailerons.- One of the problems often associated with spoiler-slot-deflector ailerons is that the yawing moments due to control projection, although favorable, are larger than desirable. A possible method of reducing these yawing moments is to project the deflector part of the control on one wing panel simultaneously with projection of the complete control on the opposite wing panel. A shortcoming in this solution, however, is that the roll contribution of the deflector part of the control would probably be reversed at moderately high angles

~~CONFIDENTIAL~~

of attack. The effects on this reversal problem of deflector projection and of a gap between the deflector trailing edge and the wing surface were, therefore, studied in a brief investigation.

Results presented in figure 8 at a Mach number of 0.90 for a low deflector projection ( $\delta_d = 0.016c$ ) show an expected favorable pressure rise on the lower wing surface ahead of the deflector. On the lower wing surface behind the deflector the pressures were decreased by adding the deflector. The flow in this region, however, was not generally separated. As the angle of attack was increased, the region of pressure reduction became larger at the outboard stations and the region of pressure rise tended to become smaller. These pressure changes resulted in rolling-moment reversal at moderate angles of attack as shown by the force data of reference 3.

As would be expected from the chordwise pressure distributions of figure 9, the force data presented in reference 3 also show reversals in rolling-moment effectiveness at moderately high angles of attack when the deflector projection was increased to  $0.045c$ . The effects on the wing pressures of adding a  $0.02c$  gap between the deflector trailing edge and the wing (see fig. 10) were also too small to prevent reversals in rolling-moment effectiveness at the moderately high angles of attack. (See ref. 3.)

#### Wing-Section Loading

At  $M = 0.60$  for low angles of attack, figure 11(a) shows that the addition of the spoiler aileron to the model caused the largest reductions in the semispan load distributions between 40 and 80 percent of the wing semispan. Apparently, the large reduction in pressure which occurred on the wing surface behind the spoiler caused considerable reduction in control effectiveness inboard of  $\frac{y}{b/2} = 0.40$ . (See fig. 4.) Increasing Mach number caused the region of maximum load change at low angles to shift outboard to about  $\frac{y}{b/2} = 0.80$ . (See fig. 11.) As indicated in the discussion of the chordwise pressure distributions, the reduction in loading due to the spoiler aileron was much smaller at high angles of attack than at the low angles.

For low angles of attack, figure 11 shows that adding the spoiler-slot-deflector aileron to the model caused larger decreases in loading at the inboard stations and smaller decreases in loading at the outboard stations than did the spoiler aileron. At high angles of attack, the spoiler-slot-deflector aileron caused a reduction in the outboard loading which was as large or larger than that caused by the spoiler aileron.

Reasons for these reductions were indicated in the pressure-distribution discussion of figure 7.

At several Mach numbers and angles near  $13^{\circ}$ , figure 11 also shows load increases over about the outboard 20 percent of the wing semispan that were caused by adding either lateral control to the model. These increases were also considered in the discussion of figures 4 and 7.

Figure 12 shows that, below an angle of attack of about  $8^{\circ}$ , addition of the spoiler aileron to the model usually caused the section centers of pressure to shift forward at stations outboard of  $\frac{y}{b/2} = 0.25$ .

This shift occurred because the wing loading behind the spoiler aileron became progressively less across the wing semispan. (See fig. 4.) At high angles of attack where its effectiveness was considerably reduced the addition of the spoiler aileron had only small effects on the section center-of-pressure locations.

Addition of the spoiler-slot-deflector aileron to the model generally caused a larger forward shift of the section centers of pressure than did the addition of the spoiler aileron. This shift generally occurred at all spanwise stations for all angles of attack except those near  $0^{\circ}$ . The larger forward shift resulted primarily because the addition of the slot deflector greatly reduced the trailing-edge loading.

#### Wing-Panel Loading

The effects of the spoiler aileron and spoiler-slot-deflector aileron on the wing-panel loading characteristics are analogous to their effects on the section pressures and loadings. These characteristics (see figs. 13 to 15) are, therefore, presented without discussion.

#### Spoiler and Deflector Pressure Distributions

The pressure distributions of figure 16 show that the pressures on the front of the spoiler decreased from positive values at low angles of attack to negative values at high angles. This trend seemed to be influenced mainly by wing flow separation spreading inboard from the wing tip as angle of attack was increased. The chord-extension effects on wing flow separation (see ref. 6) delayed the trend in the spoiler pressures at the outboard station for angles of attack of about  $12^{\circ}$  to  $17^{\circ}$ . With this exception, figure 16 shows very little effect of configuration on the pressures over the front of the spoiler.

At low angles of attack the spoiler front-face pressures at the inboard stations were apparently influenced considerably by circulation in the separated flow upstream of the spoiler trailing edge. As indicated in the discussion of figure 4, this circulatory flow probably resulted in the pressures in the region of the spoiler base being less than the immediately preceding wing pressures or the pressures at about the midchord of the spoiler. A somewhat similar pressure pattern is shown in reference 1 for a spoiler which essentially extended perpendicular to the wing surface. This reference shows, however, that the two high-pressure regions occurred at the top and bottom of the spoiler front face. This effect of spoiler deflection angle on the pressures also agrees with results obtained at supersonic speeds. (See ref. 9.) It seems probable that the position of the high-pressure region nearest the upper edge of the spoilers gives an indication of the height of the separated flow.

Figure 16 also shows that the negative pressures on the rear face of the spoiler were affected by the addition of the slot deflector; that is, flow through the slot caused the pressures nearest to the wing to increase.

The pressure distributions for the deflector, as shown in figure 17, were only slightly affected by angle-of-attack changes. Also, adding the chord-extensions had very little effect on these distributions. The positive pressures on the front of the deflector usually decreased as the distance to the wing became less probably because of flow through the slot. On the rear face of the deflector the pressure variations shown in figure 17 at the two inboard stations were probably caused by the separated flow phenomena indicated in the discussion of figure 7.

#### Spoiler and Deflector Spanwise Loading

Some of the results for the spoiler and deflector span-load distributions shown in figures 18 and 19, respectively, have been summarized in reference 2. This reference shows that at low angles of attack the shape of the load distributions was similar for the deflector and the spoiler (with and without the slot deflector added to the model). It also indicates that Mach number had very little effect on the shape of the span-load distributions.

The large loads at the inboard stations of the spoiler and deflector (see figs. 18 and 19) occurred because the typical effects of sweep did not exist at these stations. Similar results have also been found at supersonic speeds. (See ref. 9.) The spoiler loads decreased with increasing angle of attack primarily because wing-flow separation caused the spoiler front-face pressures to decrease. (See fig. 16.) The effect of the flow through the slot was to reduce the spoiler loads at all angles

~~CONFIDENTIAL~~

of attack. The chord-extensions caused a slight increase in the spoiler loading at the outboard stations for angles of attack from about  $12^{\circ}$  to  $17^{\circ}$ . Chord-extension effects on deflector loading, however, were negligible. The unexplained flow phenomena noted at an angle of attack of  $8.5^{\circ}$  in the discussion of the chordwise pressure distributions of figures 4 and 7 resulted in decreased spoiler loads as shown in figure 18.

With regard to total control normal force, reference 2 indicates that, for large control deflections, tests need only be made at low angles of attack to establish the maximum control loads; that is, the spoiler loads decreased and the deflector loads varied only slightly with increasing angle of attack. Increasing Mach number caused small increases in the total control normal-force coefficients (ref. 2).

Although no methods are known for estimating the control loads, references 10 and 1 show that, for retractable spoiler ailerons, spoiler load at any spanwise position can be determined by measurement at the wing surface of the pressure drop across the spoiler. Studies utilizing the wing orifices at  $0.65c$  and  $0.75c$  indicate that this statement also generally applies to the spoiler aileron of this paper. It does not apply, however, in the case of the spoiler and deflector of a spoiler-slot-deflector aileron. In these cases, flow through the wing slot, as previously indicated, has a large effect on the control pressure distributions. This effect will probably vary with control geometry.

In figure 20, spoiler center-of-pressure locations for the spoiler configuration have been omitted in many cases at the higher angles of attack because the spoiler loads became very small. For the spoiler (without the slot deflector on the model) or the deflector (see figs. 20 and 21, respectively), the section center-of-pressure locations generally varied only slightly across the control span. In both cases these center-of-pressure locations were usually slightly ahead of the control 50-percent chord line.

The addition of the slot deflector to the spoiler configuration, however, caused large rearward shifts in the spoiler center-of-pressure locations below an angle of attack of about  $8^{\circ}$  (see fig. 20); these shifts were caused by the flow through the wing slot. (See fig. 16.) At higher angles where the spoiler loads were small, inconsistent shifts were caused by both wing flow separation and the flow through the wing slot.

Adding the chord-extensions to the spoiler-slot-deflector configurations had a small effect on the spoiler center-of-pressure locations except for angles of attack where the spoiler loads became small. In the case of the deflector, however, the effect was negligible through the angle-of-attack and Mach number range.

~~CONFIDENTIAL~~

## CONCLUSIONS

An investigation was made with spoiler ailerons, deflector ailerons, and a spoiler-slot-deflector aileron mounted on a  $45^{\circ}$  swept-wing-fuselage combination. These controls were located in the vicinity of the 70-percent wing chord line and extended outboard to 87 percent of the wing semispan. Pressures were measured on the wing and some of the control components at several spanwise stations for Mach numbers from 0.60 to 1.03 and for an angle-of-attack range of about  $0^{\circ}$  to  $20^{\circ}$ . This investigation is a closely related extension of a previously reported study of retractable spoiler ailerons (NACA RM L54C17a).

1. Effects of flap spoiler ailerons and retractable spoiler ailerons on the wing pressures are generally similar.
2. Adding a slot deflector to a spoiler-aileron configuration creates low pressures on the rear surface of the deflector and the subsequent wing lower surface, which have a favorable effect on rolling moment, particularly at high angles of attack.
3. At low angles of attack the low pressures associated with a slot deflector have their largest effects on the spanwise and chordwise loadings for a swept wing at the inboard stations. These low pressures tend to be of the same magnitude as the upper-surface pressures behind a spoiler which are lowest at the inboard stations.
4. At high angles of attack where a spoiler has a rather small effect on wing loading, the low pressures associated with a slot deflector affect the loadings over most of the wing span.
5. Flow through the wing slot had a large effect on the chordwise loadings of the spoiler and deflector, but at low angles of attack the spanwise load distributions were similar in shape for the spoiler aileron and the spoiler and deflector components of the spoiler-slot-deflector aileron.

Langley Aeronautical Laboratory,  
National Advisory Committee for Aeronautics,  
Langley Field, Va., September 12, 1957.

~~CONFIDENTIAL~~

## REFERENCES

1. Hallissy, Joseph M., Jr., West, F. E., Jr., and Liner, George: Effects of Spoiler Ailerons on the Aerodynamic Load Distribution Over a 45° Sweptback Wing at Mach Numbers From 0.60 to 1.03. NACA RM L54C17a, 1954.
2. West, F. E., Jr., and Czarnecki, K. R.: Loads Due to Controls at Transonic and Low Supersonic Speeds. NACA RM L57D26a, 1957.
3. West, F. E., Jr., Whitcomb, Charles F., and Schmeer, James W.: Investigation of Spoiler-Slot-Deflector Ailerons and Other Spoiler Ailerons on a 45° Sweptback-Wing—Fuselage Combination at Mach Numbers From 0.60 to 1.03. NACA RM L56F15, 1956.
4. Ward, Vernon G., Whitcomb, Charles F., and Pearson, Merwin D.: Air-Flow and Power Characteristics of the Langley 16-Foot Transonic Tunnel With Slotted Test Section. NACA RM L52E01, 1952.
5. West, F. E., Jr., Liner, George, and Martz, Gladys S.: Effect of Leading-Edge Chord-Extensions on the Aerodynamic Characteristics of a 45° Sweptback Wing-Fuselage Combination at Mach Numbers of 0.40 to 1.03. NACA RM L53B02, 1953.
6. West, F. E., Jr., and Henderson, James H.: Relationship of Flow Over a 45° Sweptback Wing With and Without Leading-Edge Chord-Extensions to Longitudinal Stability Characteristics at Mach Numbers From 0.60 to 1.03. NACA RM L53H18b, 1953.
7. Whitcomb, Charles F., and Osborne, Robert S.: An Experimental Investigation of Boundary Interference on Force and Moment Characteristics of Lifting Models in the Langley 16- and 8-Foot Transonic Tunnels. NACA RM L52L29, 1953.
8. Hammond, Alexander D.: Low-Speed Pressure Distribution Investigation of a Spoiler and a Spoiler-Slot-Deflector on a 30° Sweptback Wing-Fuselage Model Having an Aspect Ratio of 3, a Taper Ratio of 0.5, and NACA 65A004 Airfoil Section. NACA RM L55I29, 1956.
9. Lord, Douglas R., and Czarnecki, K. R.: Aerodynamic Loadings Associated With Swept and Unswept Spoilers on a Flat Plate at Mach Numbers of 1.61 and 2.01. NACA RM L55L12, 1956.
10. Hammond, Alexander D., and West, F. E., Jr.: Loads Due to Flaps and Spoilers on Sweptback Wings at Subsonic and Transonic Speeds. NACA RM L53D29a, 1953.

~~CONFIDENTIAL~~



TABLE L - WING WITH SPOILER - Continued

Percent chord	Pressure coefficient													
	0.135b/2	0.25b/2	0.40b/2	0.55b/2	0.70b/2	0.85b/2	0.95b/2	0.135b/2	0.25b/2	0.40b/2	0.55b/2	0.70b/2	0.85b/2	
<b>M = 0.60 c = 12.32°</b>														
Upper surface														
	<b>M = 0.60 c = 16.40°</b>													
Lower surface														
Upper surface														
	<b>M = 0.60 c = 26.26°</b>													
Lower surface														
Upper surface														
	<b>M = 0.80 c = 4.29°</b>													
Lower surface														

CONFIDENTIAL









TABLE I. - WING WITH SPOILER - Continued







TABLE I. - WING WITH SPOILER - Concluded

TABLE II. - WING WITH SPOILER-SLOT-DEFLECTOR

		Pressure coefficient													
Per-	cent	0.135b/2	0.26b/2	0.40b/2	0.65b/2	0.70b/2	0.85b/2	0.95b/2	0.135b/1	0.26b/1	0.40b/1	0.65b/1	0.70b/1	0.85b/1	0.95b/1
Upper surface	chord	M = 0.60							M = 0.60						
		M = 0.60	c = -0.06°	M = 0.60	c = 4.02°										
	0.0	.204	.444	.440	.439	.361	.440	.176	.200	.097	.145	.102	.206	.082	.302
1.2	.242	.033	.112	.198	.222	.222	.194	.090	.752	.775	.681	.671	.539	.568	
2.4	.116	-.010	.072	.123	.144	.157	.113	.159	.620	.440	.412	.353	.248	.261	
3.6	-.005	-.005	.057	.100	.127	.114	.061	.203	.246	.302	.244	.219	.229	.232	
4.8	.051	-.013	.057	.086	.096	.086	.032	.203	.282	.223	.197	.184	.177	.195	
6.0	-.008	-.027	.042	.042	.073	.068	.091	.002	.180	.221	.137	.116	.108	.107	
7.5	.003	-.027	.042	.048	.073	.068	.091	.012	.180	.194	.135	.137	.108	.114	
10.0	-.017	-.024	.028	.079	.091	.091	.002	.002	.180	.188	.135	.137	.109	.114	
12.5	-.032	.001	.076	.079	.103	.078	.012	.146	.184	.141	.049	.037	.031	.026	
15.0	-.012	.017	.096	.090	.103	.078	.012	.146	.149	.109	.009	.006	.002	.001	
17.5	-.027	.046	.115	.122	.125	.091	.015	.150	.061	.038	.040	.045	.035	.030	
20.0	-.006	.091	.147	.140	.156	.110	.010	.114	.008	.094	.086	.096	.081	.070	
22.5	.049	-.155	.194	.182	.192	.158	.021	.084	.043	.107	.144	.147	.127	.131	
25.0	.047	.238	.250	.231	.244	.204	.002	.079	.040	.126	.181	.177	.140	.148	
27.5	.107	.236	.214	.303	.225	.193	.070	.031	.287	.223	.191	.220	.179	.145	
30.0	.033	.401	.327	.342	.322	.284	.085	.151	.302	.209	.224	.228	.175	.178	
32.5	.381	.375	.322	.277	.105	.323	.079	.190	.223	.146					
35.0	.011	.106	.114	.104	.106	.104	.104	.106	.001	.104	.104	.106	.106	.108	
37.5	.944	-.1784	-.570	-.459	-.359	-.288	-.123	-.887	-.749	-.539	-.436	-.369	-.273	-.125	
40.0	-.883	-.756	-.592	-.449	-.377	-.288	-.119	-.845	-.742	-.554	-.426	-.382	-.289	-.130	
42.5	.780	-.797	-.623	-.494	-.364	-.281	-.119	-.772	-.728	-.588	-.466	-.377	-.263	-.137	
45.0	-.696	-.731	-.641	-.506	-.372	-.271	-.117	-.710	-.714	-.609	-.467	-.377	-.252	-.137	
47.5	-.637	-.684	-.505	-.312	-.363	-.259	-.110	-.672	-.653	-.583	-.472	-.376	-.243	-.128	
	1.3	.131	-.095	-.137	-.203	-.249	-.242	-.196	.308	.367	.374	.362	.342	.347	.278
2.5	.087	-.099	.130	.182	.156	.154	.155	.269	.301	.292	.269	.262	.276	.204	
5.0	.025	-.074	.087	.100	.099	.118	.129	.231	.197	.213	.201	.202	.196	.184	
7.5	.011	-.070	.101	.103	.103	.107	.111	.217	.197	.205	.247	.193	.195	.197	
10.1	-.032	-.086	.001	.115	.089	.080	.108	.159	.127	.129	.126	.122	.120	.053	
12.5	.040	-.124	.121	.121	.089	.090	.101	.119	.080	.093	.074	.094	.090	.002	
15.0	-.074	-.103	.106	.086	.096	.073	.096	.107	.081	.092	.045	.077	.064	.005	
17.5	.082	-.124	.111	.099	.082	.076	.088	.062	.020	.035	.044	.059	.051	.033	
20.0	-.099	-.124	.102	.087	.068	.058	.060	.034	.001	.023	.034	.049	.045	.025	
22.5	.109	-.124	.088	.075	.045	.035	.054	.018	-.001	.018	.031	.049	.045	.012	
25.0	-.120	-.110	.067	.045	.013	.017	.053	.000	-.007	.020	.040	.059	.047	.045	
27.5	-.050	.012	.030	.082	.071	.071	.029	.022	.063	.063	.081	.103	.097	.074	
30.0	.093	.034	.085	.100	.144	.133	.079	.005	.058	.122	.136	.139	.147	.090	
32.5	.127	.173	.173	.157	.204	.194	.089	.045	.157	.194	.221	.220	.210	.180	
35.0	.192	.204	.121	.245	.216	.183	.195	.028	.234	.228	.273	.260	.228	.216	
37.5	-.188	-.044	.162	.175	.267	.249	.195	.055	.193	.197	.241	.253	.241	.231	
40.0	.641	-.641	-.666	.136	.188	.195	.159	.177	.227	.237	.253	.253	.249	.246	









TABLE II. - WING WITH SPOILER-SLOT-DEFLECTOR - Continued.

Percent chord		Pressure coefficient														
		0.135b/2			0.25b/2			0.40b/2			0.55b/2			0.70b/2		
		M = 0.90	c = 21.20°		M = 0.94	c = 0.26°										
Upper surface	0.0	+0.40	-0.89	+0.872	-0.737	-0.603	-0.607	-0.972	+0.279	+0.535	+0.567	+0.563	+0.485	+0.525	+0.297	
	1.2	-0.44	-0.867	+0.838	-0.716	-0.595	-0.604	-0.951	+0.324	+0.003	+0.040	+0.164	+0.187	+0.176		
	2.4	-0.84	-0.867	+0.826	-0.716	-0.590	-0.603	-0.950	+0.192	+0.022	+0.029	+0.101	+0.121	+0.101		
	5.0	-0.85	-0.867	+0.816	-0.708	-0.587	-0.602	-0.958	+0.194	+0.009	+0.024	+0.064	+0.084	+0.049		
	7.5	-0.88	-0.866	+0.809	-0.703	-0.589	-0.602	-0.968	+0.081	+0.119	+0.049	+0.087	+0.064	+0.027		
	10.0	-0.89	-0.856	+0.805	-0.703	-0.589	-0.602	-0.969	+0.081	+0.028	+0.044	+0.086	+0.064	+0.027		
	12.5	-0.84	-0.856	+0.809	-0.703	-0.589	-0.602	-0.968	+0.081	+0.028	+0.044	+0.085	+0.064	+0.027		
	15.0	-0.85	-0.856	+0.805	-0.703	-0.589	-0.602	-0.969	+0.081	+0.028	+0.044	+0.085	+0.064	+0.027		
	17.5	-0.85	-0.856	+0.805	-0.703	-0.589	-0.602	-0.968	+0.081	+0.028	+0.044	+0.085	+0.064	+0.027		
	20.0	-0.85	-0.856	+0.805	-0.703	-0.589	-0.602	-0.968	+0.081	+0.028	+0.044	+0.085	+0.064	+0.027		
	22.5	-0.84	-0.856	+0.805	-0.703	-0.589	-0.602	-0.968	+0.081	+0.028	+0.044	+0.085	+0.064	+0.027		
	25.0	-0.84	-0.856	+0.805	-0.703	-0.589	-0.602	-0.968	+0.081	+0.028	+0.044	+0.085	+0.064	+0.027		
	27.5	-0.84	-0.856	+0.805	-0.703	-0.589	-0.602	-0.968	+0.081	+0.028	+0.044	+0.085	+0.064	+0.027		
	30.0	-0.84	-0.856	+0.805	-0.703	-0.589	-0.602	-0.968	+0.081	+0.028	+0.044	+0.085	+0.064	+0.027		
Lower surface	0.0	+0.40	-0.89	+0.872	-0.737	-0.603	-0.607	-0.972	+0.279	+0.535	+0.567	+0.563	+0.485	+0.525	+0.297	
	1.2	-0.89	-0.849	+0.838	-0.716	-0.595	-0.604	-0.951	+0.324	+0.003	+0.040	+0.164	+0.187	+0.176		
	2.4	-0.797	-0.854	+0.771	-0.858	-0.623	-0.602	-0.930	+0.087	+0.022	+0.029	+0.101	+0.121	+0.101		
	5.0	-0.771	-0.841	+0.749	-0.874	-0.627	-0.602	-0.930	+0.087	+0.022	+0.029	+0.093	+0.085	+0.035		
	7.5	-0.755	-0.856	+0.816	-0.865	-0.630	-0.628	-0.920	+0.083	+0.031	+0.083	+0.110	+0.105	+0.024		
	10.0	-0.854	-0.867	+0.804	-0.855	-0.625	-0.628	-0.925	+0.085	+0.031	+0.083	+0.112	+0.104	+0.018		
	12.5	-0.854	-0.867	+0.804	-0.855	-0.625	-0.628	-0.925	+0.085	+0.031	+0.083	+0.112	+0.104	+0.018		
	15.0	-0.854	-0.867	+0.804	-0.855	-0.625	-0.628	-0.925	+0.085	+0.031	+0.083	+0.112	+0.104	+0.018		
	17.5	-0.854	-0.867	+0.804	-0.855	-0.625	-0.628	-0.925	+0.085	+0.031	+0.083	+0.112	+0.104	+0.018		
	20.0	-0.854	-0.867	+0.804	-0.855	-0.625	-0.628	-0.925	+0.085	+0.031	+0.083	+0.112	+0.104	+0.018		
	22.5	-0.854	-0.867	+0.804	-0.855	-0.625	-0.628	-0.925	+0.085	+0.031	+0.083	+0.112	+0.104	+0.018		
	25.0	-0.854	-0.867	+0.804	-0.855	-0.625	-0.628	-0.925	+0.085	+0.031	+0.083	+0.112	+0.104	+0.018		
	27.5	-0.854	-0.867	+0.804	-0.855	-0.625	-0.628	-0.925	+0.085	+0.031	+0.083	+0.112	+0.104	+0.018		
	30.0	-0.854	-0.867	+0.804	-0.855	-0.625	-0.628	-0.925	+0.085	+0.031	+0.083	+0.112	+0.104	+0.018		
Upper surface	0.0	+0.40	-0.89	+0.872	-0.737	-0.603	-0.607	-0.972	+0.279	+0.535	+0.567	+0.563	+0.485	+0.525	+0.297	
	1.2	-0.89	-0.849	+0.838	-0.716	-0.595	-0.604	-0.951	+0.324	+0.003	+0.040	+0.164	+0.187	+0.176		
	2.4	-0.797	-0.854	+0.771	-0.858	-0.623	-0.602	-0.930	+0.087	+0.022	+0.029	+0.101	+0.121	+0.101		
	5.0	-0.771	-0.841	+0.749	-0.874	-0.627	-0.602	-0.930	+0.087	+0.022	+0.029	+0.093	+0.085	+0.035		
	7.5	-0.755	-0.856	+0.816	-0.865	-0.630	-0.628	-0.920	+0.083	+0.031	+0.083	+0.110	+0.105	+0.024		
	10.0	-0.854	-0.867	+0.804	-0.855	-0.625	-0.628	-0.925	+0.085	+0.031	+0.083	+0.112	+0.104	+0.018		
	12.5	-0.854	-0.867	+0.804	-0.855	-0.625	-0.628	-0.925	+0.085	+0.031	+0.083	+0.112	+0.104	+0.018		
	15.0	-0.854	-0.867	+0.804	-0.855	-0.625	-0.628	-0.925	+0.085	+0.031	+0.083	+0.112	+0.104	+0.018		
	17.5	-0.854	-0.867	+0.804	-0.855	-0.625	-0.628	-0.925	+0.085	+0.031	+0.083	+0.112	+0.104	+0.018		
	20.0	-0.854	-0.867	+0.804	-0.855	-0.625	-0.628	-0.925	+0.085	+0.031	+0.083	+0.112	+0.104	+0.018		
	22.5	-0.854	-0.867	+0.804	-0.855	-0.625	-0.628	-0.925	+0.085	+0.031	+0.083	+0.112	+0.104	+0.018		
	25.0	-0.854	-0.867	+0.804	-0.855	-0.625	-0.628	-0.925	+0.085	+0.031	+0.083	+0.112	+0.104	+0.018		
	27.5	-0.854	-0.867	+0.804	-0.855	-0.625	-0.628	-0.925	+0.085	+0.031	+0.083	+0.112	+0.104	+0.018		
	30.0	-0.854	-0.867	+0.804	-0.855	-0.625	-0.628	-0.925	+0.085	+0.031	+0.083	+0.112	+0.104	+0.018		
Lower surface	0.0	+0.40	-0.89	+0.872	-0.737	-0.603	-0.607	-0.972	+0.279	+0.535	+0.567	+0.563	+0.485	+0.525	+0.297	
	1.2	-0.89	-0.849	+0.838	-0.716	-0.595	-0.604	-0.951	+0.324	+0.003	+0.040	+0.164	+0.187	+0.176		
	2.4	-0.797	-0.854	+0.771	-0.858	-0.623	-0.602	-0.930	+0.087	+0.022	+0.029	+0.101	+0.121	+0.101		
	5.0	-0.771	-0.841	+0.749	-0.874	-0.627	-0.602	-0.930	+0.087	+0.022	+0.029	+0.093	+0.085	+0.035		
	7.5	-0.755	-0.856	+0.816	-0.865	-0.630	-0.628	-0.920	+0.083	+0.031	+0.083	+0.110	+0.105	+0.024		
	10.0	-0.854	-0.867	+0.804	-0.855	-0.625	-0.628	-0.925	+0.085	+0.031	+0.083	+0.112	+0.104	+0.018		
	12.5	-0.854	-0.867	+0.804	-0.855	-0.625	-0.628	-0.925	+0.085	+0.031	+0.083	+0.112	+0.104	+0.018		
	15.0	-0.854	-0.867	+0.804	-0.855	-0.625	-0.628	-0.925	+0.085	+0.031	+0.083	+0.112	+0.104	+0.018		
	17.5	-0.854	-0.867	+0.804	-0.855	-0.625	-0.628	-0.925	+0.085	+0.031	+0.083	+0.112	+0.104	+0.018		
	20.0	-0.854	-0.867	+0.804	-0.855	-0.625	-0.628	-0.925	+0.085	+0.031	+0.083	+0.112	+0.104	+0.018		
	22.5	-0.854	-0.867	+0.804	-0.855	-0.625	-0.628	-0.925	+0.085	+0.031	+0.083	+0.112	+0.104	+0.018		
	25.0	-0.854	-0.867	+0.804	-0.855	-0.625	-0.628	-0.925	+0.085	+0.031	+0.083	+0.112	+0.104	+0.018		
	27.5	-0.854	-0.867	+0.804	-0.855	-0.625	-0.628	-0.925	+0.085	+0.031	+0.083	+0.112	+0.104	+0.018		
	30.0	-0.854	-0.867	+0.804	-0.855	-0.625	-0.628	-0.925	+0.085	+0.031	+0.083	+0.112	+0.104	+0.018		

TABLE II. - WING WITH SPOILER-SLOT-DEFLECTOR - Continued

Per-		Pressure coefficient													
		0.135b/2		0.25b/2		0.40b/2		0.55b/2		0.70b/2		0.85b/2			
		cent	chord	M = 0.94	a = 8.25°	M = 0.94	a = 12.73°	M = 0.94	a = 17.16°	M = 0.94	a = 21.35°	M = 0.94	a = 25.73°		
Upper surface	0.0	+302	-008	-089	-315	-160	-307	+016	+279	-414	-563	-699	-467	-569	-266
	1.2	+102	-1208	-1280	-765	-768	-681	-613	-081	-1304	-133	-697	-556	-508	-462
	2.4	-200	-1182	-1259	-780	-726	-697	-592	-403	-1299	-108	-652	-564	-521	-455
	5.0	-330	-1046	-1202	-726	-765	-688	-579	-494	-1244	-102	-641	-582	-534	-451
	7.5	-557	-775	-1131	-720	-874	-571	-579	-682	-1191	-1075	-643	-600	-533	-446
	10.0	-385	-665	-1091	-721	-767	-542	-575	-662	-1128	-1069	-649	-601	-533	-437
	15.0	-368	-578	-929	-709	-719	-534	-554	-618	-1059	-1046	-652	-524	-539	-423
	19.6	-352	-536	-568	-676	-202	-544	-523	-587	-1021	-1028	-661	-537	-428	
	24.5	-376	-505	-536	-684	-169	-537	-471	-570	-996	-96	-722	-440	-551	-425
	29.5	-343	-482	-613	-631	-157	-539	-436	-534	-949	-936	-777	-461	-540	-424
	34.5	-374	-424	-653	-592	-139	-525	-415	-543	-841	-828	-722	-440	-551	-425
	39.5	-360	-145	-115	-389	-126	-472	-405	-502	-876	-830	-702	-445	-545	-425
	44.5	-372	-050	-132	-159	-126	-373	-402	-526	-884	-846	-704	-450	-522	-407
	49.5	-371	+175	+127	+018	+125	+222	+412	+475	+882	+799	+860	+510	+399	
	54.5	-088	+224	+116	+108	+148	+294	+327	+381	+739	+740	+857	+457	+348	
	59.5	-088	+167	+100	+165	+178	+20	+321	+351	+022	+571	+702	+859	+482	+367
	64.5	-227	+175	+084	+198	+221	+071	+643	+128	+018	+402	+617	+554	+456	+373
	69.5	-009								+013	-010				+366
	74.6	-867	-805	-635	-505	-441	-344	-356	-831	-799	-641	-553	-448	-387	-335
	79.5	-843	-792	-635	-507	-440	-353	-353	-831	-782	-663	-572	-453	-402	-367
	84.6	-785	-778	-645	-510	-438	-350	-318	-797	-738	-718	-588	-495	-399	-340
	89.6	-717	-754	-646	-507	-448	-347	-359	-718	-746	-715	-599	-466	-390	-334
	94.6	-674	-723	-628	-505	-457	-343	-293	-681	-721	-629	-588	-458	-378	-326
Lower surface	1.3	+465	+561	+532	+527	+514	+501	+437	+514	+628	+578	+547	+524	+516	+466
	2.9	+418	+523	+487	+479	+446	+458	+408	+426	+635	+585	+556	+506	+495	
	7.6	+467	+432	+418	+418	+416	+386	+337	+395	+722	+662	+542	+530	+496	+428
	10.1	+447	+384	+365	+363	+309	+359	+346	+365	+725	+644	+642	+650	+556	+559
	15.0	+411	+347	+342	+333	+317	+303	+325	+412	+747	+636	+636	+612	+580	+517
	19.6	+368	+293	+262	+278	+259	+240	+304	+547	+456	+405	+405	+353	+325	+202
	24.5	+261	+214	+217	+208	+197	+170	+404	+436	+580	+529	+300	+283	+251	+075
	29.5	+245	+194	+197	+186	+171	+144	+411	+390	+529	+300	+272	+249	+215	+048
	34.5	+207	+181	+181	+147	+158	+122	+324	+350	+502	+277	+244	+226	+188	+016
	39.5	+183	+184	+172	+158	+155	+109	+302	+320	+290	+260	+226	+214	+186	+013
	44.5	+154	+197	+174	+162	+159	+110	+355	+284	+288	+251	+216	+208	+155	+053
	49.5	+143	+218	+187	+179	+174	+125	+101	+265	+294	+249	+219	+232	+157	+113
	54.5	+190	+273	+221	+214	+226	+175	+169	+295	+333	+288	+242	+248	+187	+189
	59.5	+233	+316	+284	+257	+276	+242	+219	+323	+360	+315	+284	+291	+244	+251
	64.5	+406	+346	+307	+331	+296	+238	+235	+471	+390	+339	+348	+317	+282	+251
	69.5	+663													
	74.6	-920	-775	-715	-595	-451	-343	-220	-472	-577	-745	-642	-521	-446	-273
	79.6	-778	-670	-715	-599	-460	-352	-232	-464	-746	-772	-651	-527	-421	-268
	84.6	-474	-1008	-695	-591	-453	-321	-228	-352	-921	-737	-641	-521	-409	-274
	89.6	-395	-672	-684	-582	-435	-324	-232	-388	-649	-648	-514	-393	-290	
	94.6	-144	-636	-636	-641	-508	-455	-315			-441	-581	-639	-503	-365
Lower surface	1.3	+457	+638	+577	+534	+518	+500	+450	+408	+606	+530	+478	+470	+446	+407
	2.6	+387	+691	+636	+594	+570	+531	+479	+214	+703	+638	+587	+572	+522	+480
	5.0	+696	+685	+628	+600	+556	+520	+452	+746	+752	+649	+628	+590	+559	+479
	7.6	+780	+697	+593	+559	+523	+495	+408	+866	+735	+650	+604	+572	+530	+449
	10.1	+767	+618	+583	+527	+492	+462	+375	+853	+706	+648	+584	+545	+506	+422
	15.1	+689	+561	+515	+473	+436	+400	+287	+783	+655	+589	+538	+476	+452	+318
	19.6	+612	+511	+471	+441	+400	+366	+203	+710	+611	+548	+464	+420	+366	+266
	24.5	+589	+472	+435	+395	+359	+320	+127	+669	+570	+509	+461	+423	+371	+176
	29.5	+520	+440	+402	+357	+325	+282	+089	+622	+596	+476	+423	+386	+330	+246
	34.5	+477	+412	+374	+327	+297	+247	+046	+574	+522	+478	+423	+386	+327	
	39.5	+444	+393	+351	+303	+277	+220	+047	+541	+480	+415	+361	+329	+258	+026
	44.5	+412	+381	+334	+285	+261	+212	+047	+505	+461	+393	+337	+305	+250	+030
	49.5	+376	+372	+321	+277	+200	+193	+106	+474	+447	+373	+319	+314	+212	+111
	54.5	+403	+405	+363	+389	+274	+214	+198	+485	+464	+372	+316	+295	+219	+216
	59.5	+429	+426	+364	+322	+312	+258	+280	+493	+474	+393	+349	+324	+257	+216
	64.5	+349	+451	+387	+375	+336	+275	+328	+612	+495	+411	+386	+345	+272	+384
	69.5	+763													
	74.6	-643	-446	-710	-780	-594	-444	-364	-666	-387	-626	-797	-663	-616	-417
	79.6	-504	-600	-753	-801	-609	-470	-350	-508	-669	-681	-683	-611	-403	
	84.6	-156	-756	-706	-833	-601	-464	-347	-622	-634	-611	-725	-595	-405	
	89.7	+111	-627	-670	-829	-586	-458	-358	-300	-391	-577	-630	-676	-563	-419
	94.6	+263	-284	-381	-724	-538	-447	-354	-292	-340	-544	-631	-672	-533	-424

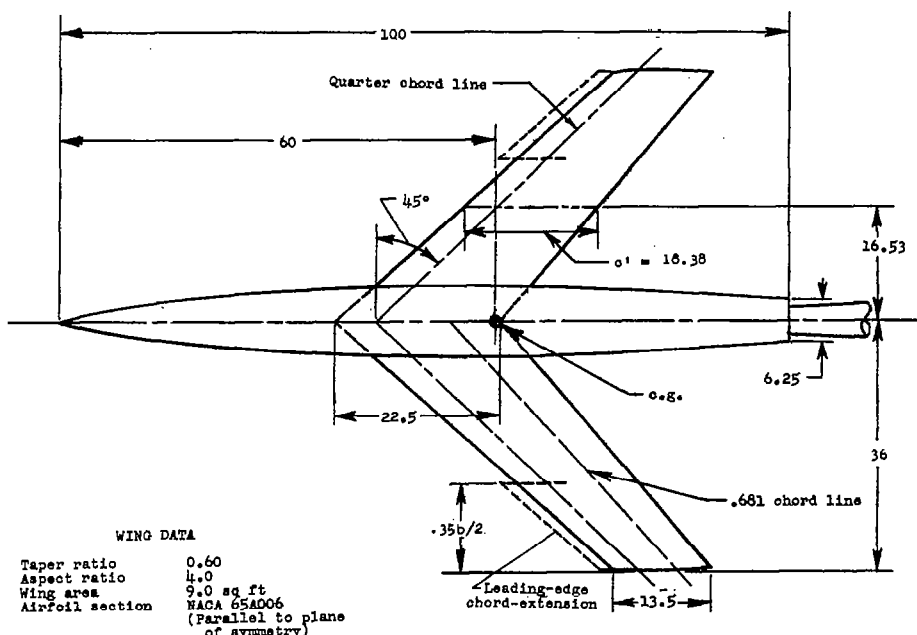
TABLE II. - WING WITH SPOILER-SLOT-DEFLECTOR - Continued

Percent chord	Pressure coefficient															
	0.135b/2				0.25b/2				0.40b/2				0.55b/2			
	M = 0.98	a = 0.26°	M = 0.98	a = 4.22°	M = 0.98	a = 6.26°	M = 0.98	a = 8.27°	M = 0.98	a = 0.98	M = 0.98	a = 0.26°	M = 0.98	a = 4.22°		
Upper surface																
0.0	.293	.546	.581	.580	.478	.523	.331	.295	.362	.342	.224	.280	.182	.342		
1.2	.337	.014	.043	.174	.165	.183	.173	.250	.757	.930	.812	.802	.857	.716		
2.4	.211	-.021	.031	.123	.141	.132	.104	.024	.709	.675	.678	.640	.777	.644		
5.0	.142	-.006	.049	.123	.119	.109	.070	-.051	.297	.711	.425	.400	.430	.390		
7.5	.101	-.006	.060	.114	.101	.086	.040	-.094	.258	.345	.181	.243	.227	.324		
10.0	.068	-.020	.059	.109	.099	.071	.010	-.121	.116	.169	.146	.186	.185	.274		
15.0	.036	-.023	.091	.113	.100	.079	-.049	-.112	.127	.149	.146	.133	.152	.226		
19.6	.027	-.027	.108	.130	.122	.114	-.053	.134	.251	.004	-.014	.072	.080	.085		
24.5	-.015	-.016	.048	.119	.118	.023	-.178	.247	.067	.002	.030	.049	.032			
29.5	.007	-.014	.100	.124	.100	.006	-.159	.258	.112	.025	.013	.022	.009			
34.5	-.014	-.118	.221	.179	.155	.114	.033	-.195	.007	.159	.057	.017	.003			
39.5	.194	.260	.203	.188	.181	.024	-.193	.152	.213	.096	.107	.059	.005			
44.5	-.041	.291	.306	.248	.230	.161	-.003	-.196	.274	.244	.139	.147	.106	.013		
49.5	.105	.396	.361	.300	.281	.200	.053	.059	.369	.252	.177	.186	.149	.080		
54.5	.210	.504	.394	.361	.354	.256	.139	.120	.400	.295	.205	.210	.173	.133		
59.5	.360	.527	.390	.380	.353	.280	.227	.261	.317	.219	.221	.219	.175	.124		
64.5	.480	.452	.372	.355	.358	.270	.302	.396	.173	.207	.232	.221	.161	.116		
69.5	.036							-.327	.020							
74.6	-.951	-.844	-.684	-.603	-.550	-.450	-.353	-.969	-.857	-.703	-.620	-.529	-.429	.349		
79.5	-.947	-.828	-.708	-.614	-.512	-.483	-.359	-.921	-.888	-.713	-.626	-.529	-.428	.355		
84.6	-.800	-.818	-.733	-.619	-.503	-.452	-.351	-.815	-.852	-.722	-.627	-.524	-.423	.360		
89.6	-.645	-.808	-.760	-.623	-.505	-.448	-.317	-.703	-.821	-.761	-.624	-.523	-.422	.350		
94.6	-.342	-.777	-.723	-.619	-.502	-.441	-.305	-.635	-.791	-.758	-.622	-.521	-.420	.340		
Lower surface																
1.3	.245	.085	.075	.042	-.041	-.099	.112	.379	.417	.428	.451	.414	.397	.345		
2.6	.226	.057	.035	.014	-.001	-.051	-.053	.350	.356	.353	.336	.329	.271			
5.0	.166	.047	.048	.068	.018	.037	.087	.327	.272	.279	.297	.271	.238	.211		
7.6	.123	.031	.025	.036	.001	-.041	-.081	.285	.224	.232	.244	.221	.205	.183		
10.1	.092	.019	.037	.017	-.019	-.045	-.089	.248	.194	.210	.209	.180	.161	.103		
15.1	.062	-.003	.012	.003	-.030	-.055	-.158	.209	.156	.179	.173	.148	.127			
19.6	.024	-.013	.014	.019	-.030	-.050	-.187	.163	.128	.155	.155	.123	.108	.067		
24.5	.016	-.047	.016	.000	-.030	-.058	-.122	.190	.094	.134	.118	.099	.064	.125		
29.5	-.005	-.049	.027	.004	-.022	-.051	-.028	.120	.086	.124	.101	.086	.041	.073		
34.5	-.028	-.031	.041	.009	-.011	-.035	-.018	.071	.077	.101	.092	.081	.049	.034		
39.5	-.044	-.011	.058	.031	.011	-.021	-.012	.074	.107	.123	.096	.084	.048	.033		
44.5	-.060	.071	.088	.069	.044	.011	-.048	.056	.184	.158	.140	.131	.072	.083		
49.5	-.045	.131	.122	.119	.114	.063	-.049	.107	.233	.207	.186	.175	.139	.160		
54.5	.024	.223	.104	.093	.102	.150	.121	.191	.309	.274	.243	.246	.221	.250		
59.5	.153	.304	.274	.222	.244	.246	.246	.282	.377	.395	.292	.300	.258	.298		
64.5	.455	.364	.304	.275	.227	.242	.246	.295	.568							
69.5	-.019	-.1016	-.778	-.673	-.523	-.447	-.311	-.922	-.934	-.798	-.667	-.542	-.453	.314		
74.6	-.770	-.013	-.753	-.681	-.542	-.450	-.302	-.707	-.951	-.769	-.674	-.550	-.444	.322		
79.5	-.478	-.1007	-.738	-.669	-.530	-.450	-.291	-.460	-.984	-.748	-.670	-.539	-.438	.327		
84.6	-.412	-.1072	-.722	-.672	-.531	-.440	-.291	-.353	-.904	-.731	-.665	-.533	-.424	.345		
89.7	-.227	-.0953	-.701	-.691	-.528	-.408	-.286	-.180	-.827	-.711	-.680	-.592	-.403	.343		
Lower surface																
1.3	.434	.507	.497	.501	.487	.470	.404	.482	.576	.549	.536	.522	.510	.482		
2.6	.401	.456	.435	.434	.422	.407	.344	.441	.536	.502	.484	.460	.445			
5.0	.407	.362	.360	.370	.352	.319	.282	.490	.445	.452	.424	.427	.395			
7.6	.373	.314	.307	.314	.300	.278	.222	.470	.398	.380	.350	.322	.322			
10.1	.335	.286	.297	.282	.261	.240	.168	.434	.340	.330	.329	.311	.297			
15.1	.293	.231	.240	.236	.215	.198	.087	.331	.237	.223	.204	.206	.202			
19.6	.241	.194	.207	.212	.186	.170	.024	.331	.238	.266	.242	.237	.202			
24.5	.223	.161	.184	.177	.158	.131	.058	.368	.230	.229	.222	.207	.176	.012		
29.5	.187	.146	.156	.156	.136	.109	.078	.366	.212	.219	.198	.182	.147			
34.5	.156	.146	.159	.157	.137	.108	.087	.331	.202	.205	.179	.167	.126			
39.5	.135	.132	.147	.148	.124	.080	.049	.206	.196	.198	.170	.159	.103			
44.5	.105	.177	.164	.142	.133	.075	-.030	.178	.222	.199	.172	.160	.098			
49.5	.105	.210	.183	.165	.154	.092	-.090	.169	.247	.209	.186	.177	.111			
54.5	.157	.274	.222	.204	.186	.146	-.170	.216	.299	.245	.220	.221	.156			
59.5	.220	.318	.286	.253	.260	.224	-.252	.263	.340	.304	.279	.272	.232			
64.5	.401	.347	.305	.315	.276	.218	-.293	.437	.367	.324	.332	.286	.231			
69.5	.609															
74.6	-.904	-.849	-.818	-.679	-.541	-.434	-.302	-.857	-.754	-.825	-.737	-.592	-.523			
79.5	-.659	-.901	-.804	-.676	-.544	-.438	-.310	-.686	-.827	-.822	-.739	-.579	-.498			
84.6	-.458	-.976	-.793	-.673	-.539	-.427	-.318	-.438	-.950	-.791	-.742	-.592	-.484			
89.7	-.356	-.972	-.751	-.660	-.535	-.410	-.335	-.357	-.916	-.737	-.711	-.602	-.441			
94.6	-.152	-.729	-.697	-.664	-.540	-.392	-.322	-.617	-.655	-.699	-.620	-.445	-.318			

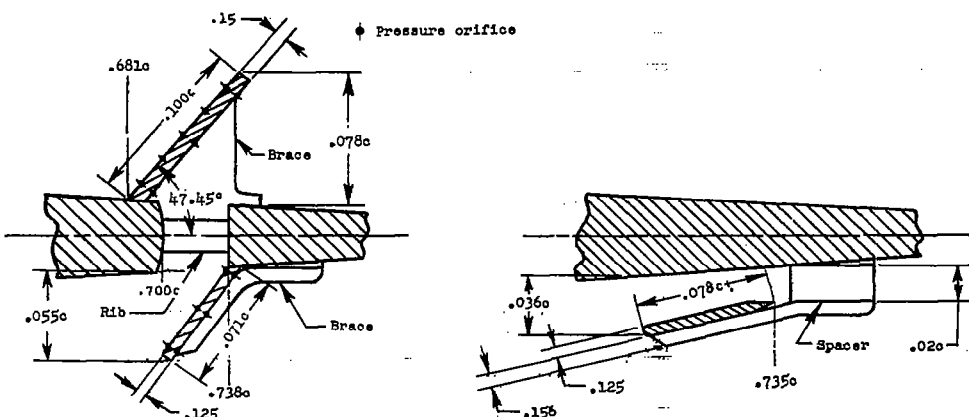








(a) Model.

(b) Spoiler-slot-deflector.  
(Section parallel to plane of symmetry.)

(c) Deflector. (Section parallel to plane of symmetry.)

Figure 1-- Diagram and dimensional details of wing-fuselage model and cross-sectional detail of two different type spoiler control configurations. (All linear dimensions are in inches, except as noted.)

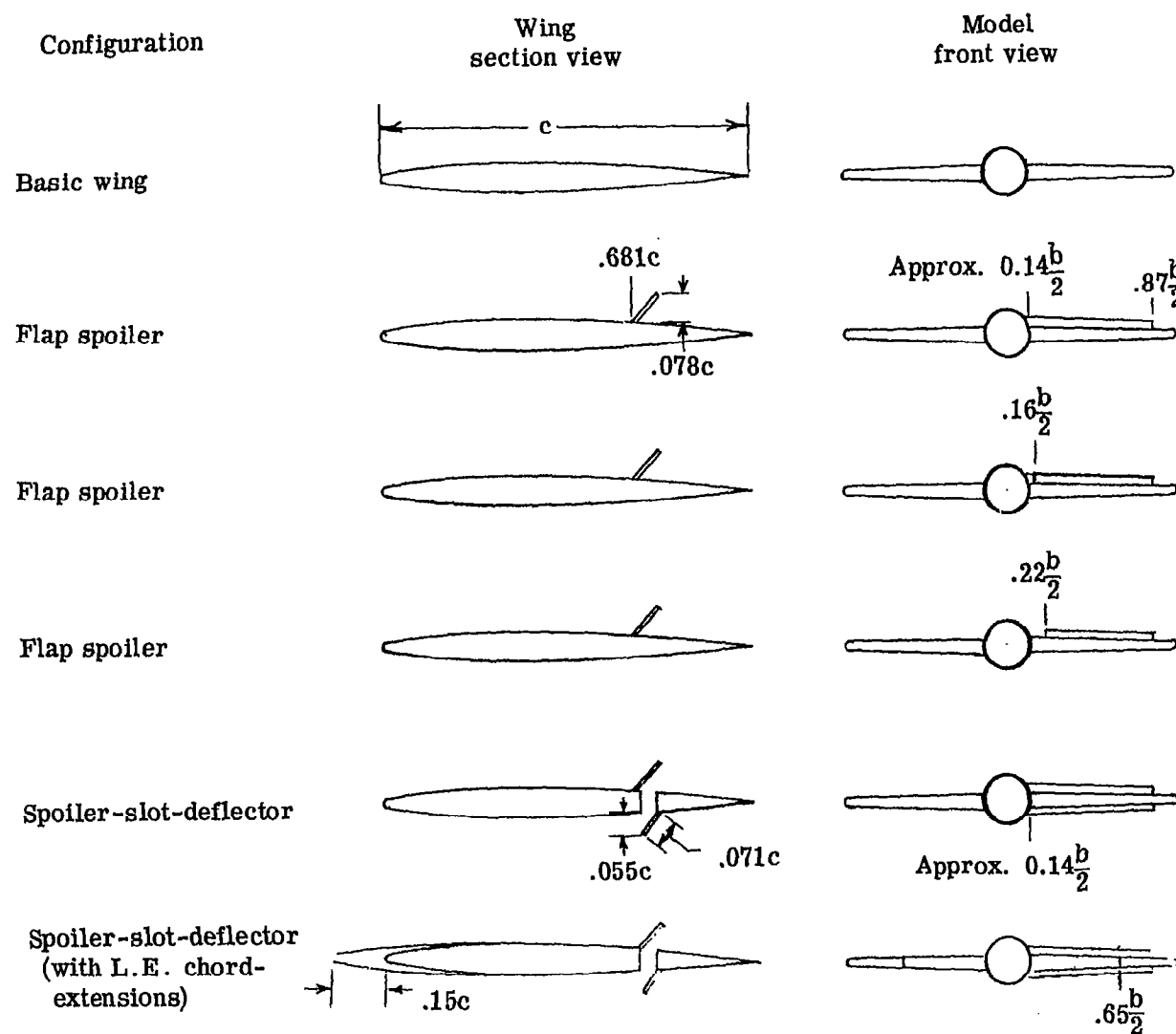


Figure 2.- Geometry of test configurations. (Not to scale.)

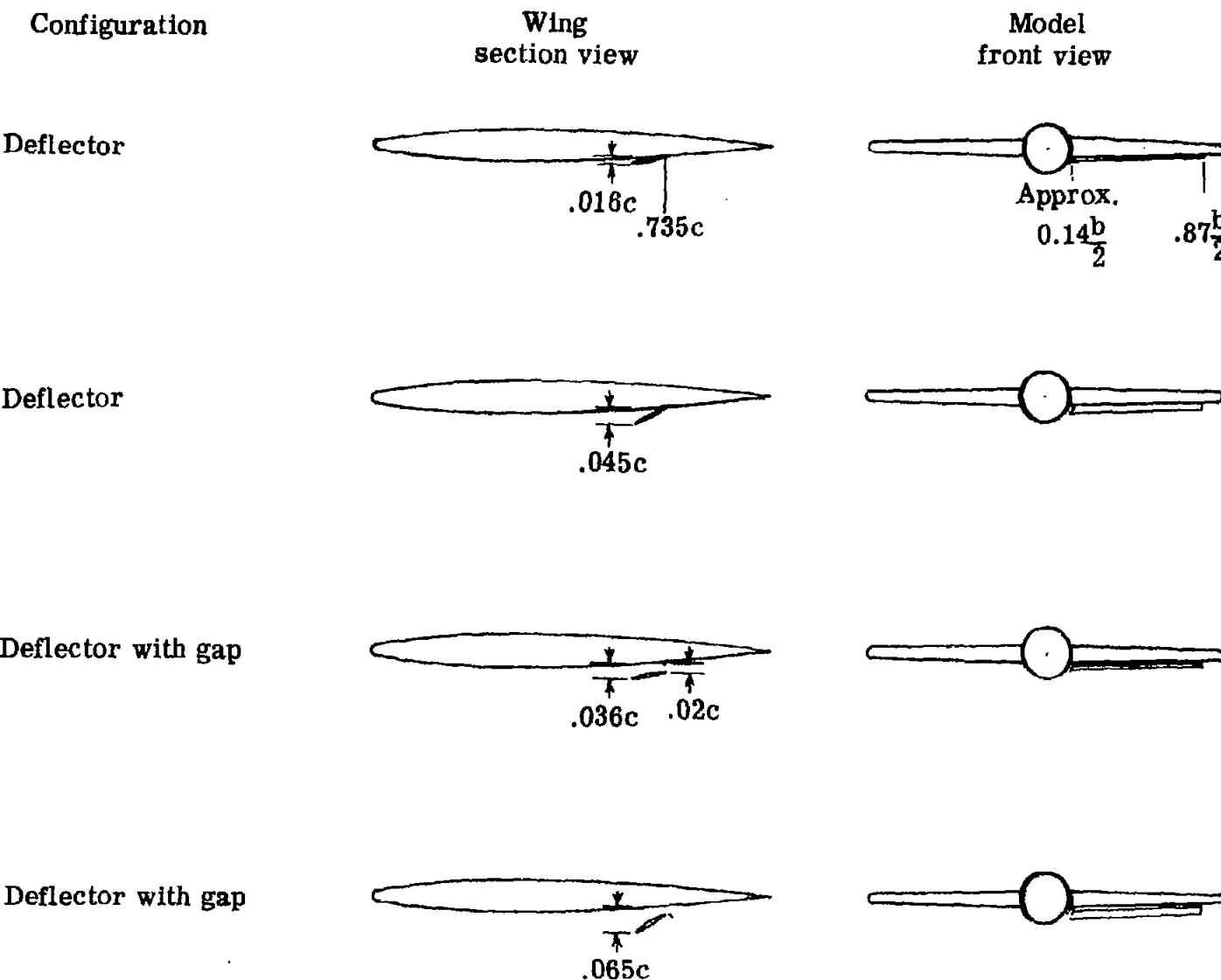


Figure 2.- Concluded.

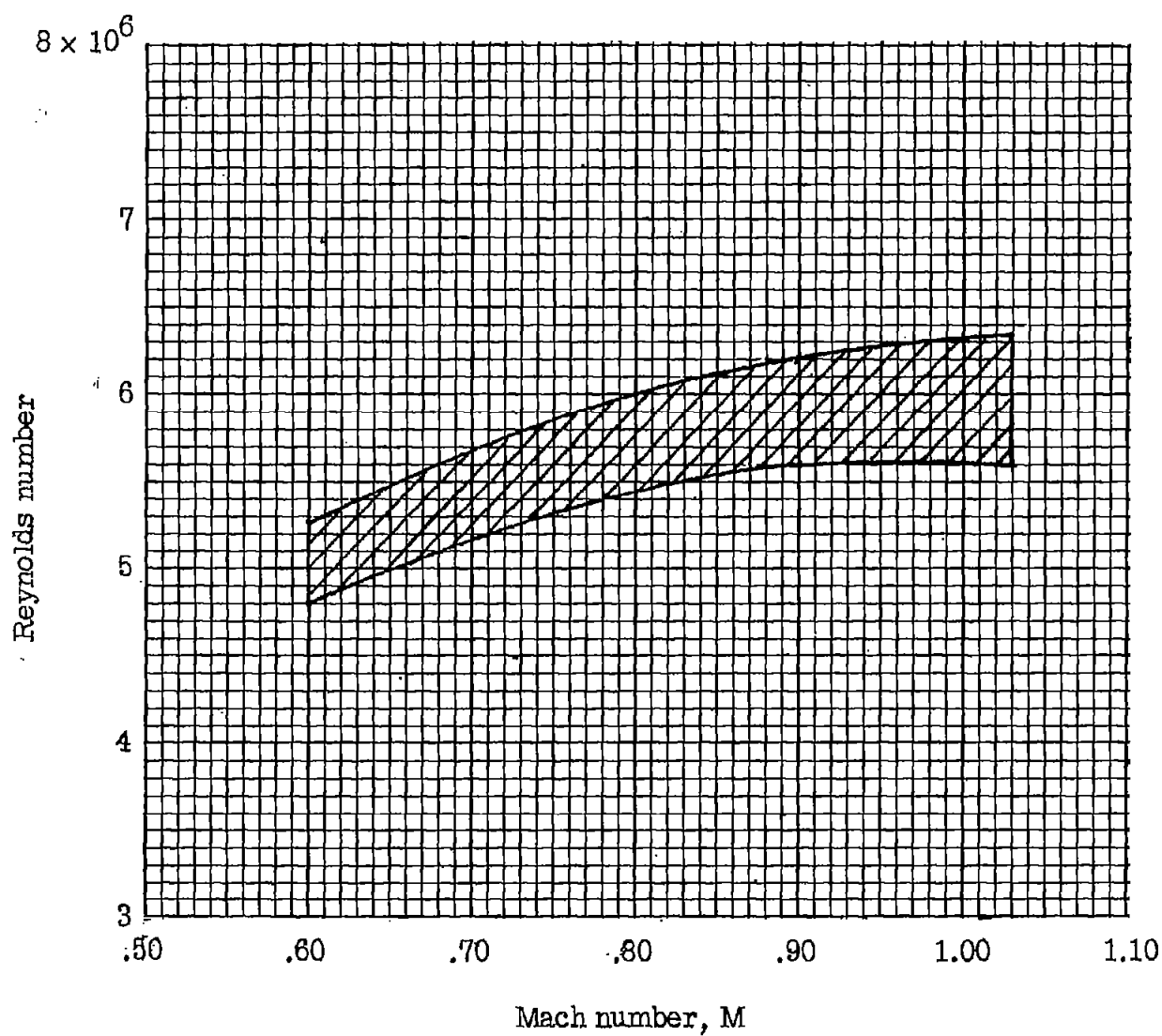


Figure 3.- Variation of Reynolds number (based on wing mean aerodynamic chord) with Mach number.

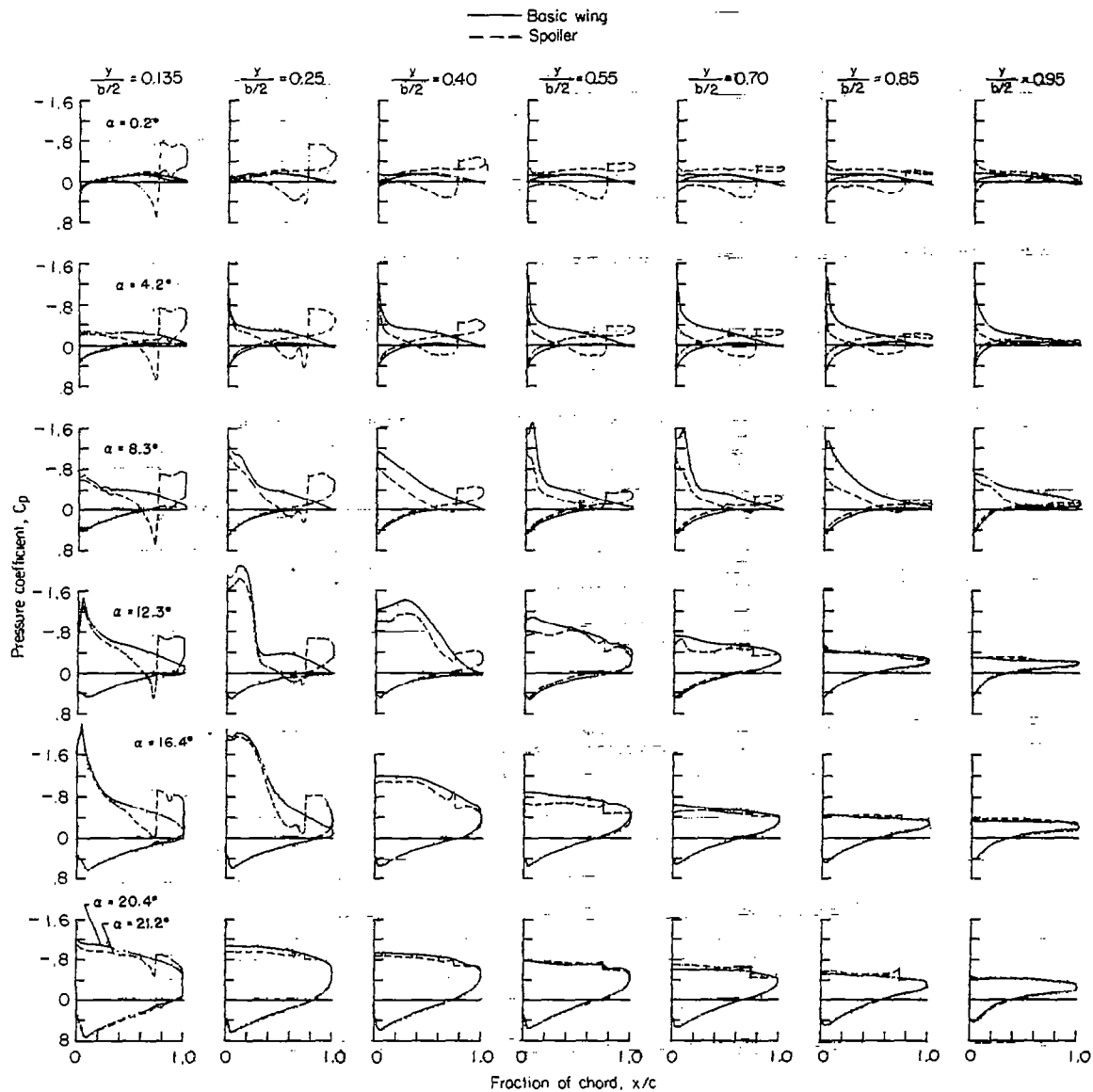
(a)  $M = 0.60.$ 

Figure 4.- Wing chordwise pressure distributions for the basic model and a spoiler aileron configuration.

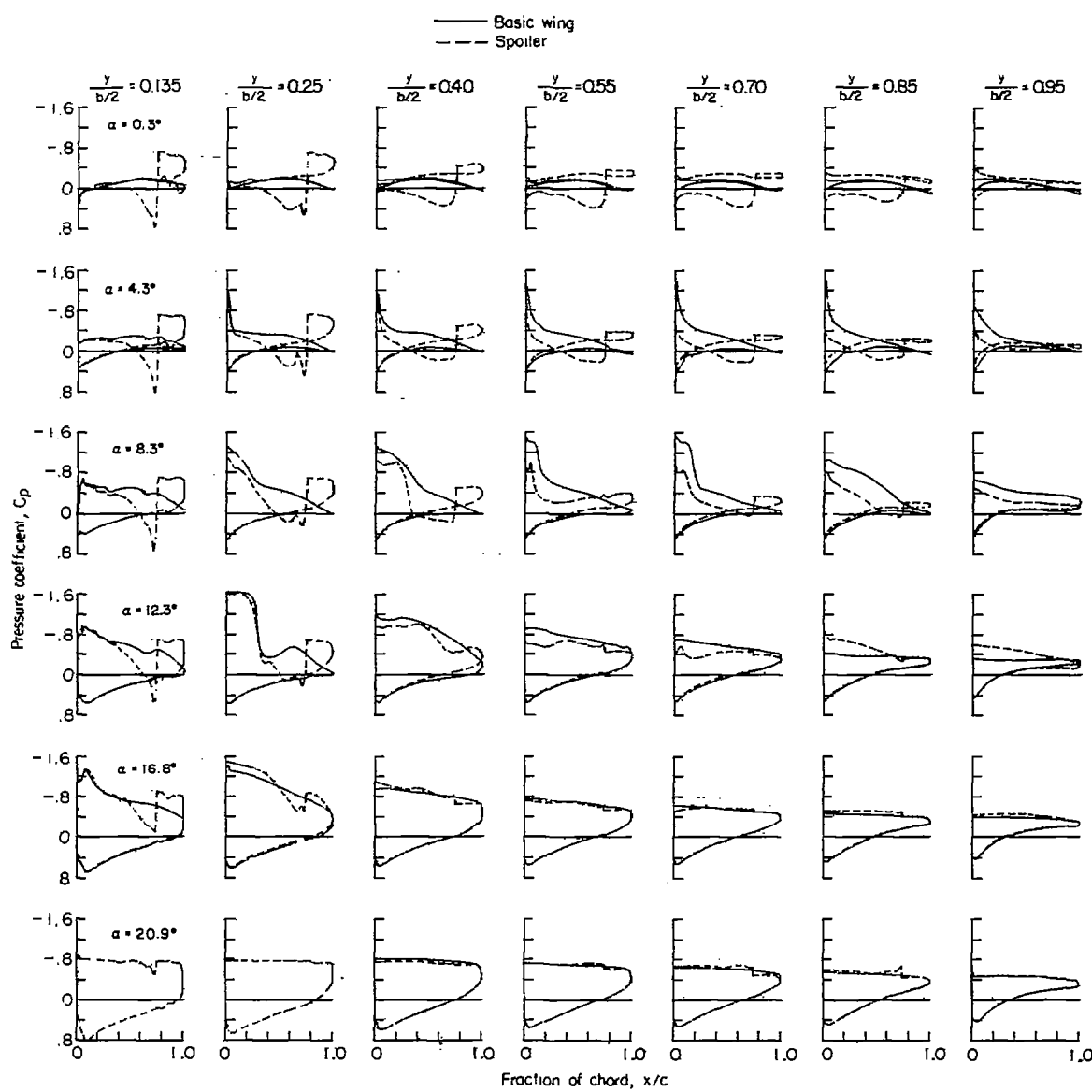
(b)  $M = 0.80$ .

Figure 4.- Continued.

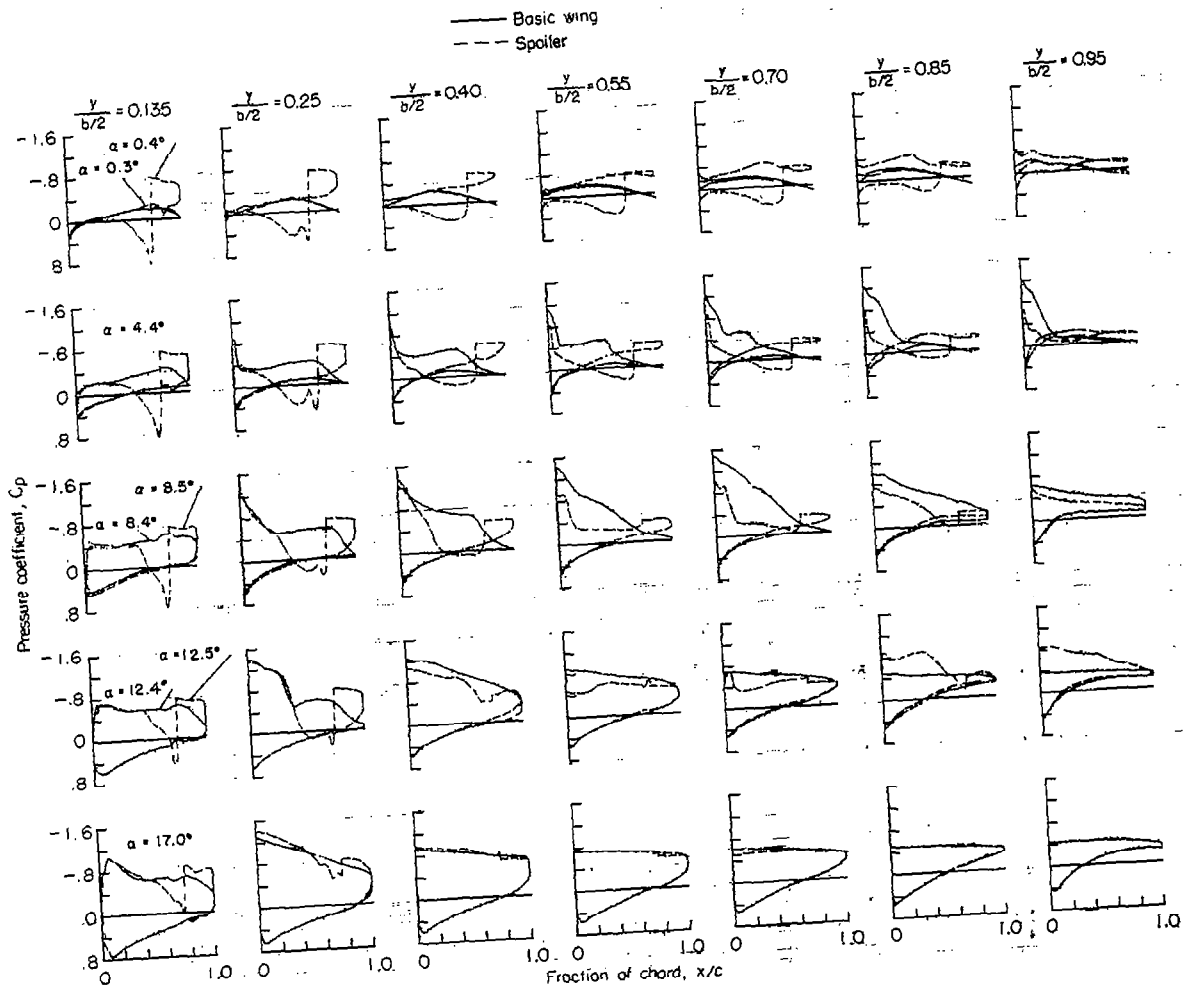
(c)  $M = 0.90$ .

Figure 4.- Continued.

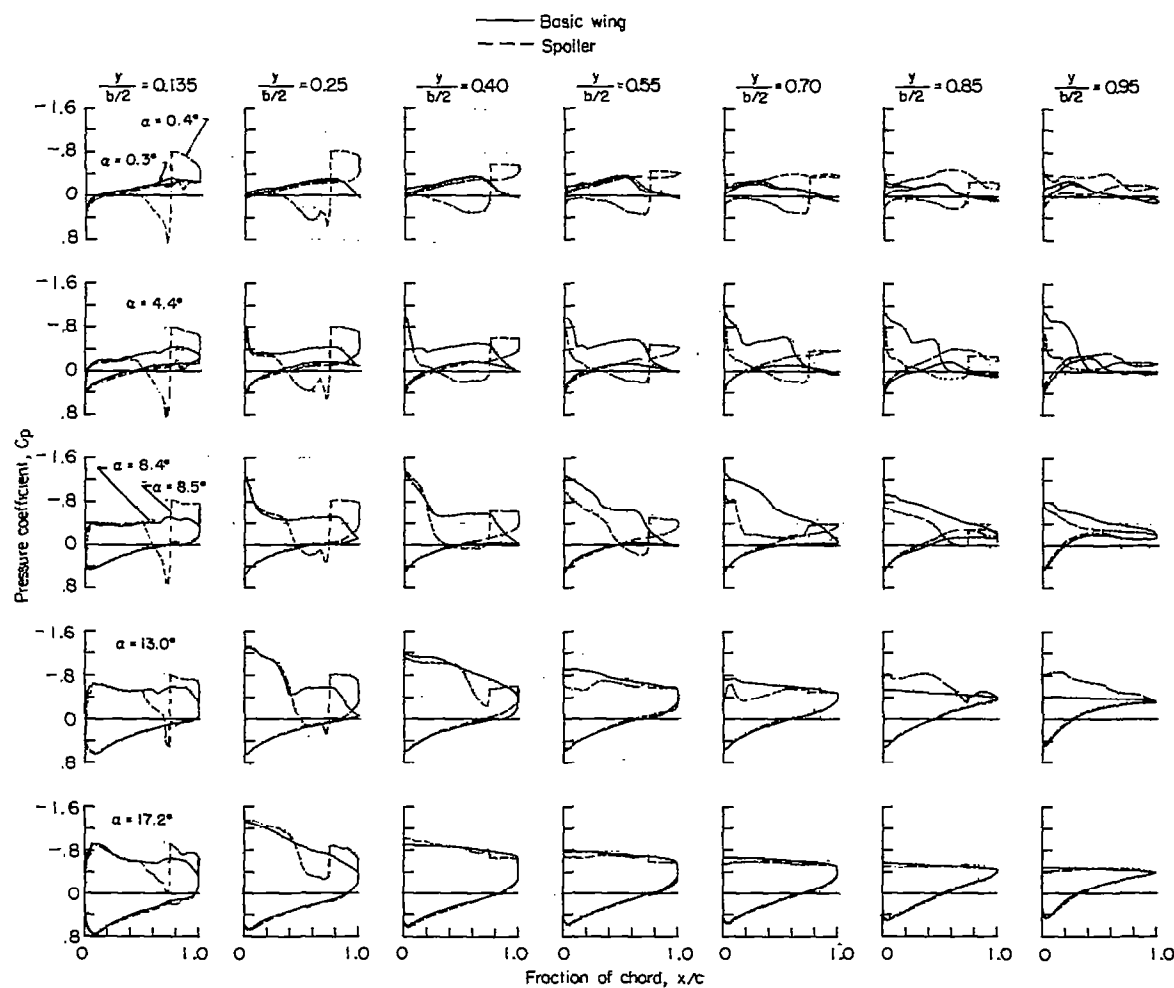
(d)  $M = 0.94$ .

Figure 4.- Continued.

CONFIDENTIAL

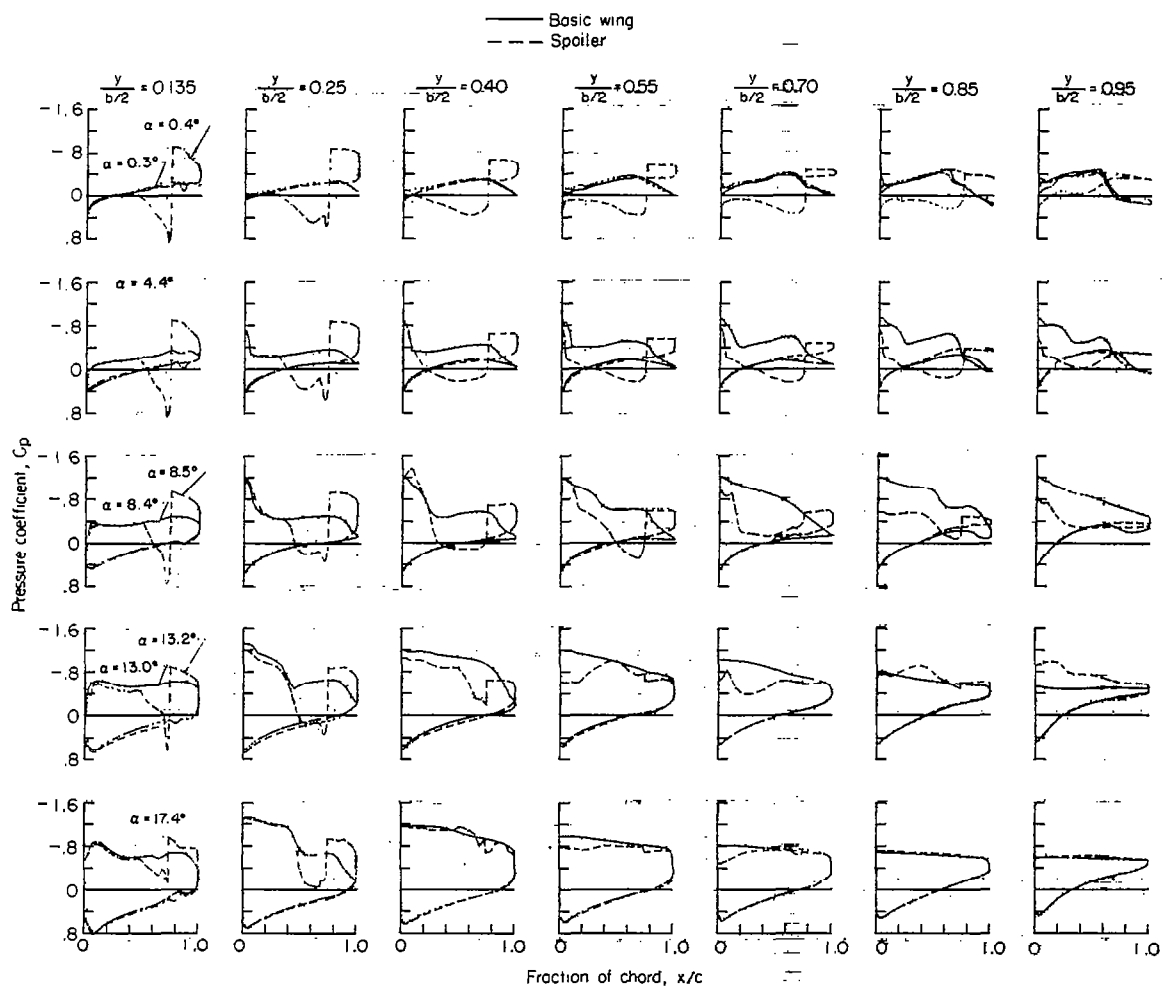
(e)  $M = 0.98$ .

Figure 4.- Continued.

CONFIDENTIAL

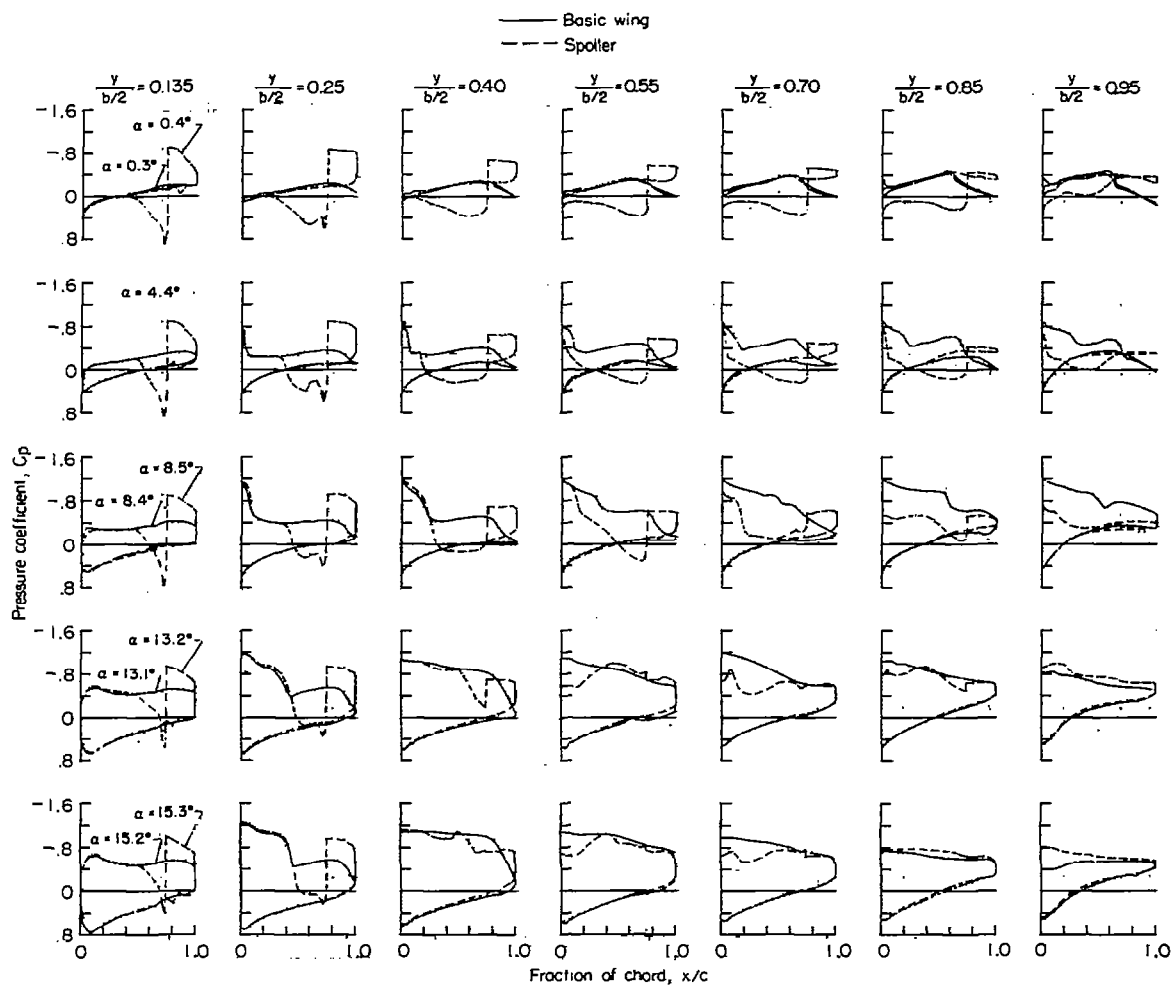
(f)  $M = 1.00$ .

Figure 4.- Continued.

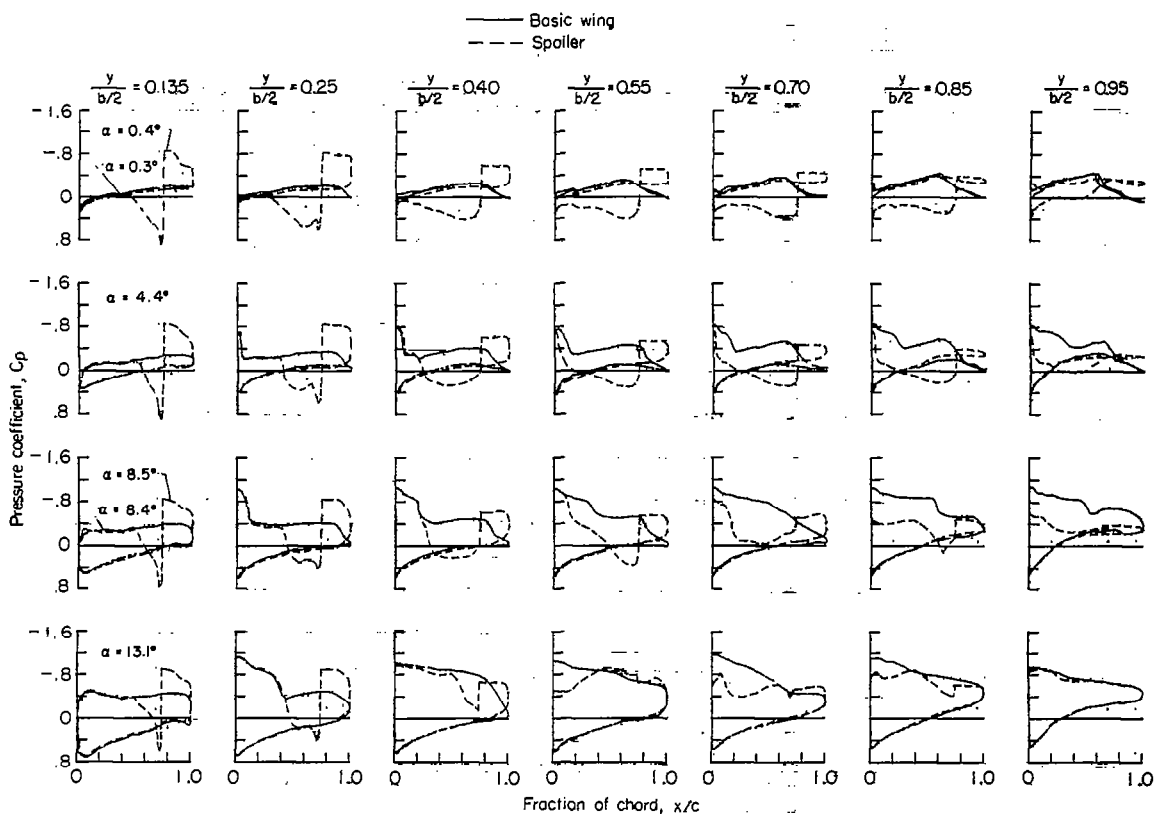
(g)  $M = 1.03.$ 

Figure 4.- Concluded.

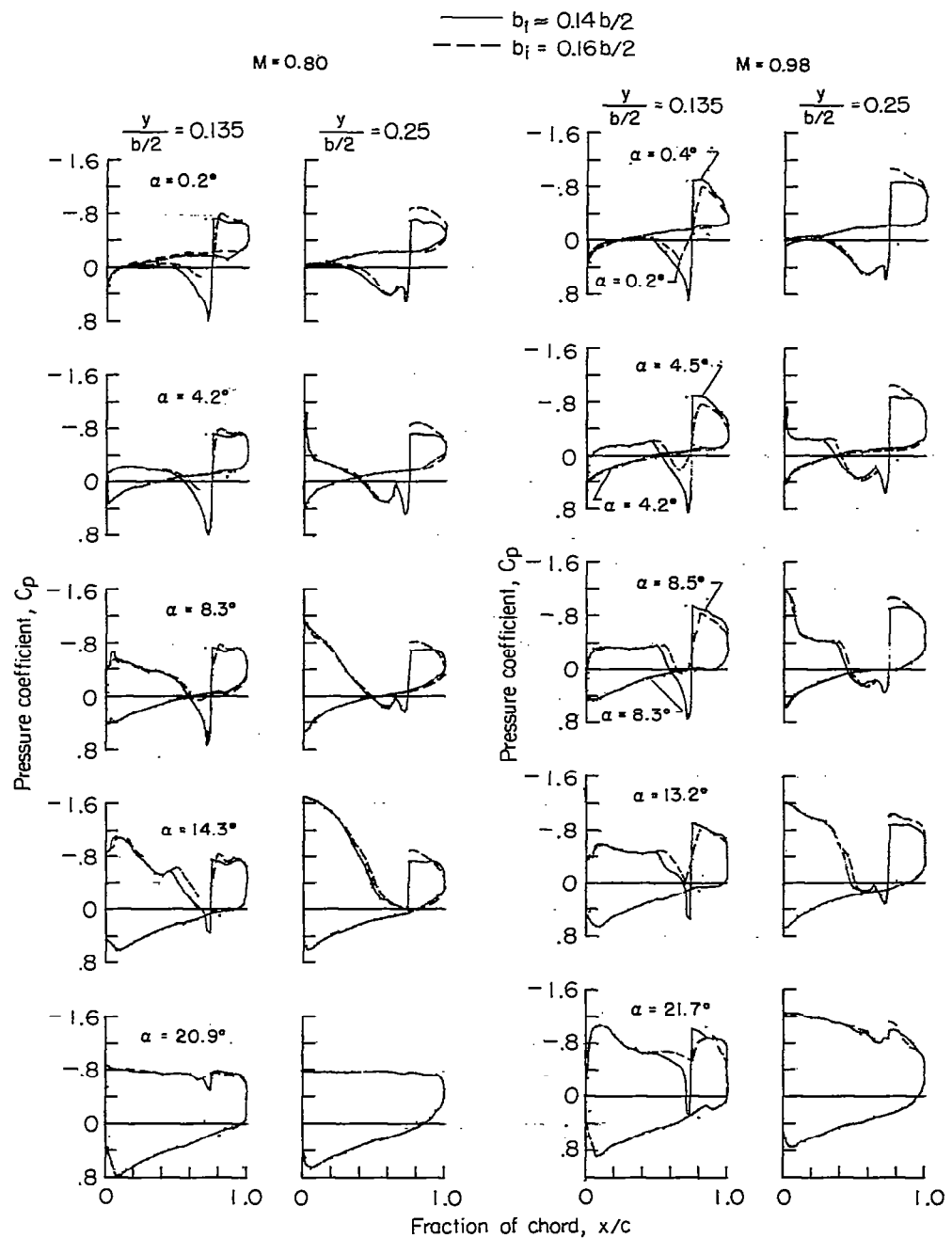


Figure 5.- Wing chordwise pressure distributions showing the effect of changing the inboard end position of a spoiler aileron from approximately 14 to 16 percent of the semispan.

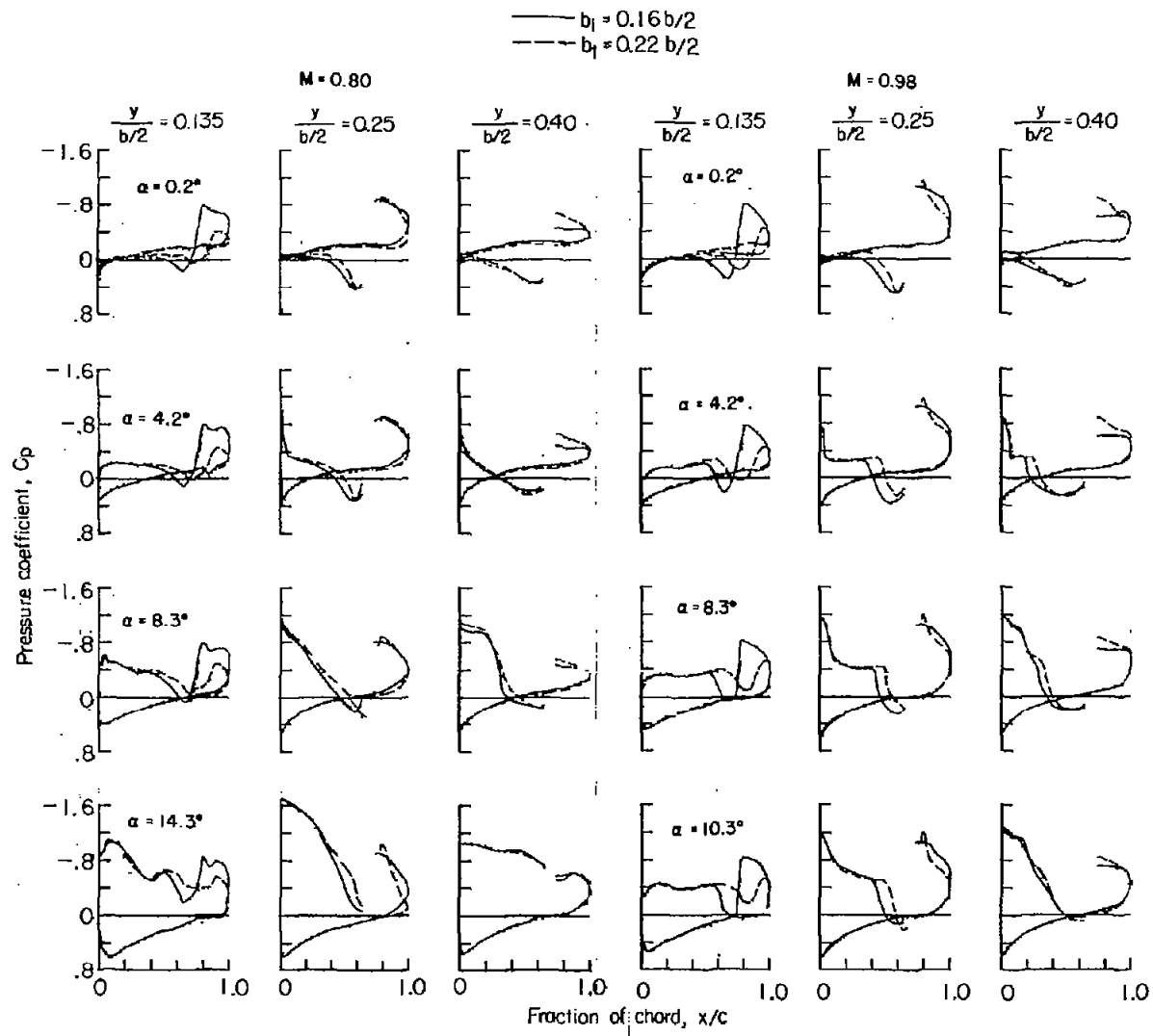


Figure 6.- Wing chordwise pressure distributions showing the effect of changing the inboard end position of a spoiler aileron from 16 to 22 percent of the semispan.

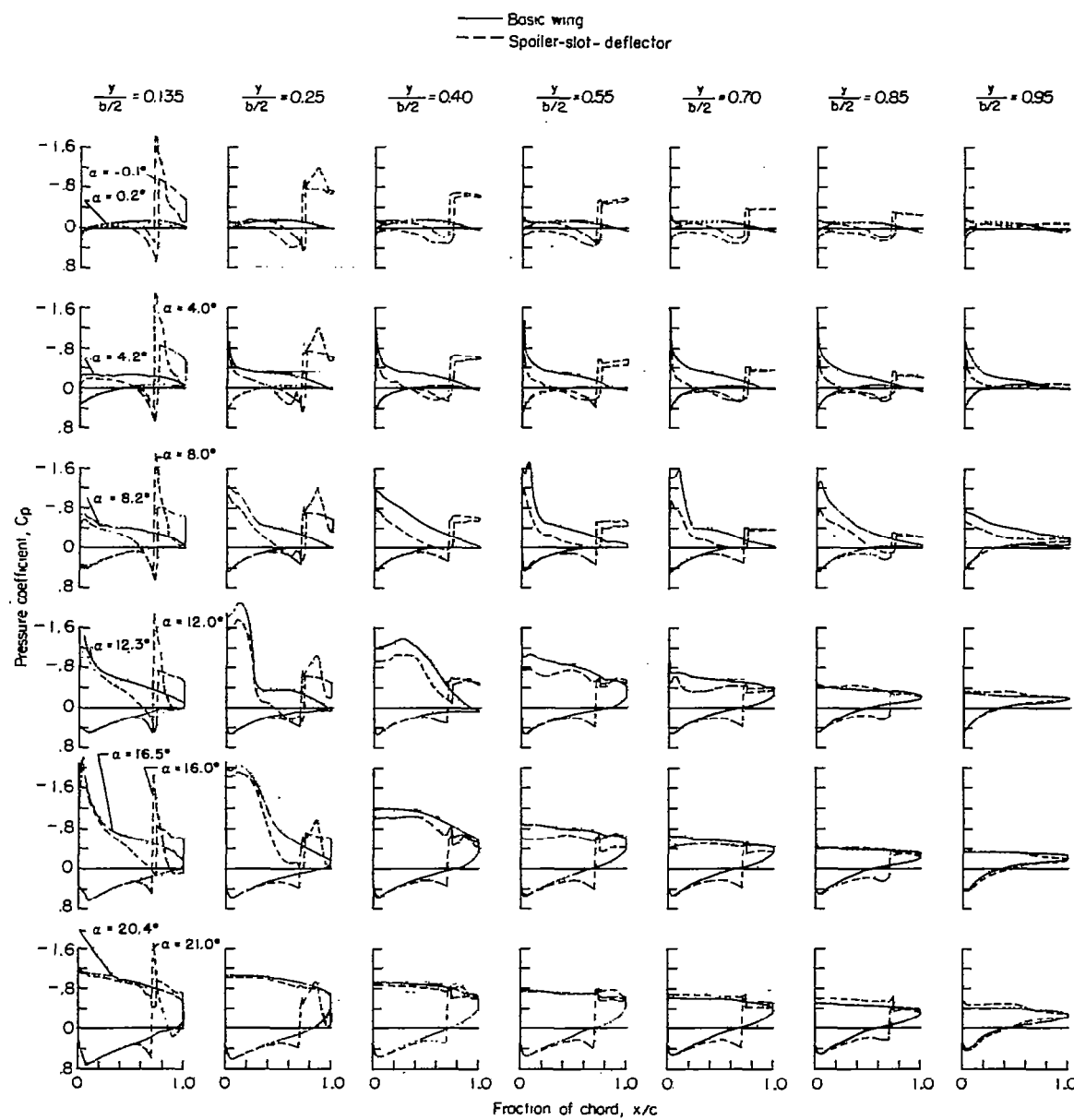
(a)  $M = 0.60.$ 

Figure 7.- Wing chordwise pressure distributions for the basic model and a spoiler-slot-deflector aileron configuration.

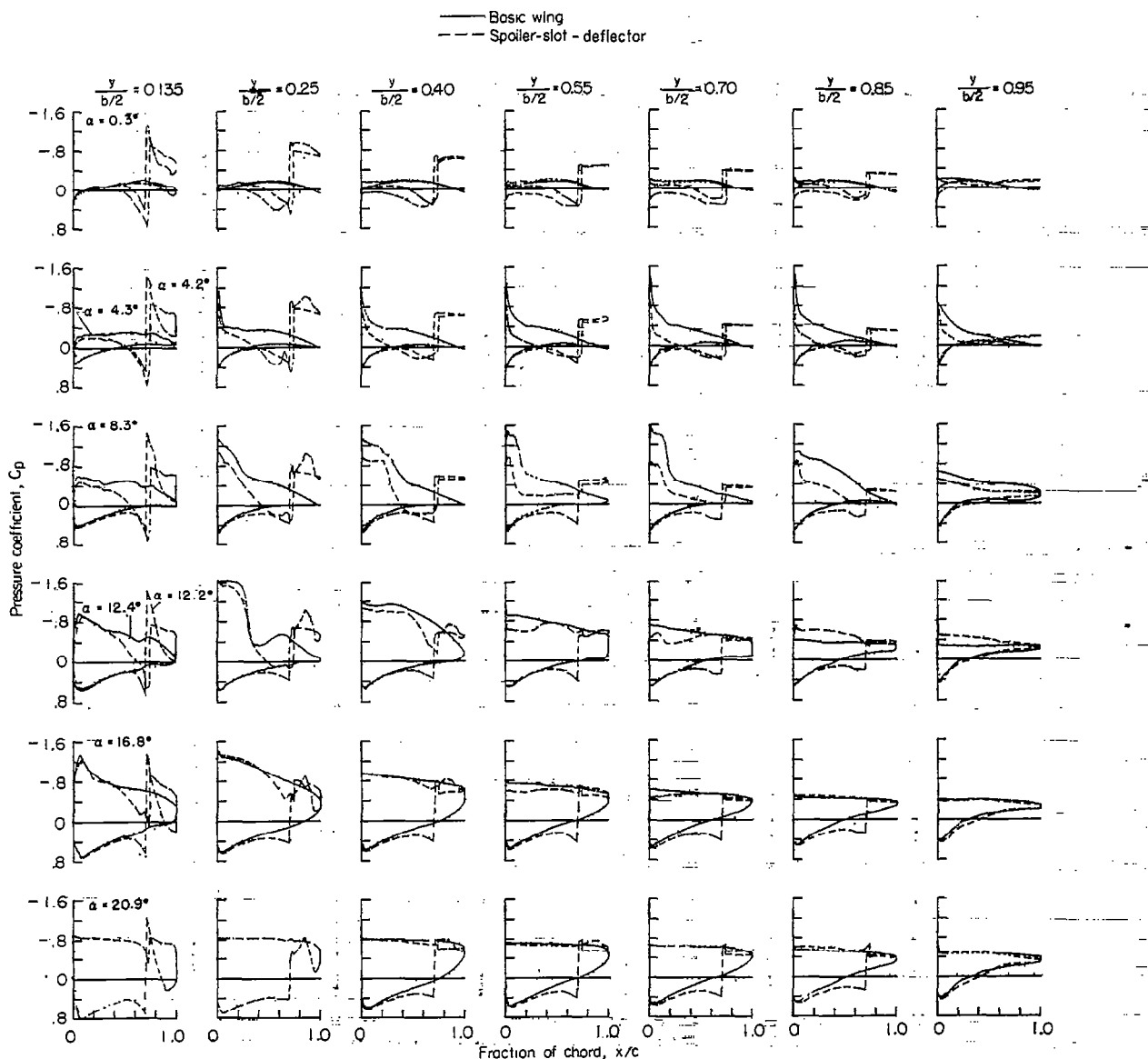
(b)  $M = 0.80$ .

Figure 7.- Continued.

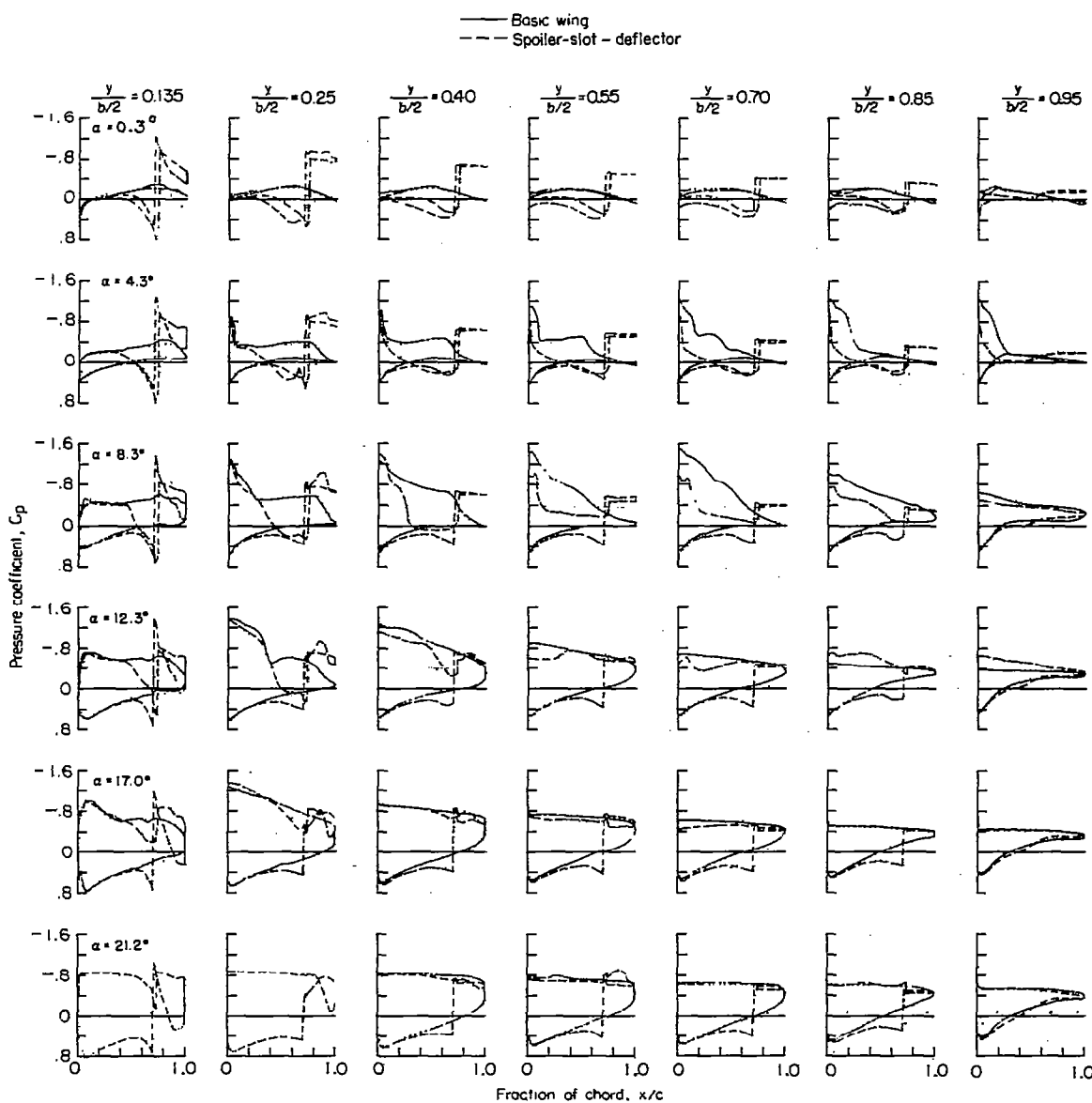
(c)  $M = 0.90.$ 

Figure 7.- Continued.

CONFIDENTIAL

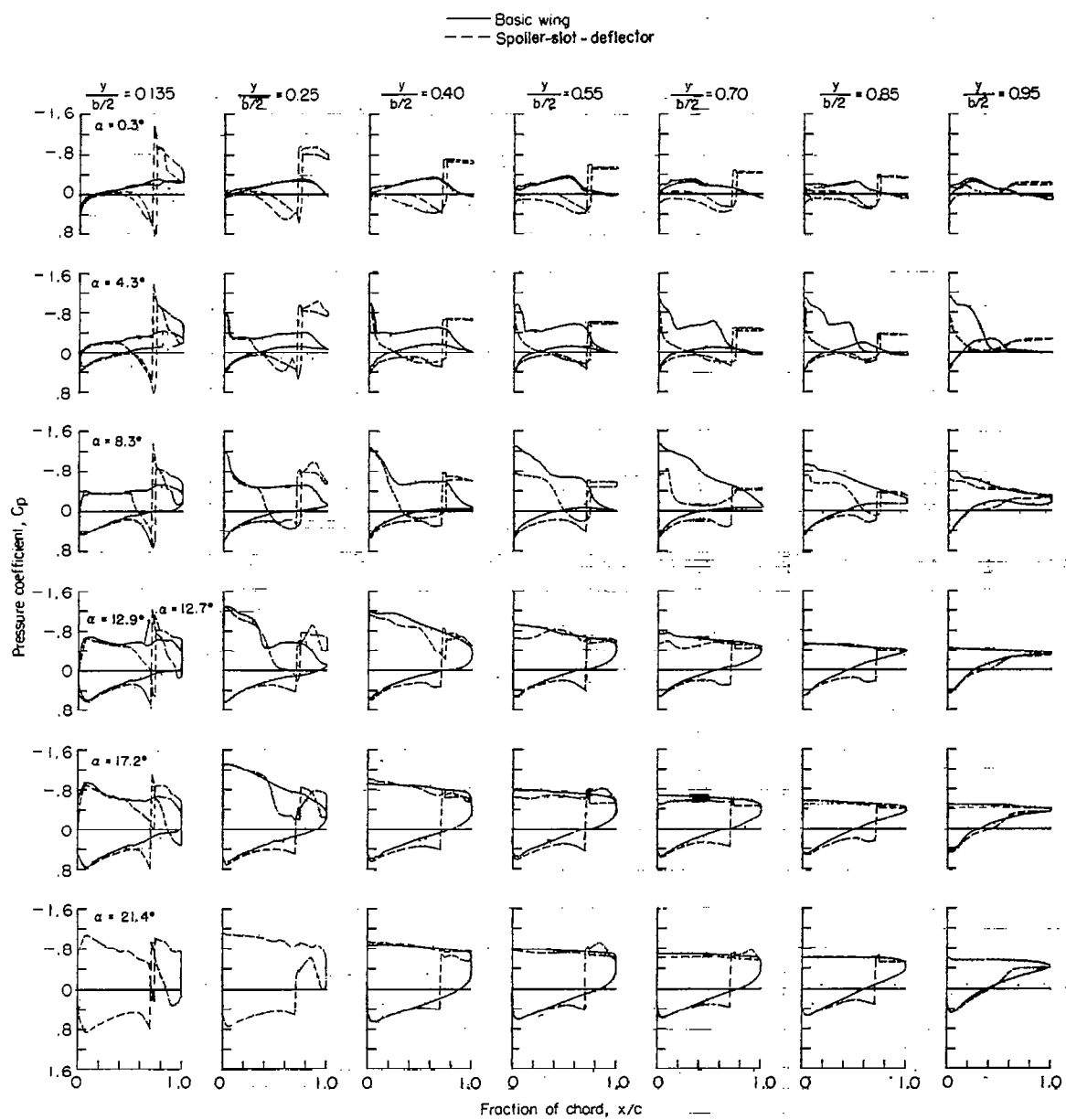
(d)  $M = 0.94$ .

Figure 7.- Continued.

CONFIDENTIAL

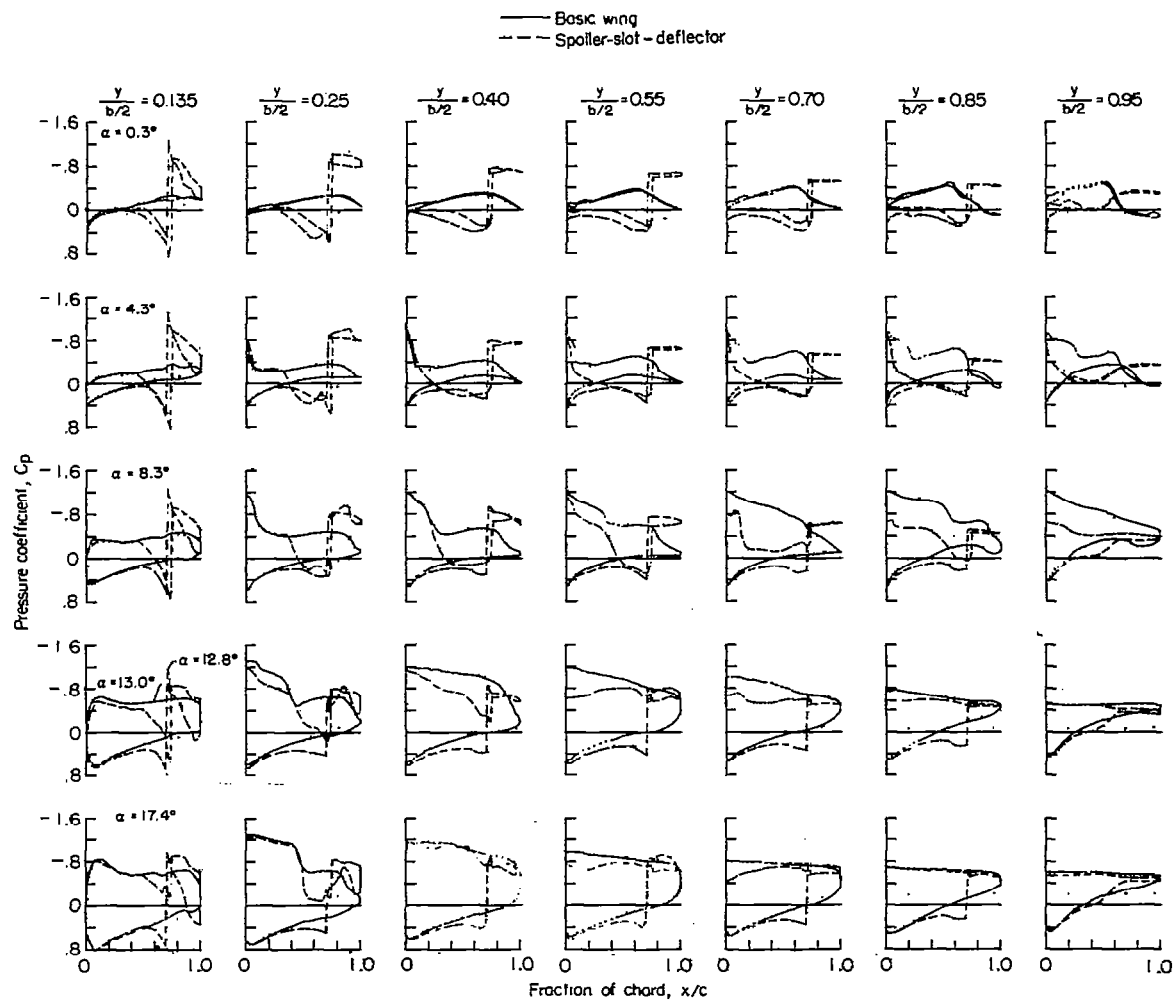
(e)  $M = 0.98$ .

Figure 7.- Continued.

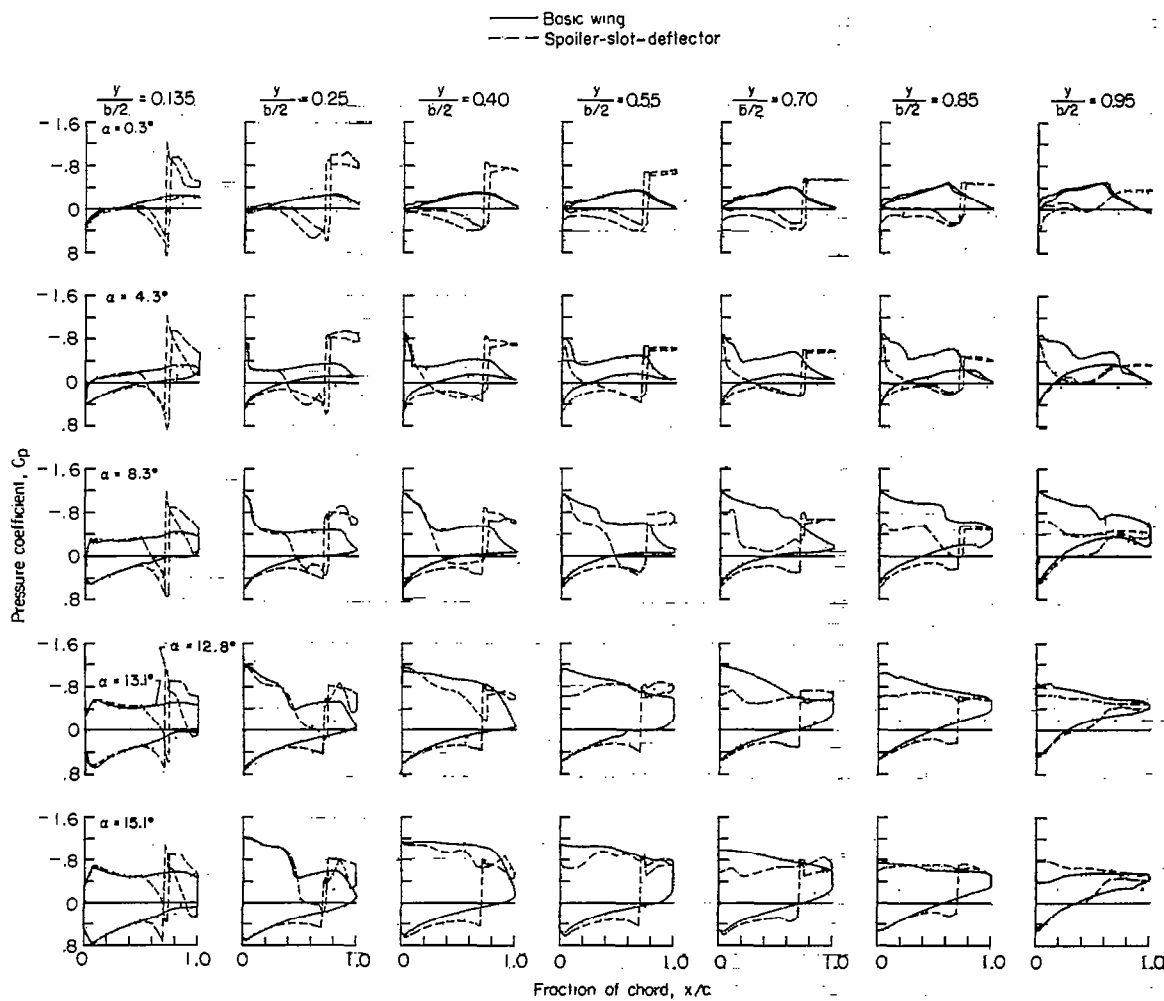
(f)  $M = 1.00$ .

Figure 7.- Continued.

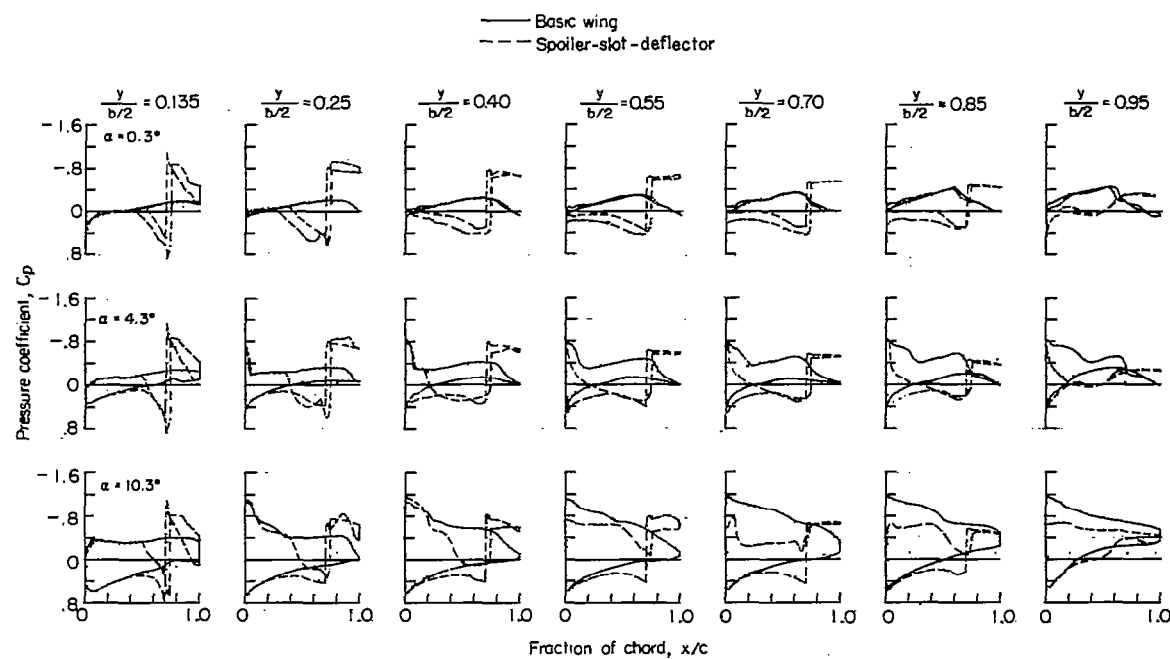
(g)  $M = 1.03$ .

Figure 7.- Concluded.

~~CONFIDENTIAL~~

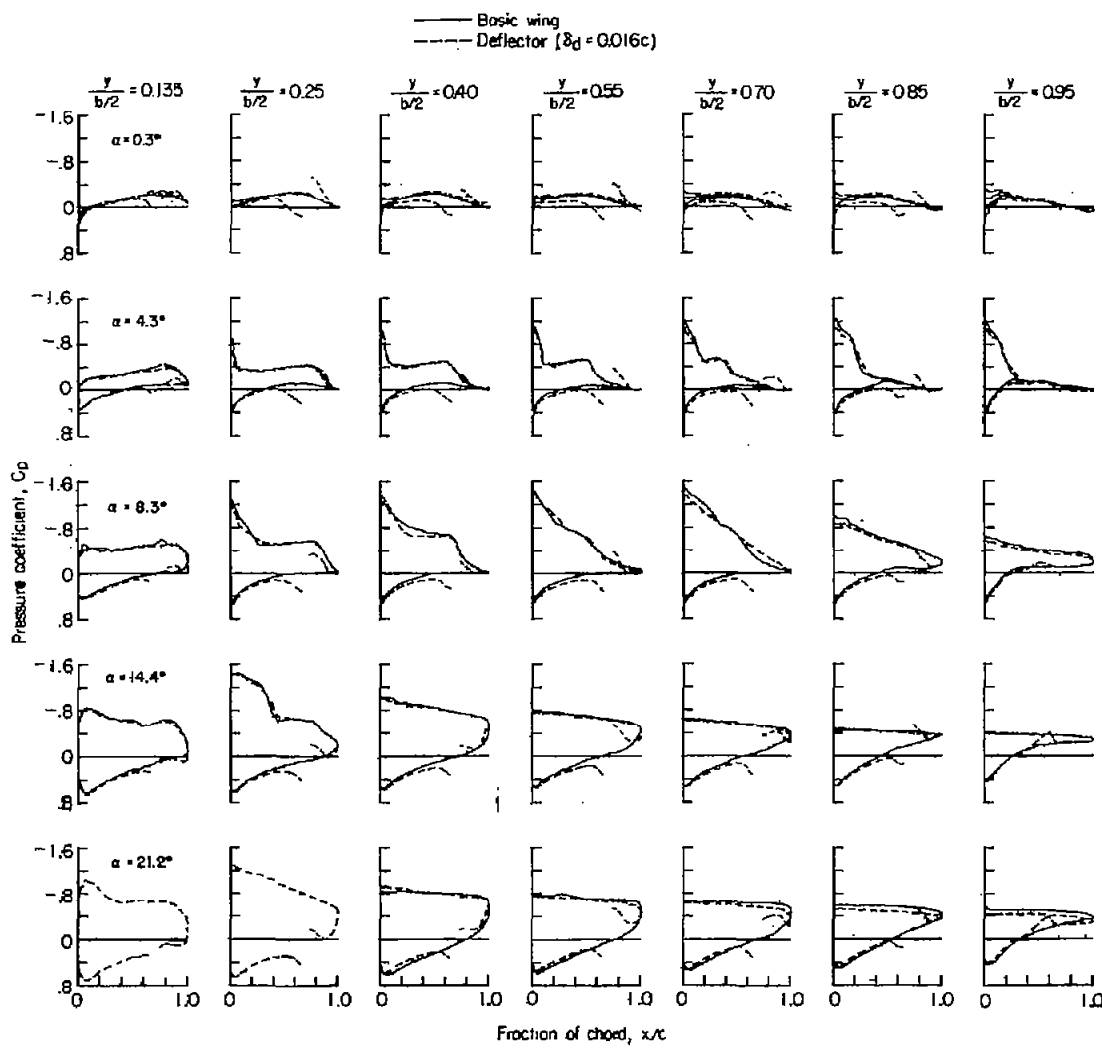


Figure 8.- Wing chordwise pressure distributions for the basic model and a deflector ( $\delta_d = 0.016c$ ) aileron configuration at a Mach number of 0.90.

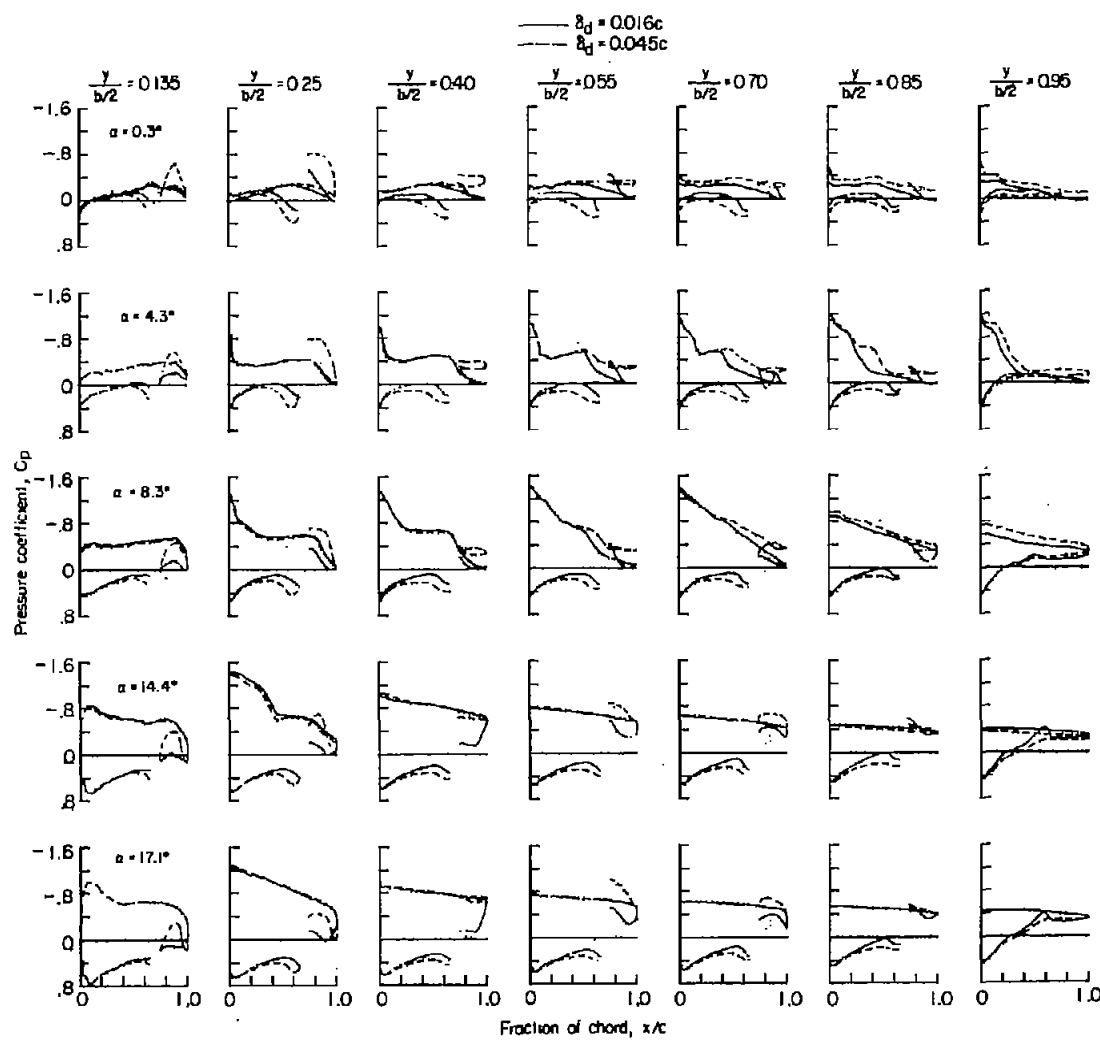
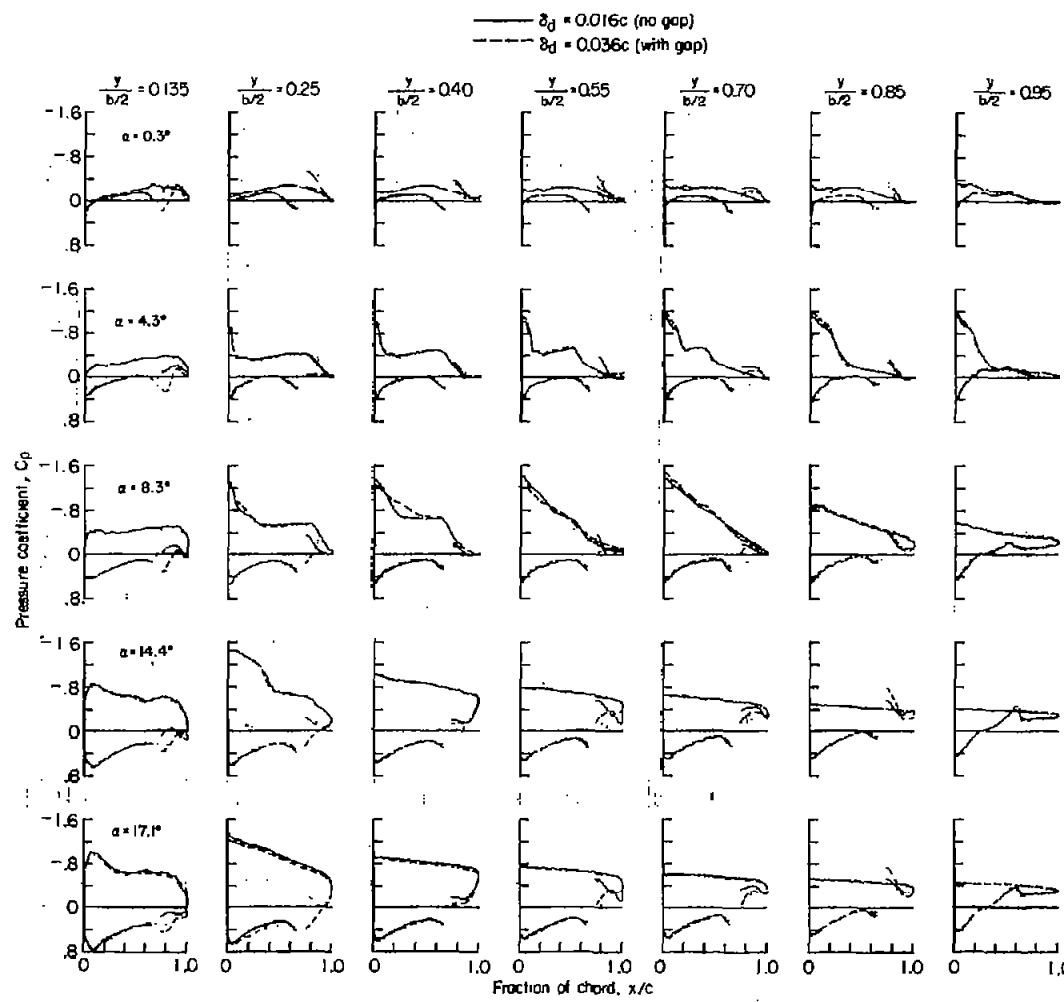


Figure 9.- Wing chordwise pressure distributions showing the effect of changing projection of a deflector aileron from  $0.016c$  to  $0.045c$  at a Mach number of 0.90.



(a)  $\delta_d = 0.016c$  (no gap);  $\delta_d = 0.036c$  (with gap).

Figure 10.- Wing chordwise pressure distributions showing the effect of a  $0.02c$  gap between a deflector aileron and the wing at a Mach number of 0.90.

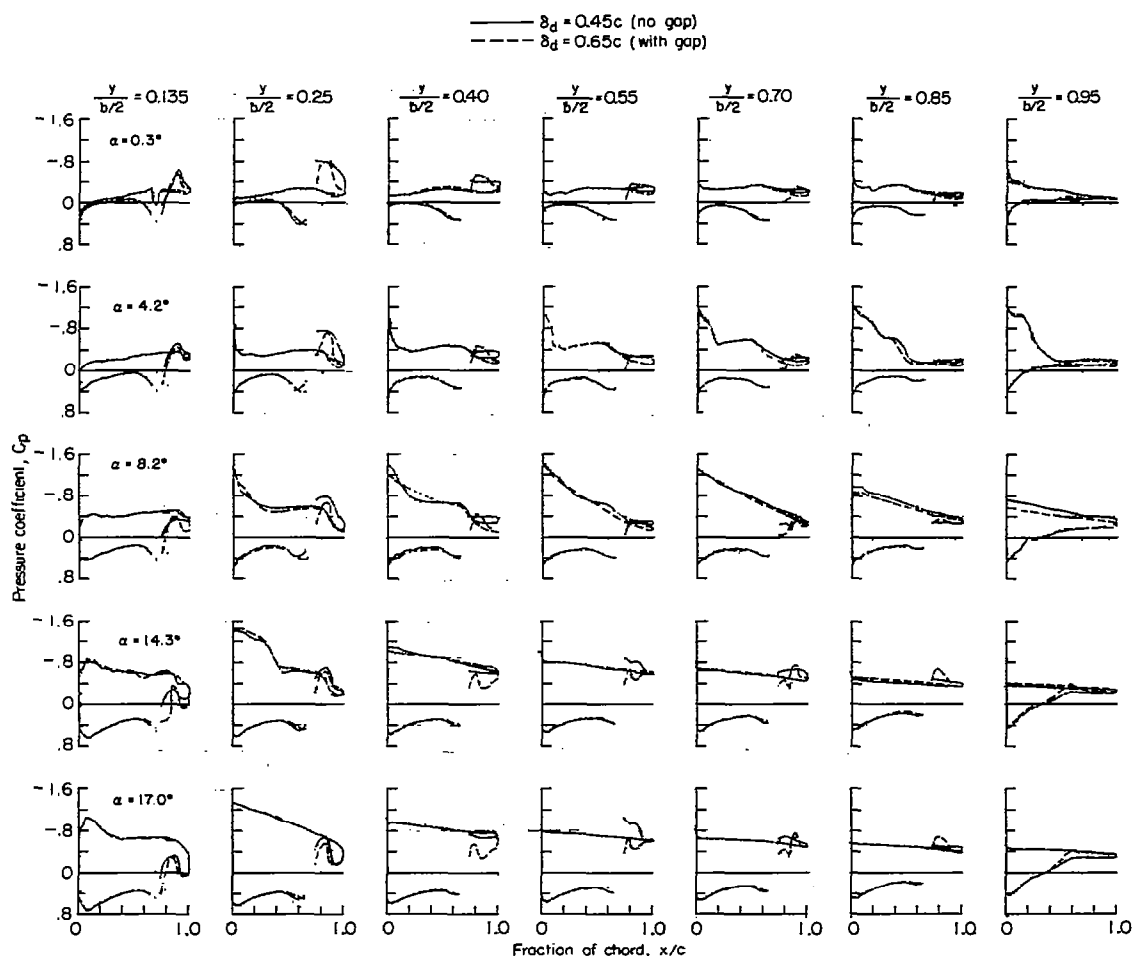
(b)  $\delta_d = 0.45c$  (no gap);  $\delta_d = 0.65c$  (with gap).

Figure 10.- Concluded.

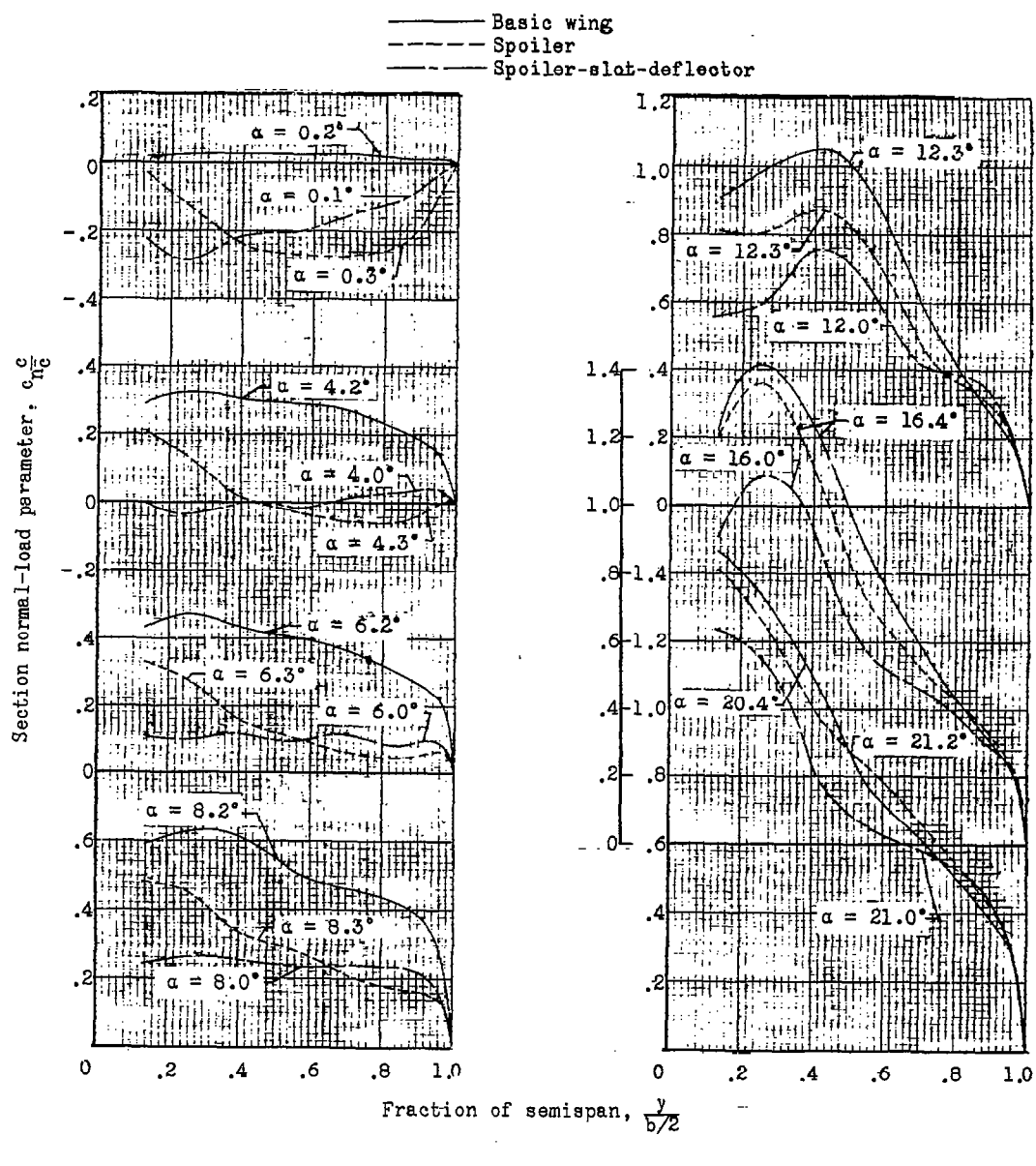


Figure 11.- Wing semispan load distributions for the basic model, a spoiler aileron configuration, and a spoiler-slot-deflector aileron configuration.

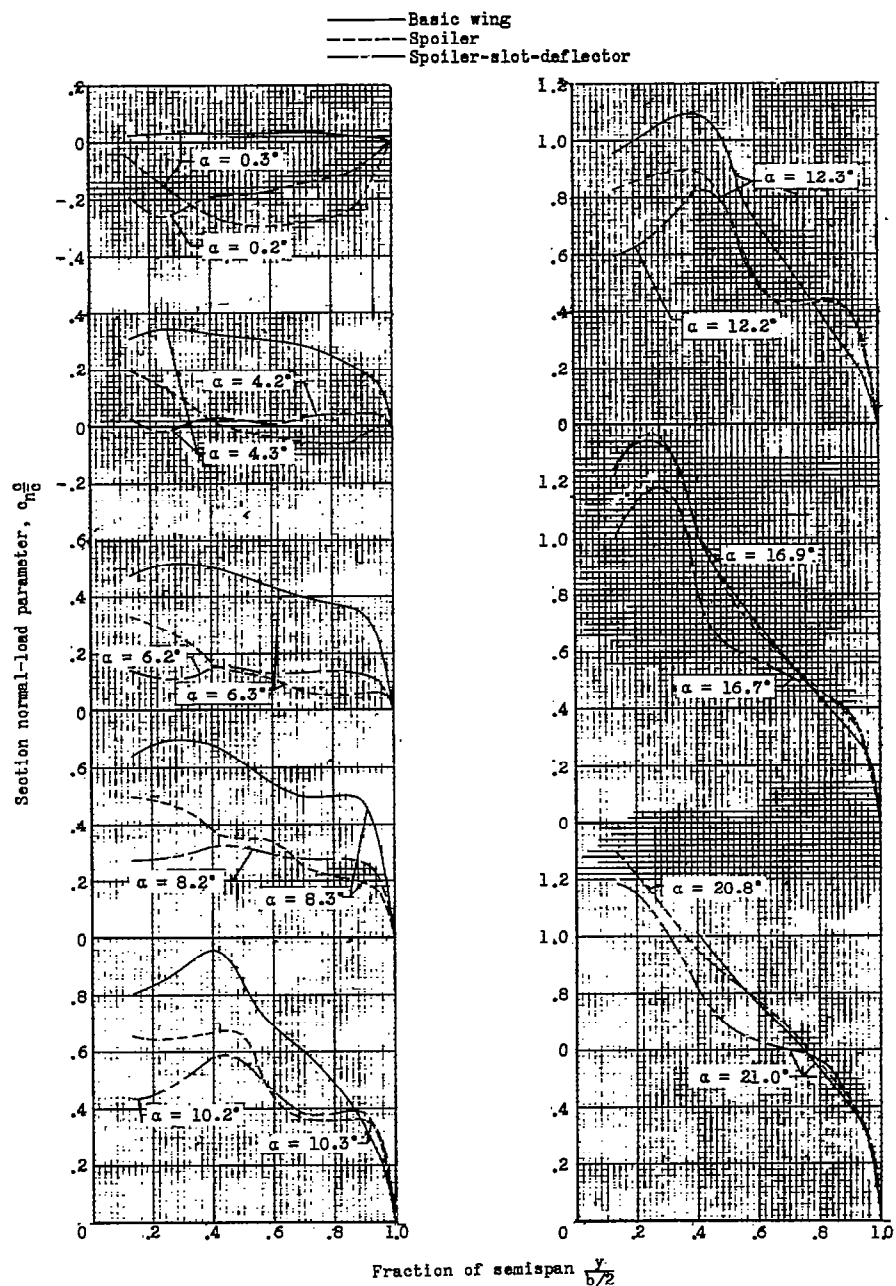
(b)  $M = 0.80$ .

Figure 11.- Continued.

CONFIDENTIAL

NACA RM L57J11

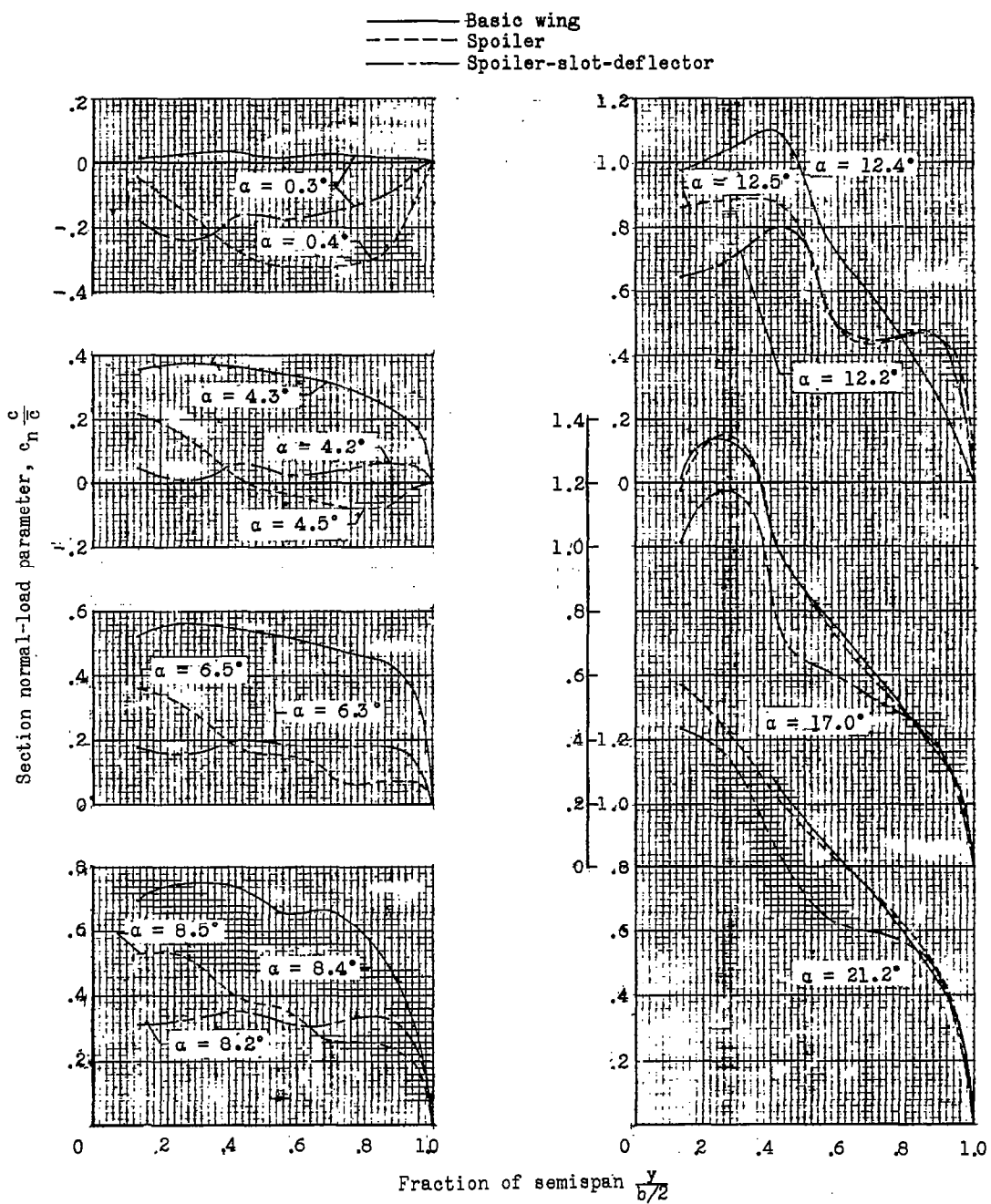
(c)  $M = 0.90$ .

Figure 11.- Continued.

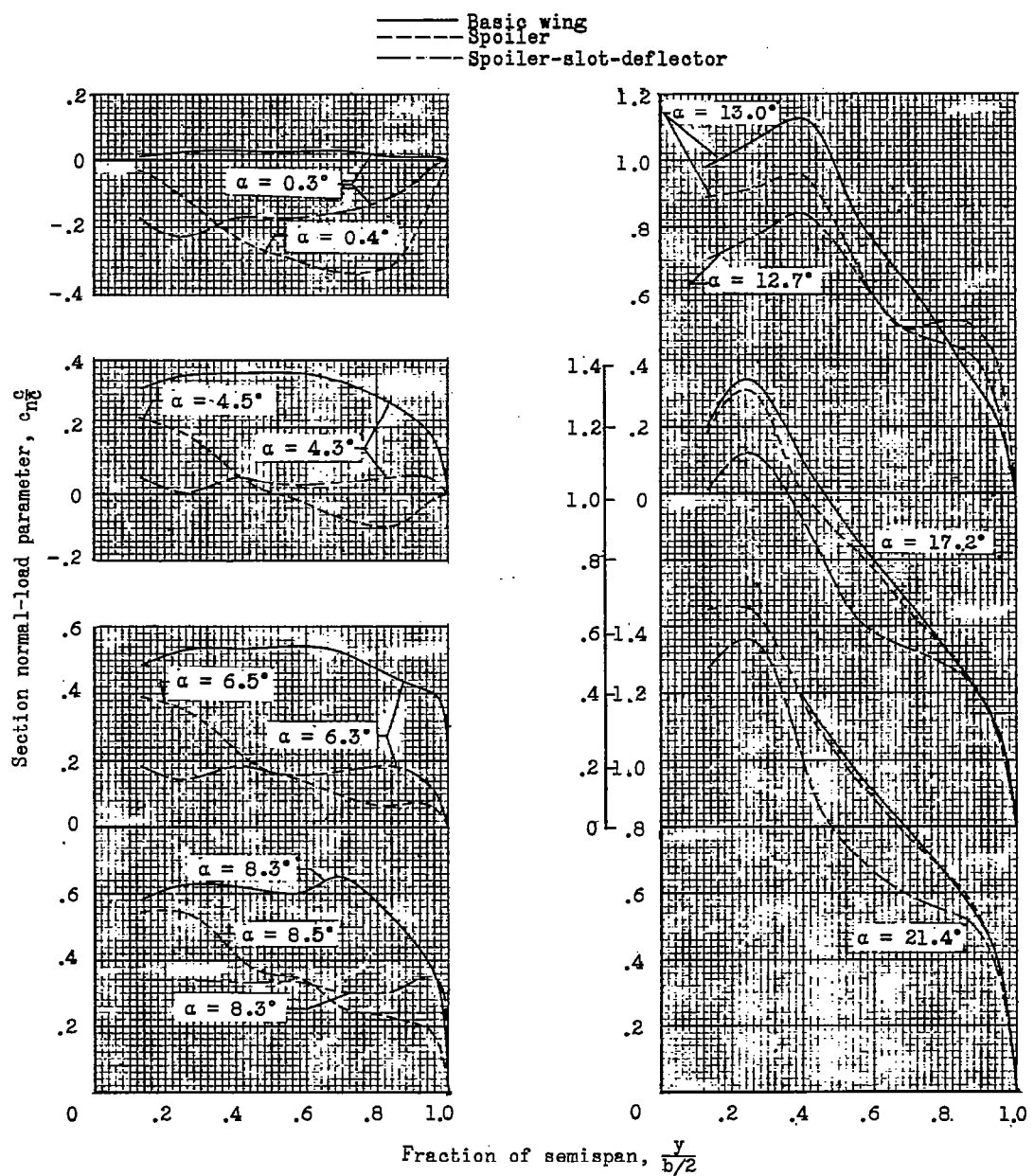
(d)  $M = 0.94$ .

Figure 11.- Continued.

CONFIDENTIAL

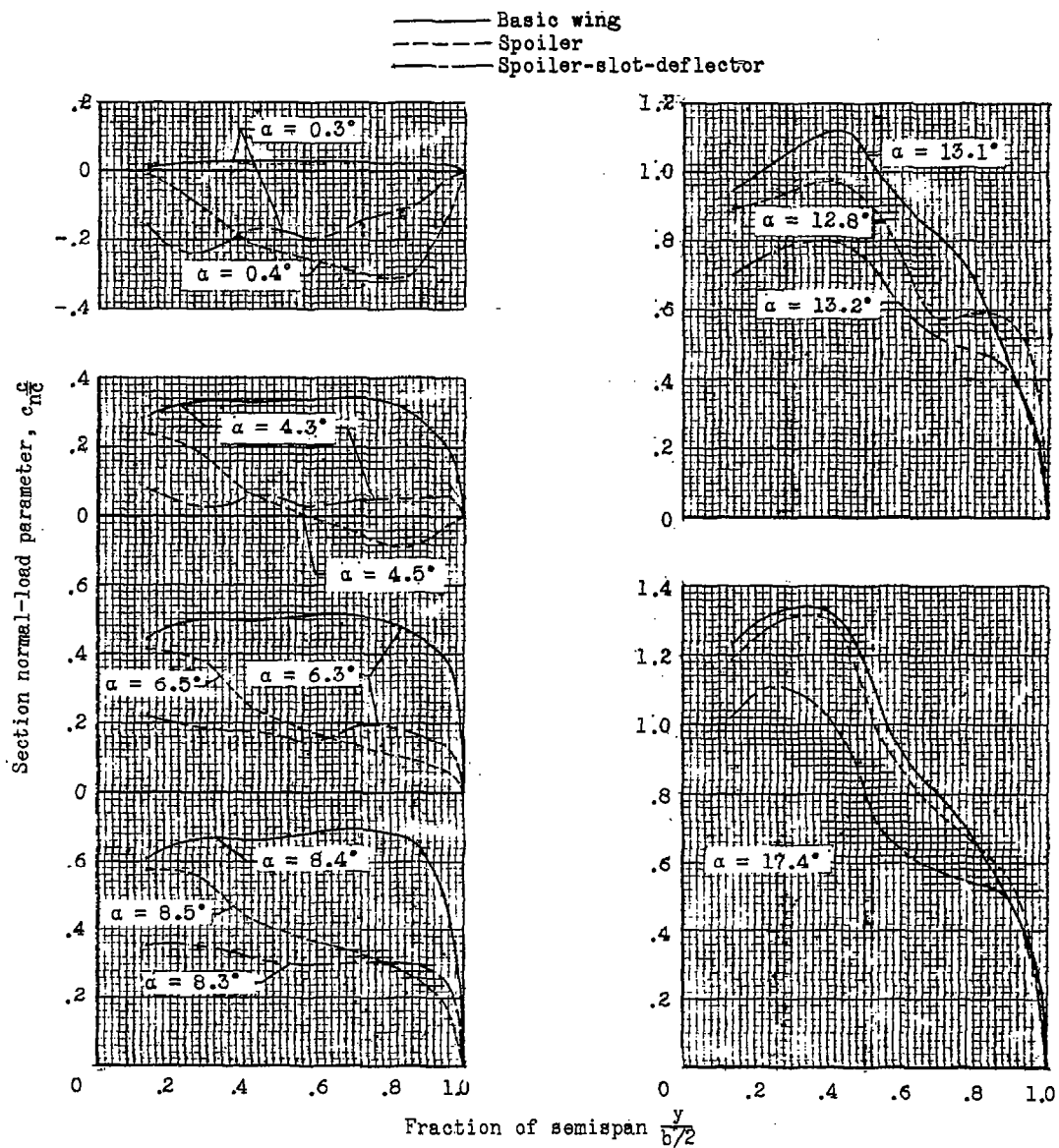
(e)  $M = 0.98$ .

Figure 11.- Continued.

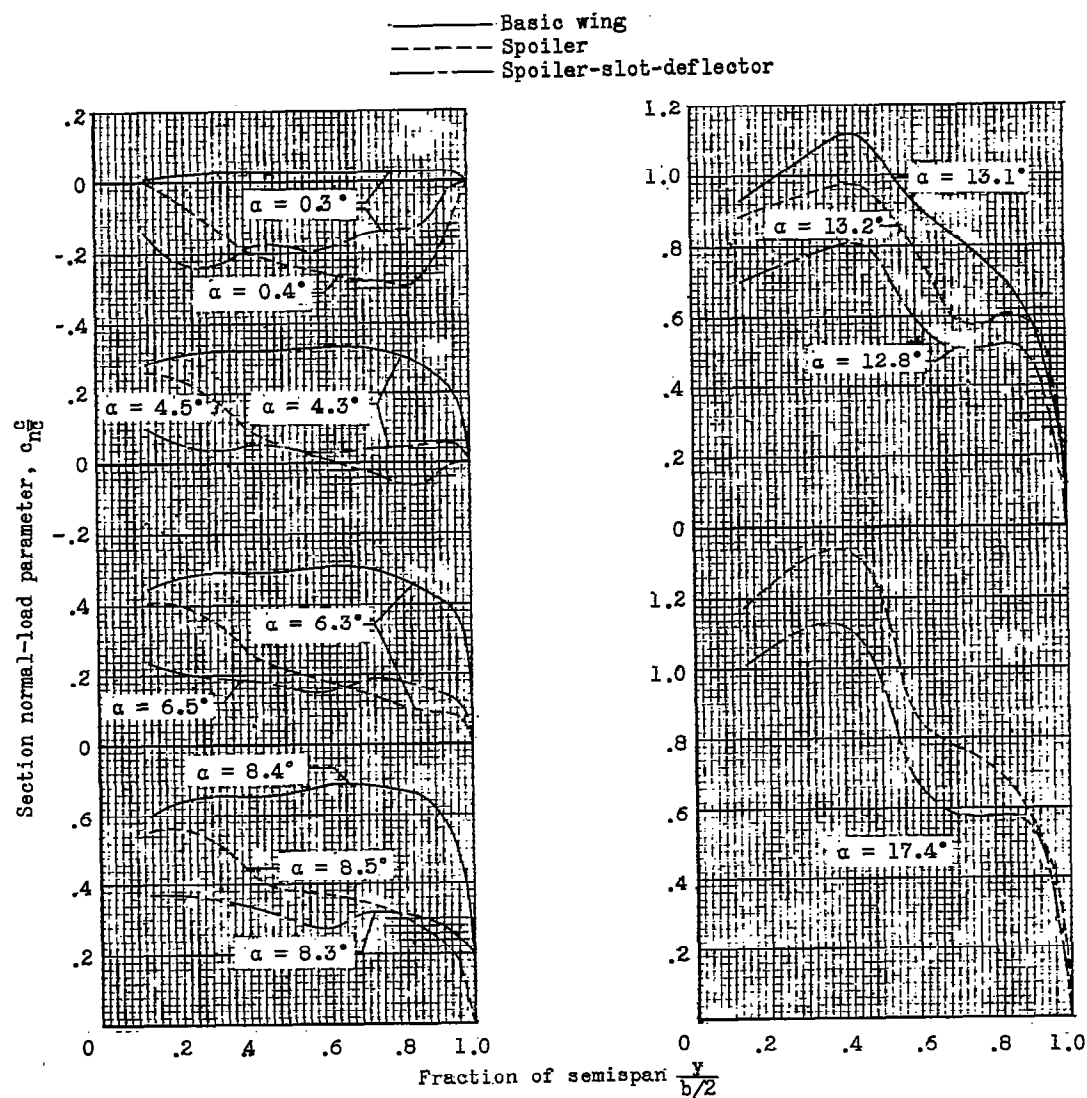
(f)  $M = 1.00$ 

Figure 11.- Continued.

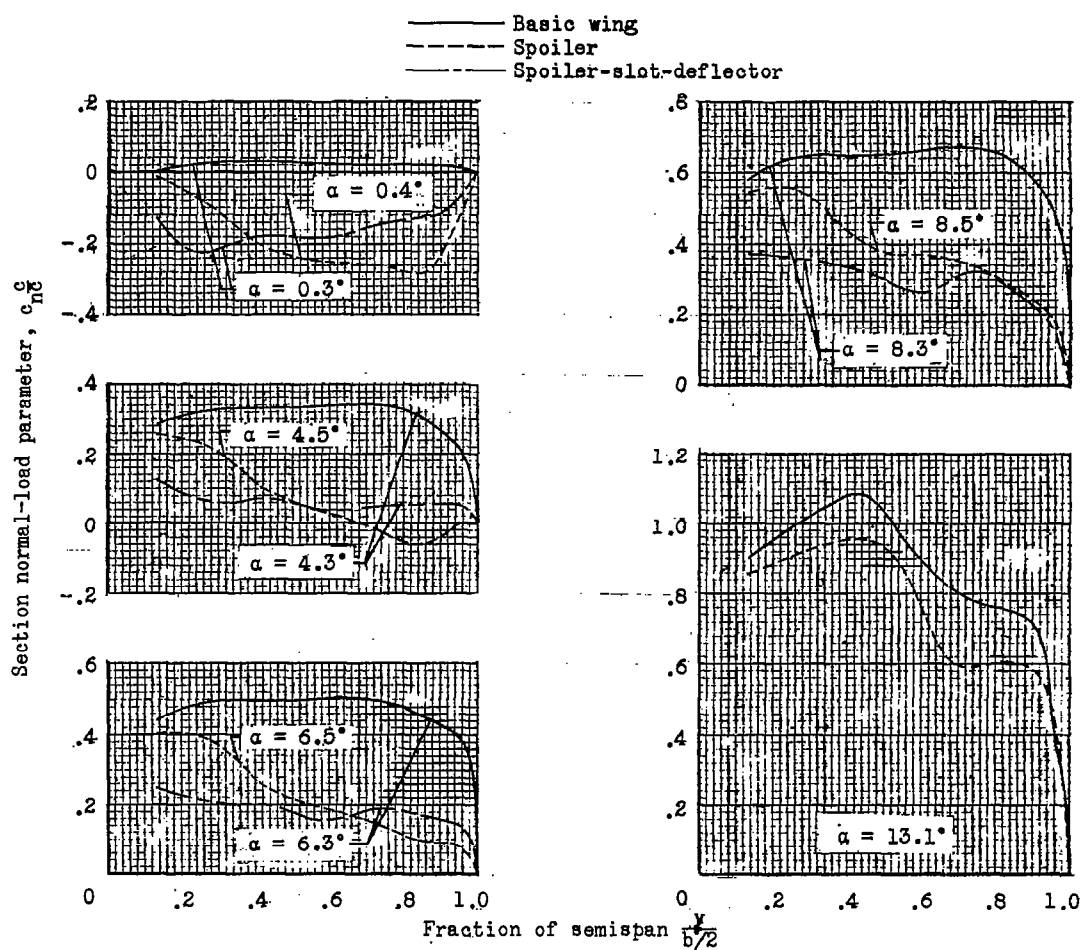
(g)  $M = 1.03$ .

Figure 11.- Concluded.

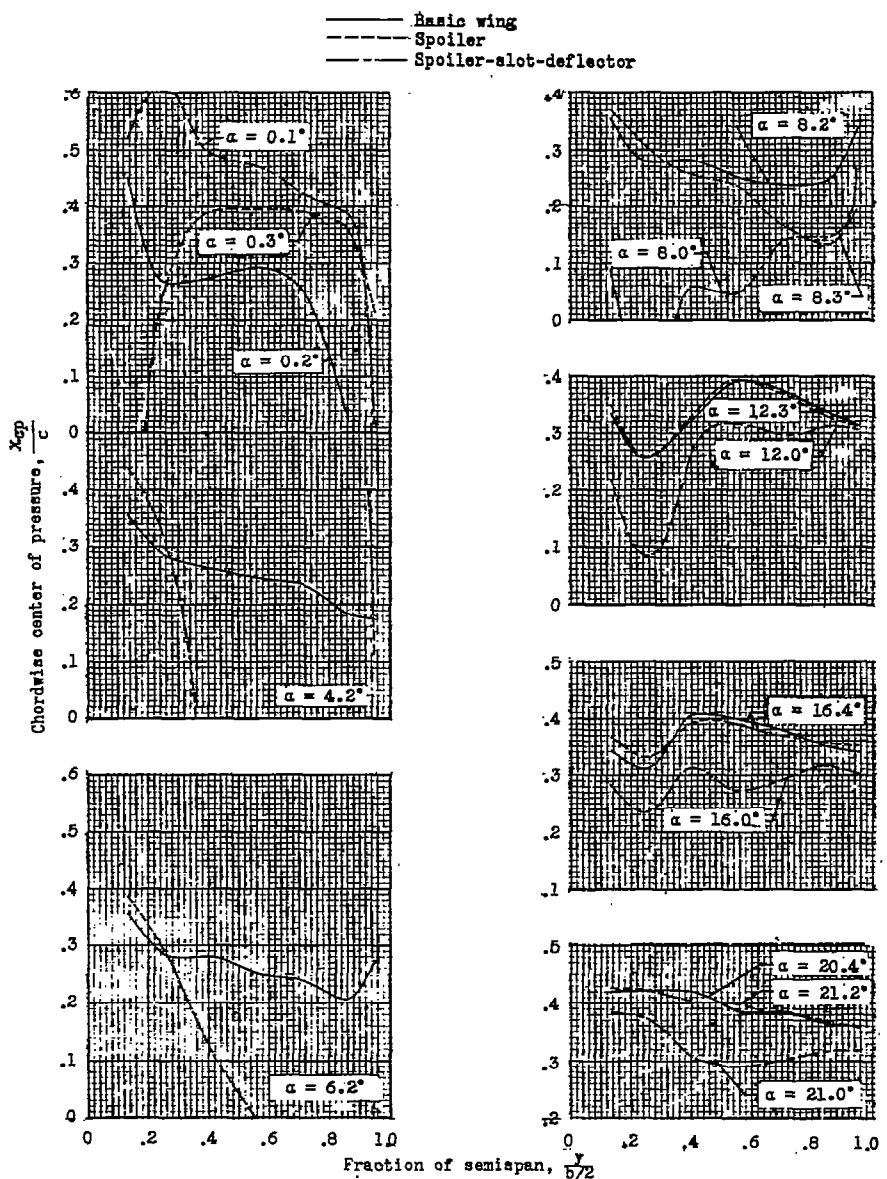
(a)  $M = 0.60$ .

Figure 12.- Wing section center of pressure for the basic model, a spoiler aileron configuration, and a spoiler-slot-deflector aileron configuration.

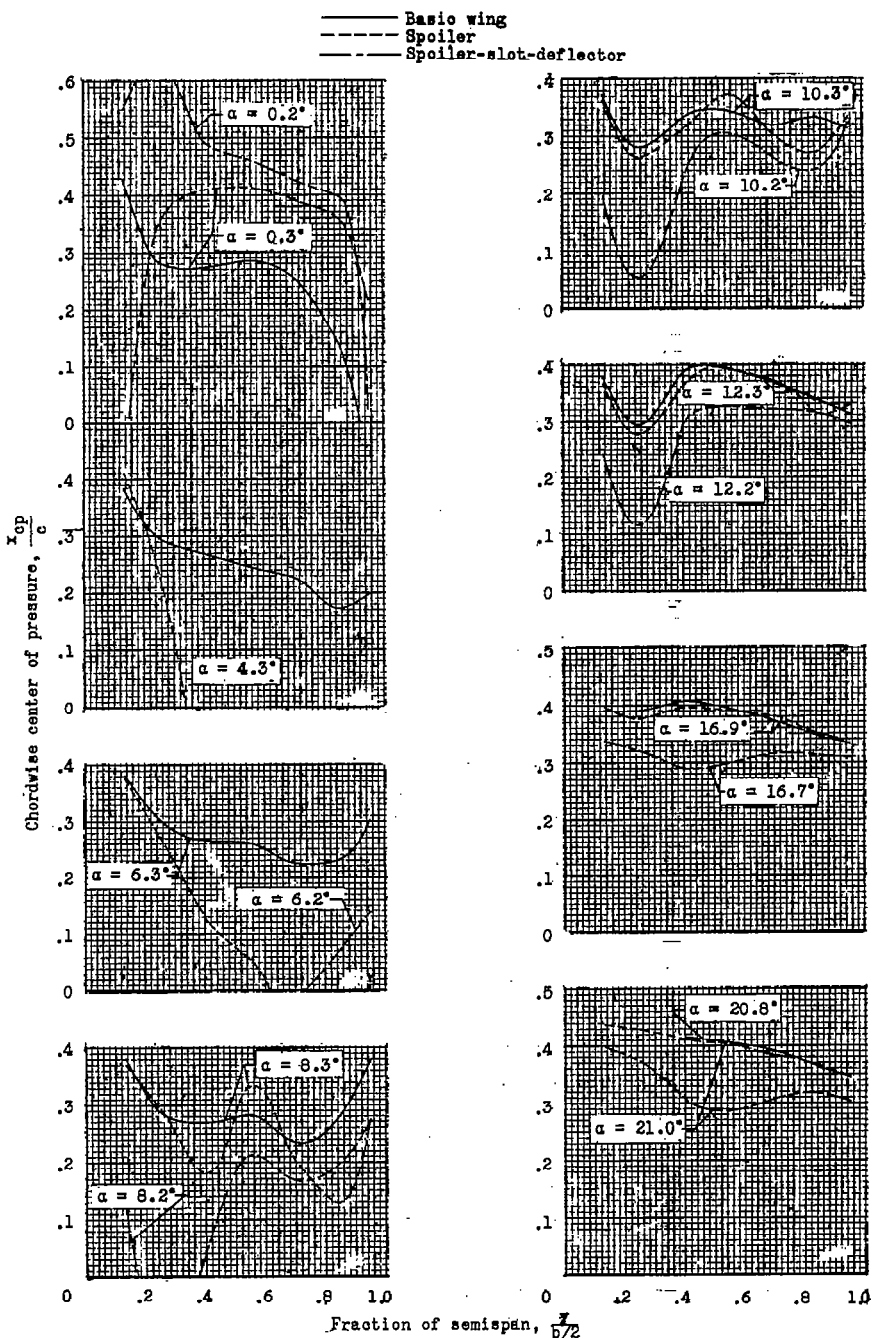
(b)  $M = 0.80$ .

Figure 12.- Continued.

CONFIDENTIAL

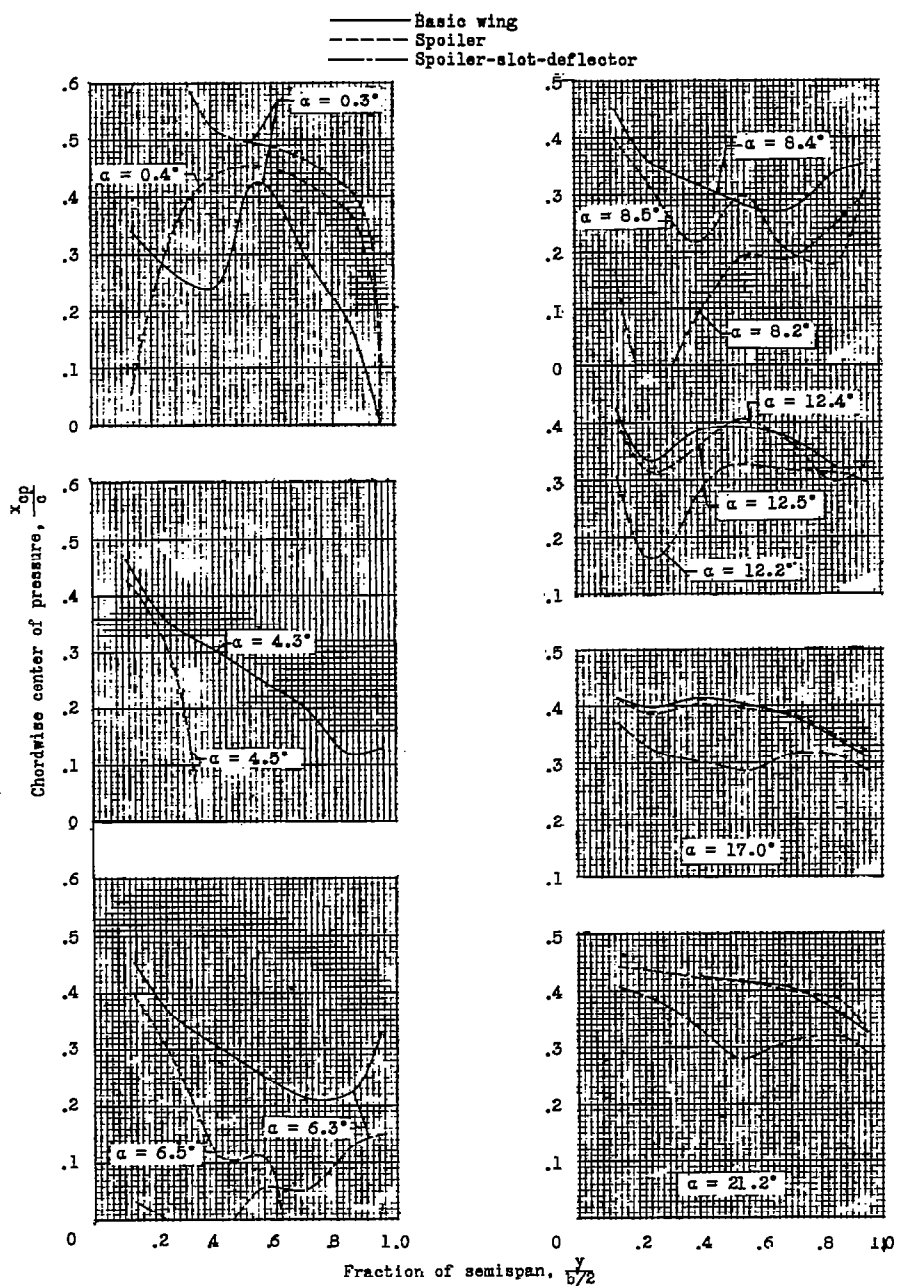
(c)  $M = 0.90$ .

Figure 12.- Continued.

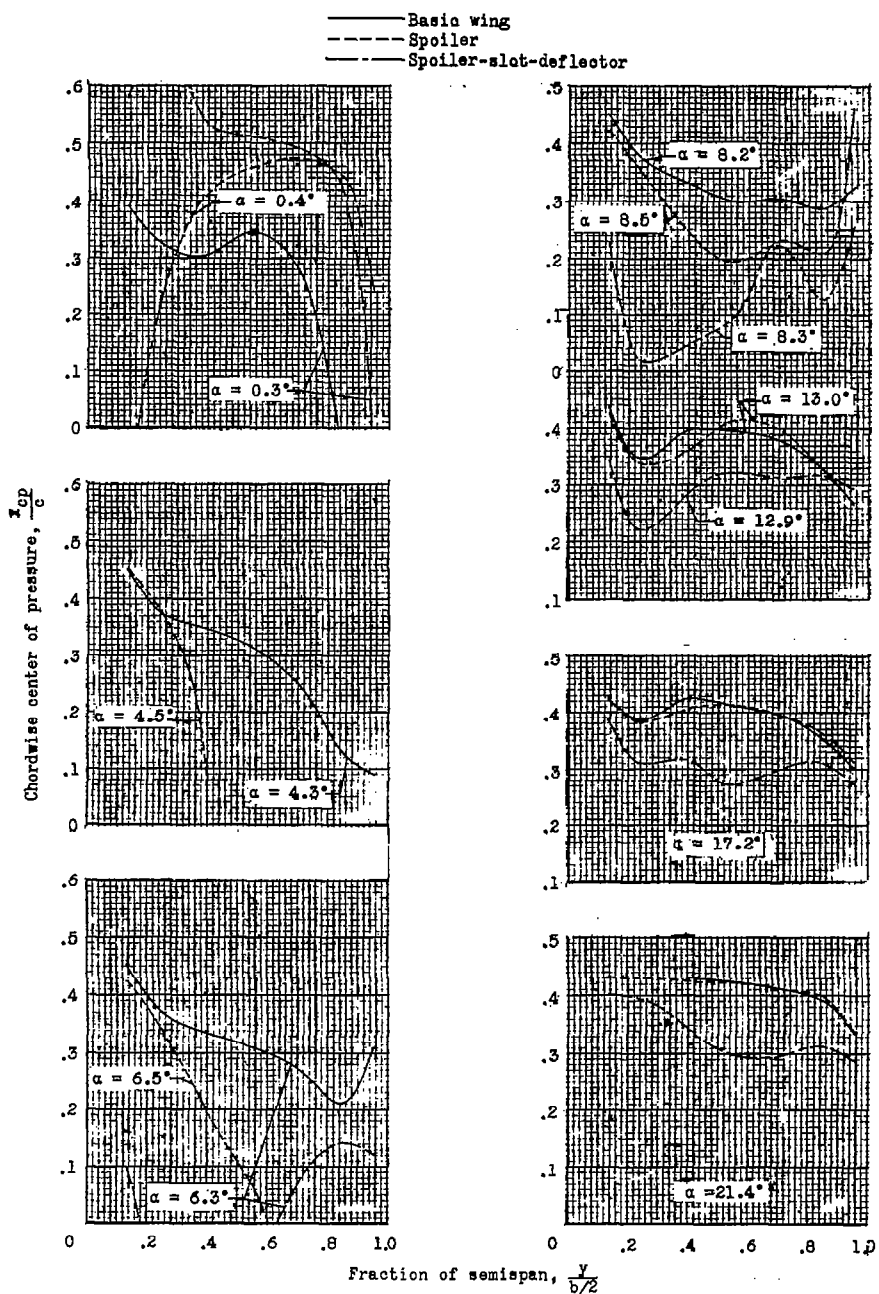
(d)  $M = 0.94$ .

Figure 12.- Continued.

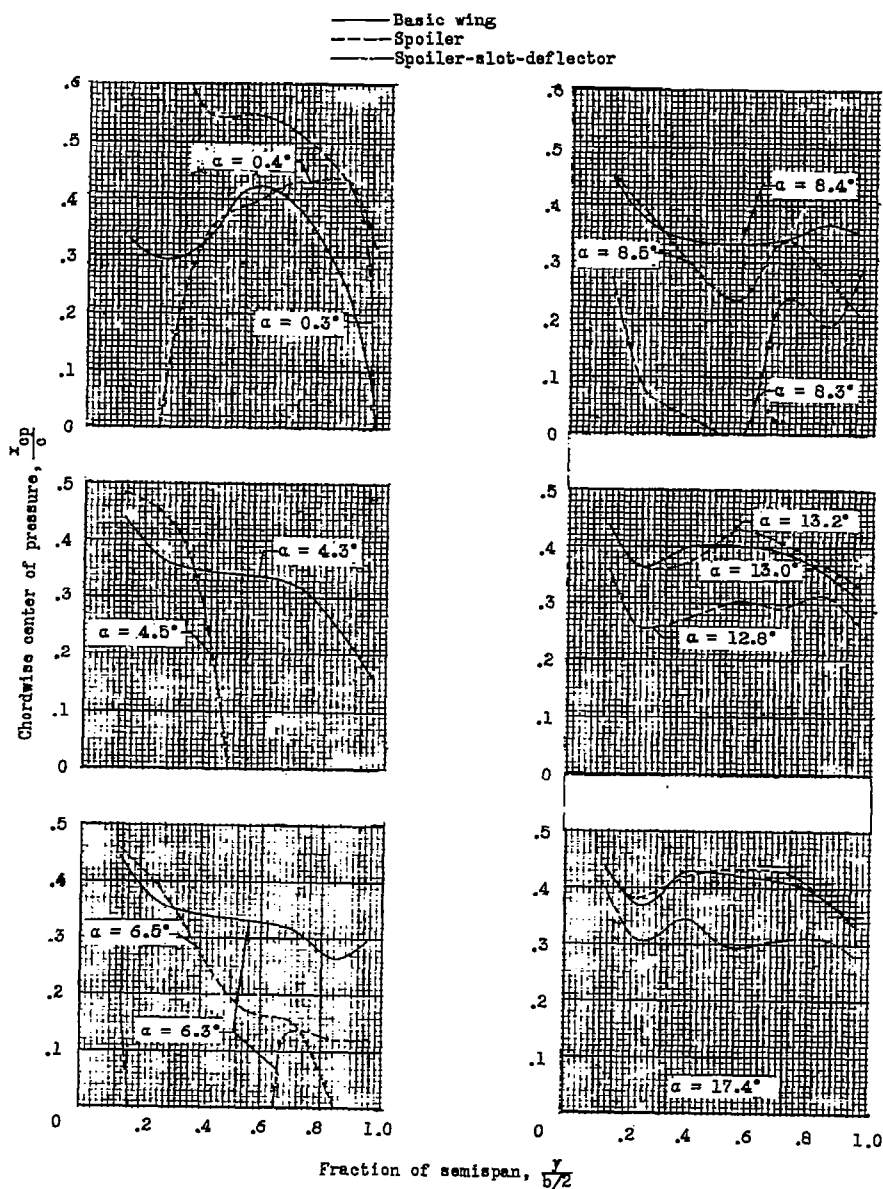
(e)  $M = 0.98$ .

Figure 12.- Continued.

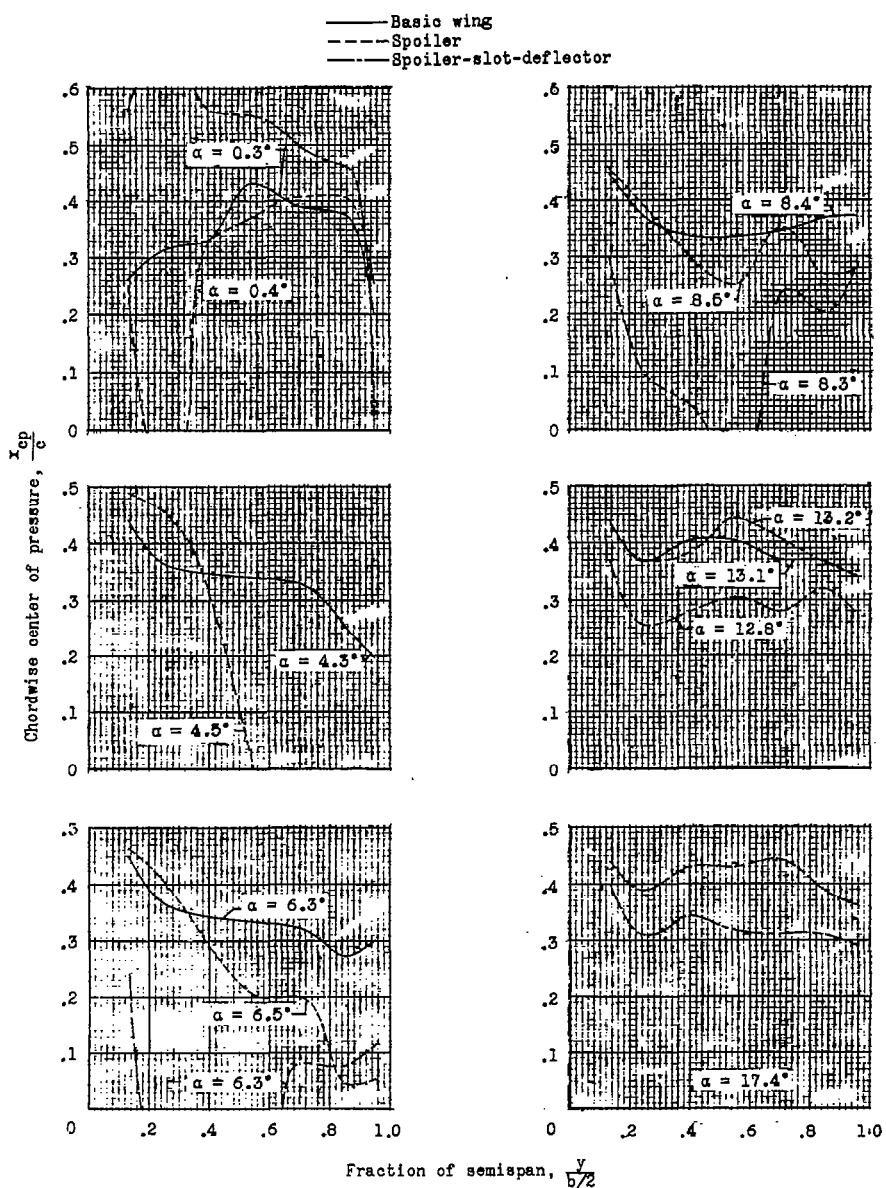
(f)  $M = 1.00$ .

Figure 12.- Continued.

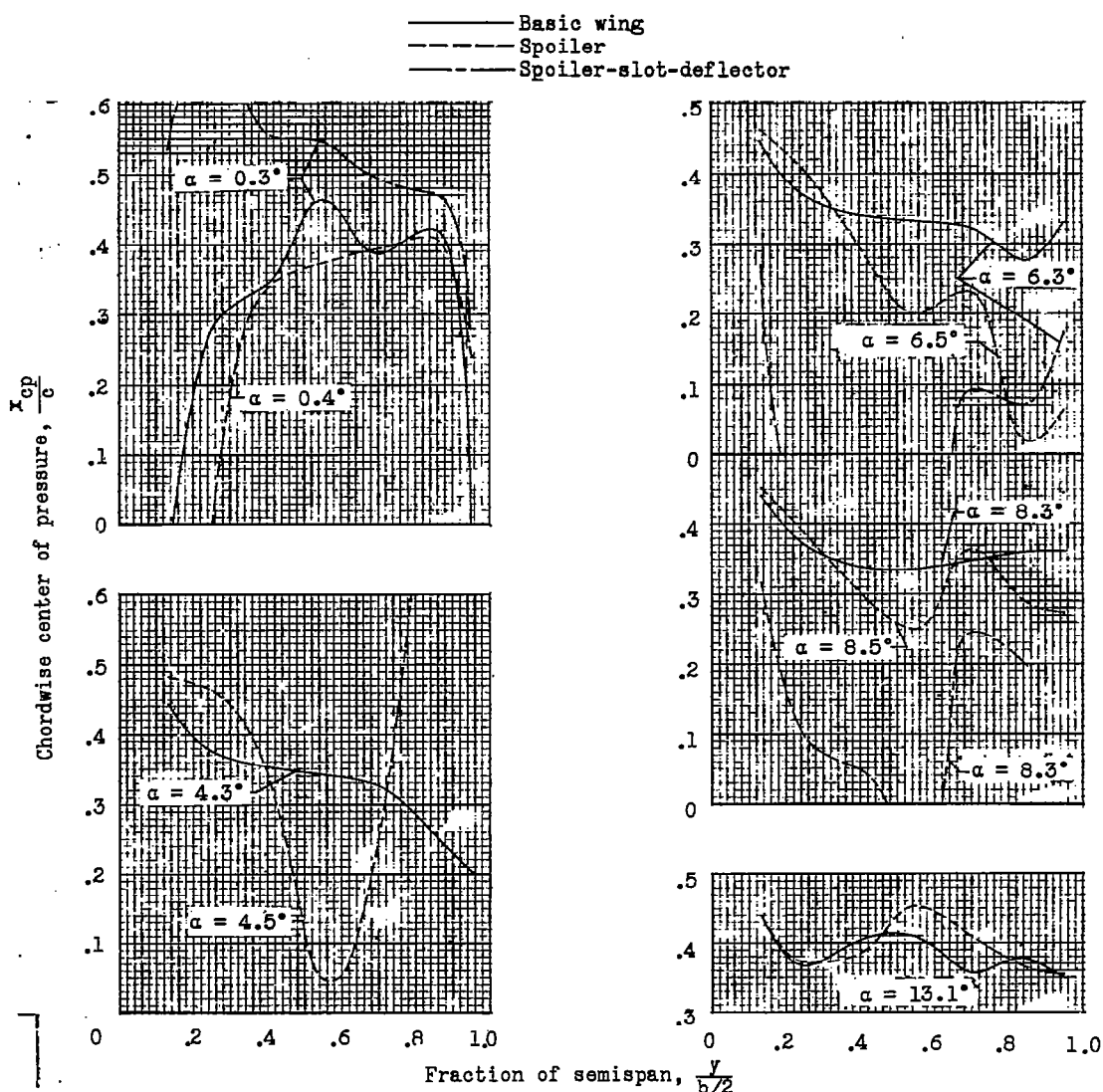
(g)  $M = 1.03$ .

Figure 12.- Concluded.

**NACA – Digidocs**

**Document processing error**

Unreadable tiff image

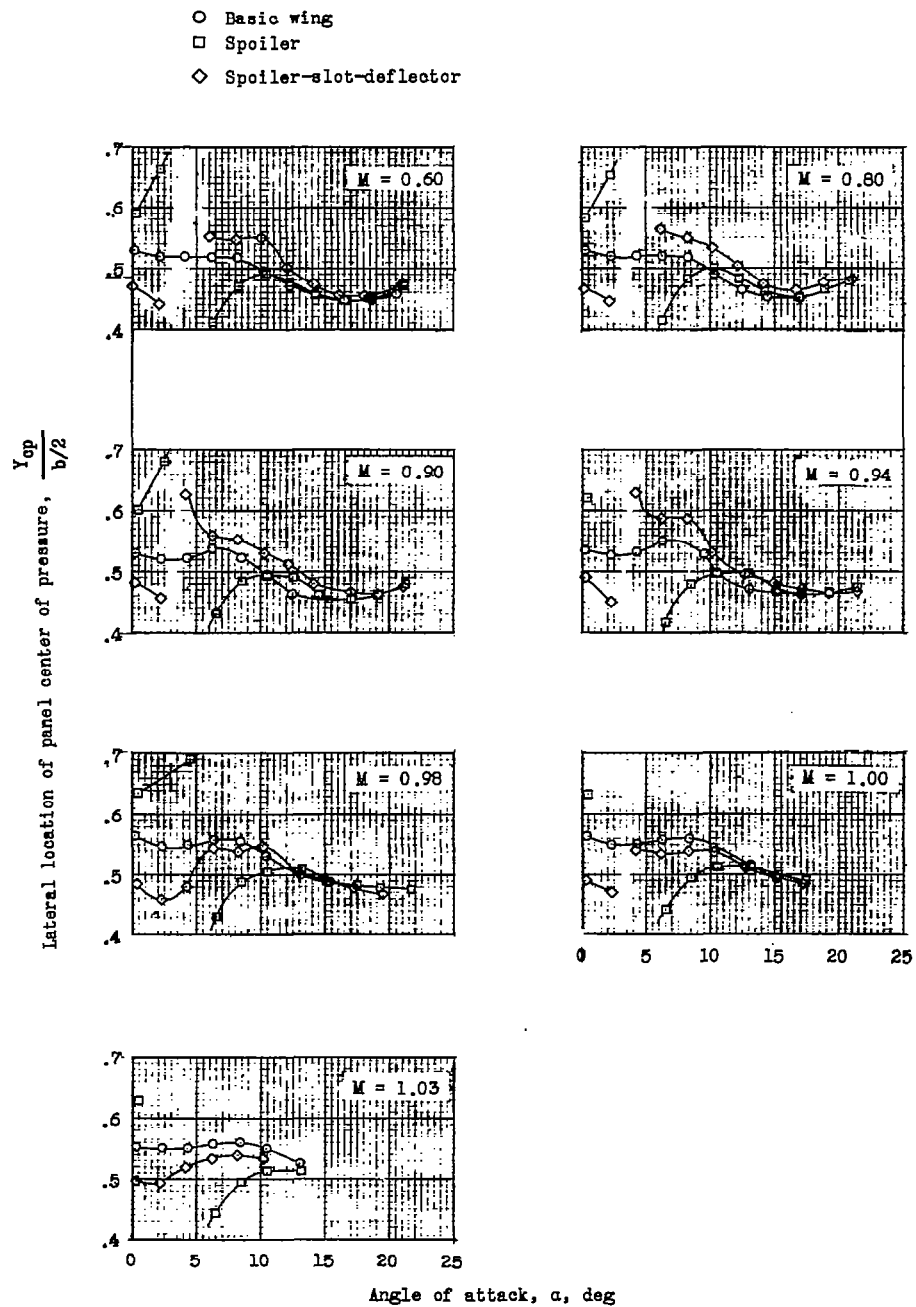


Figure 14.- Lateral position of wing center of pressure for the basic model, a spoiler aileron configuration, and a spoiler-slot-deflector aileron configuration.

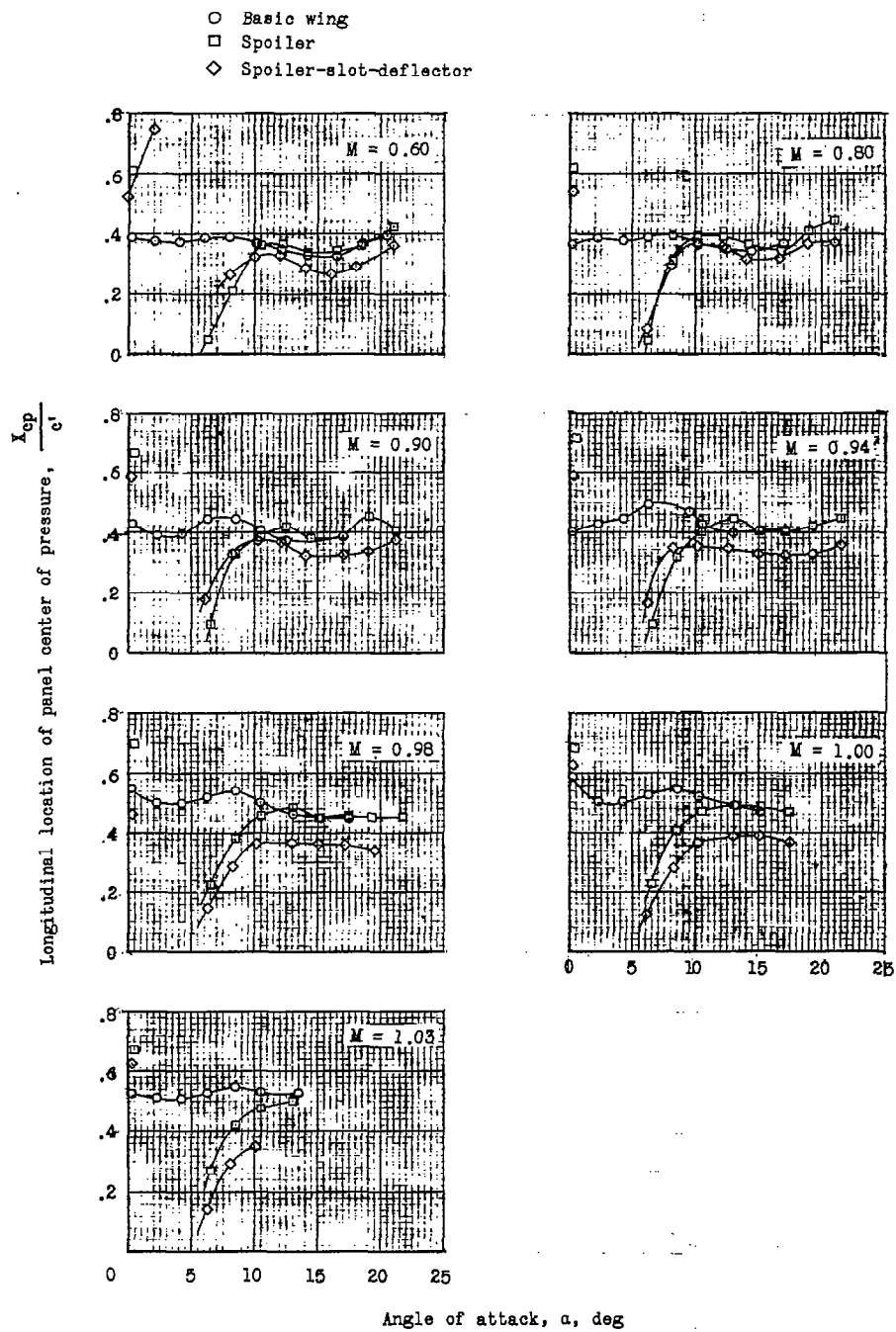


Figure 15.- Longitudinal position of wing center of pressure for the basic model, a spoiler aileron configuration, and a spoiler-slot-deflector aileron configuration.

~~CONFIDENTIAL~~

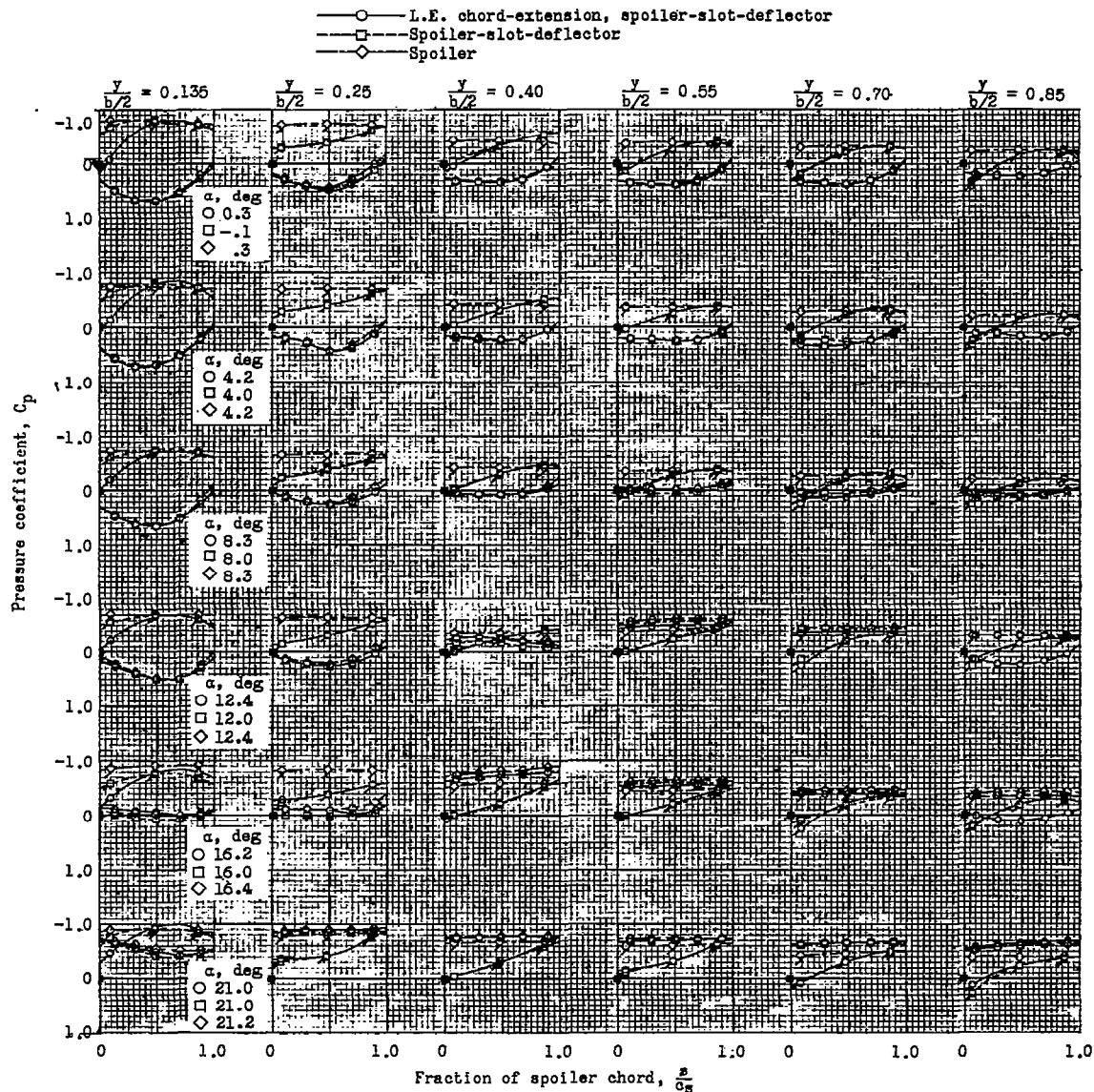
(a)  $M = 0.60.$ 

Figure 16.- Section pressure distributions for a spoiler aileron and spoilers of basic and leading-edge chord-extension spoiler-slot-deflector aileron configurations. (Flagged symbols indicate rear surface.)

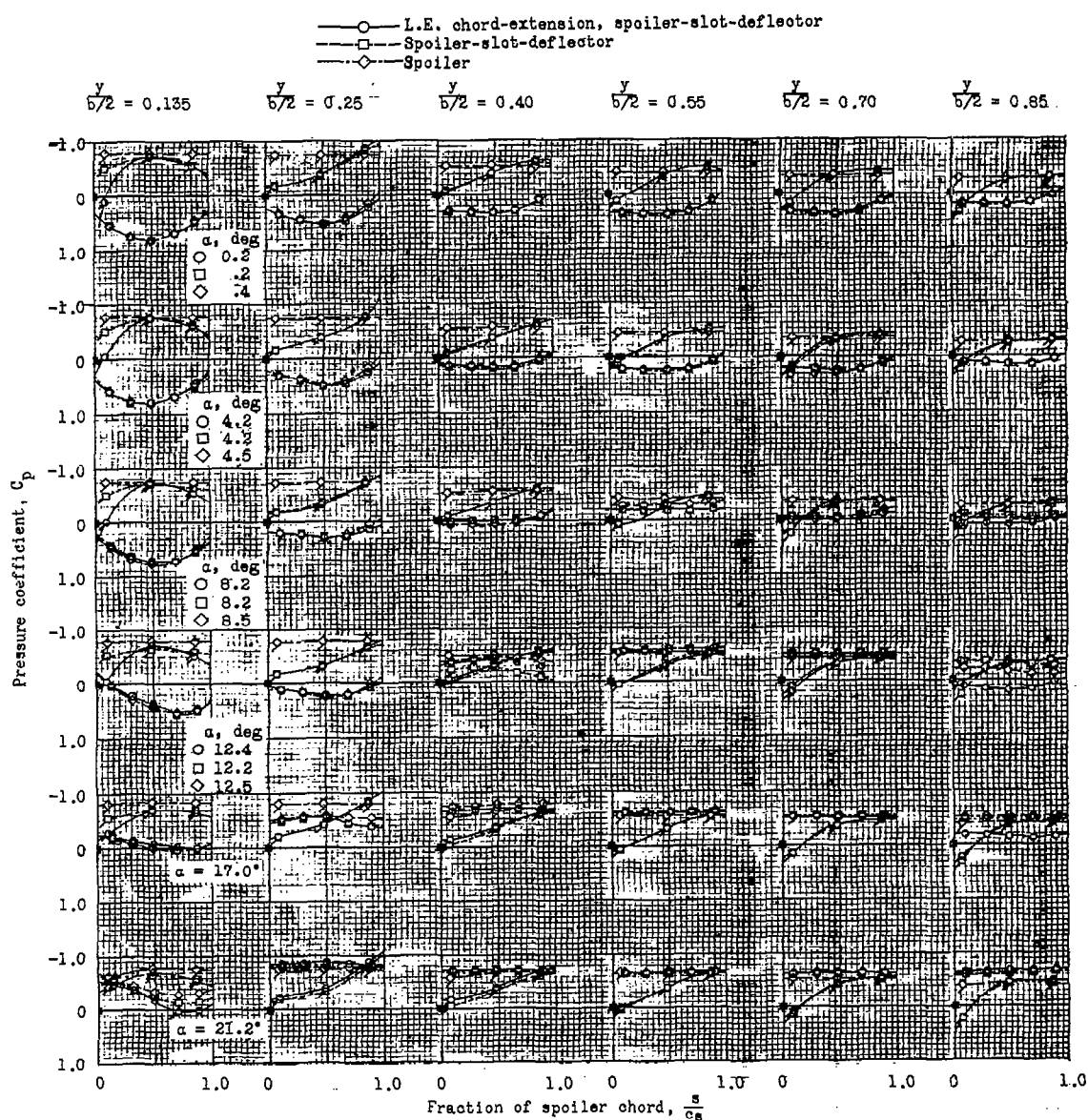
(b)  $M = 0.90$ .

Figure 16.- Continued.

**NACA – Digidocs**

**Document processing error**

Unreadable tiff image

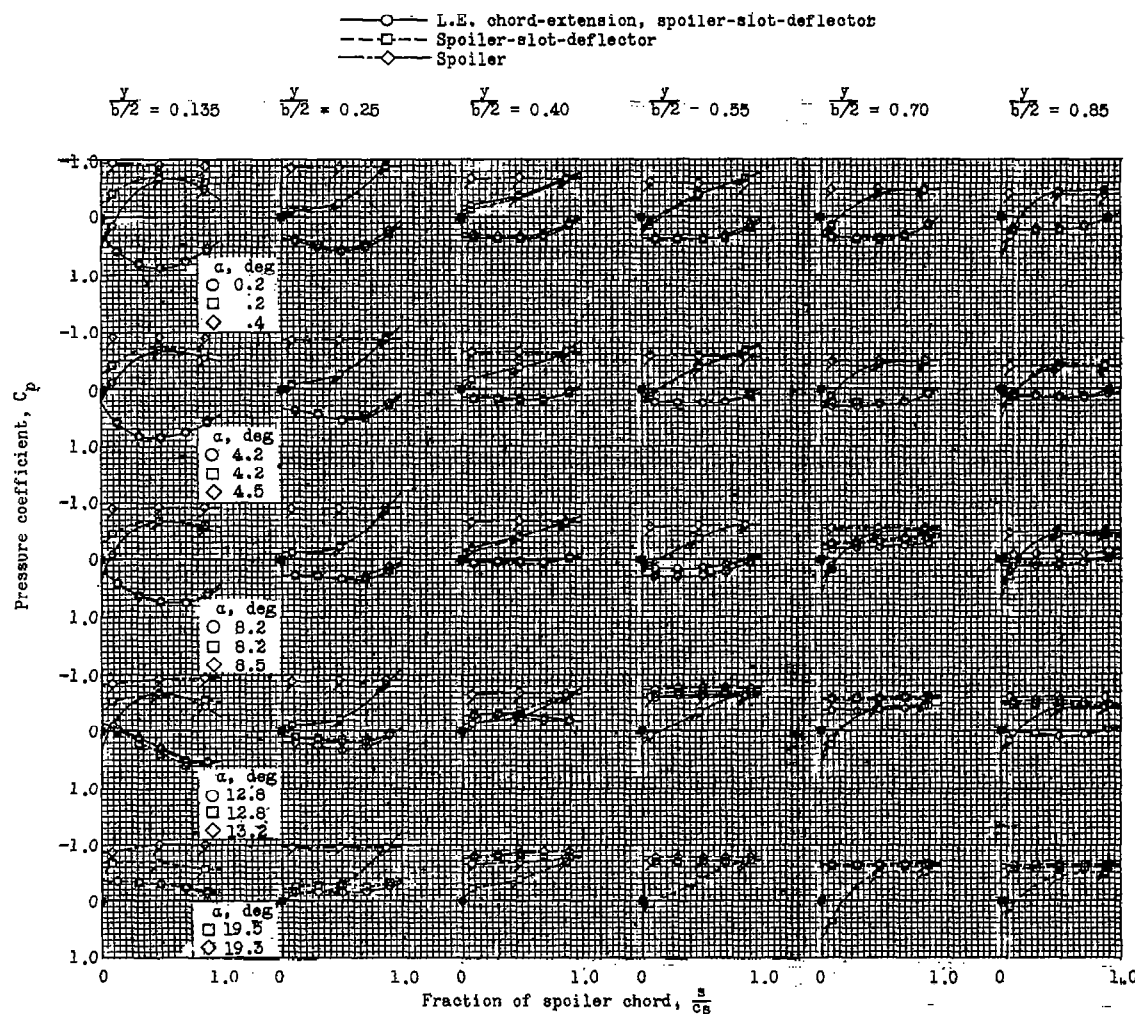
(d)  $M = 0.98$ .

Figure 16.- Continued.

~~CONFIDENTIAL~~

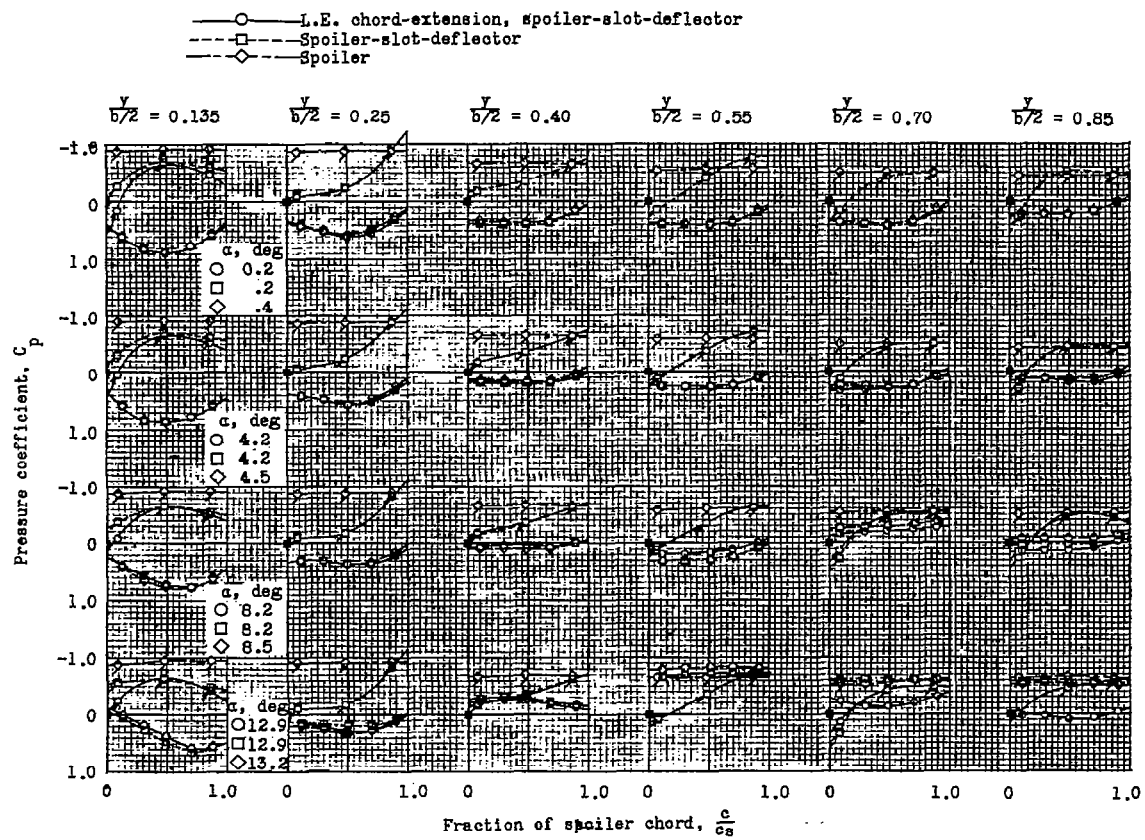
(e)  $M = 1.00.$ 

Figure 16.- Concluded.

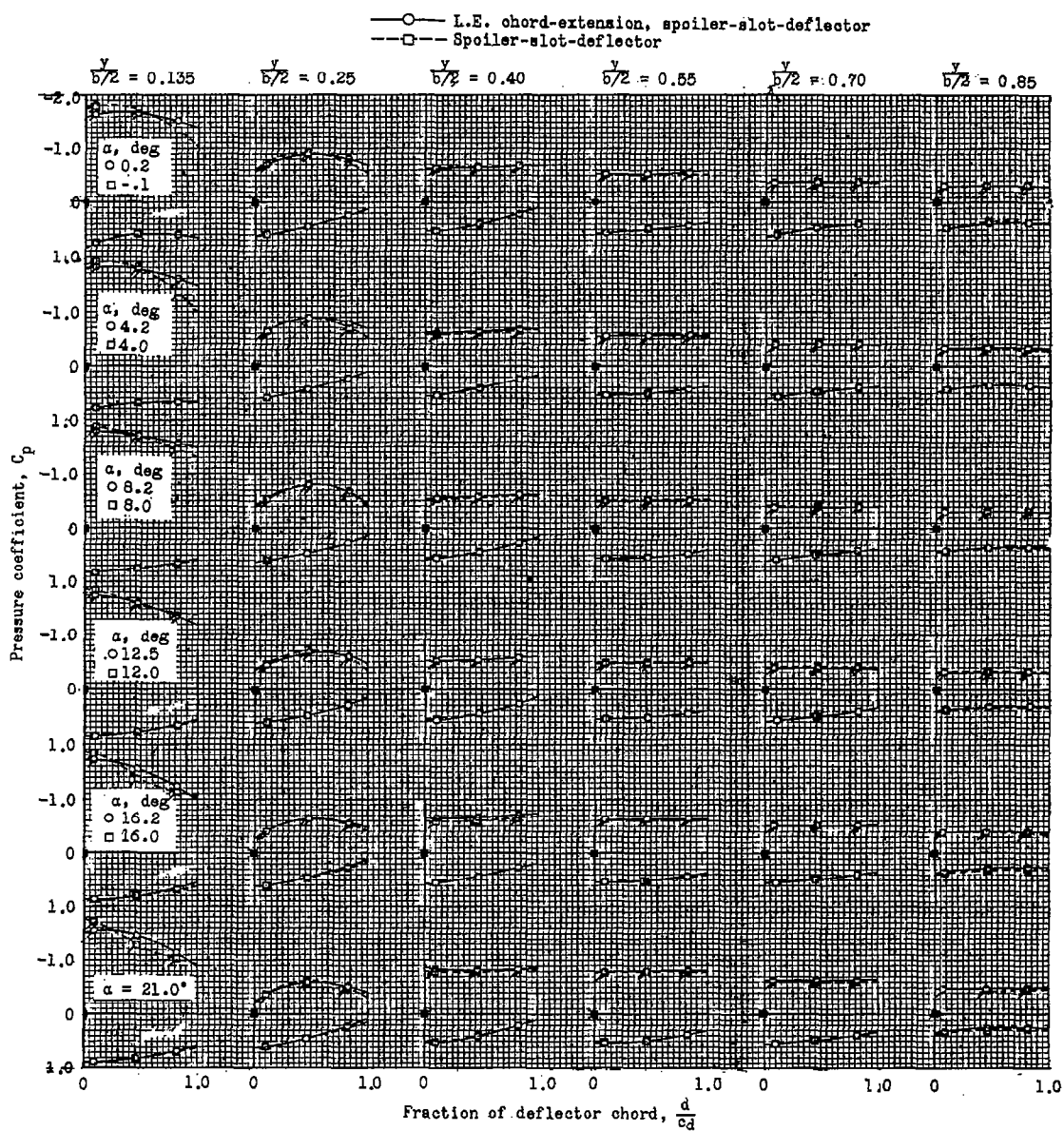
(a)  $M = 0.60.$ 

Figure 17.- Section pressure distribution for deflectors of the basic and leading-edge chord-extension spoiler-slot-deflector aileron configurations. (Flagged symbols indicate rear surface.)

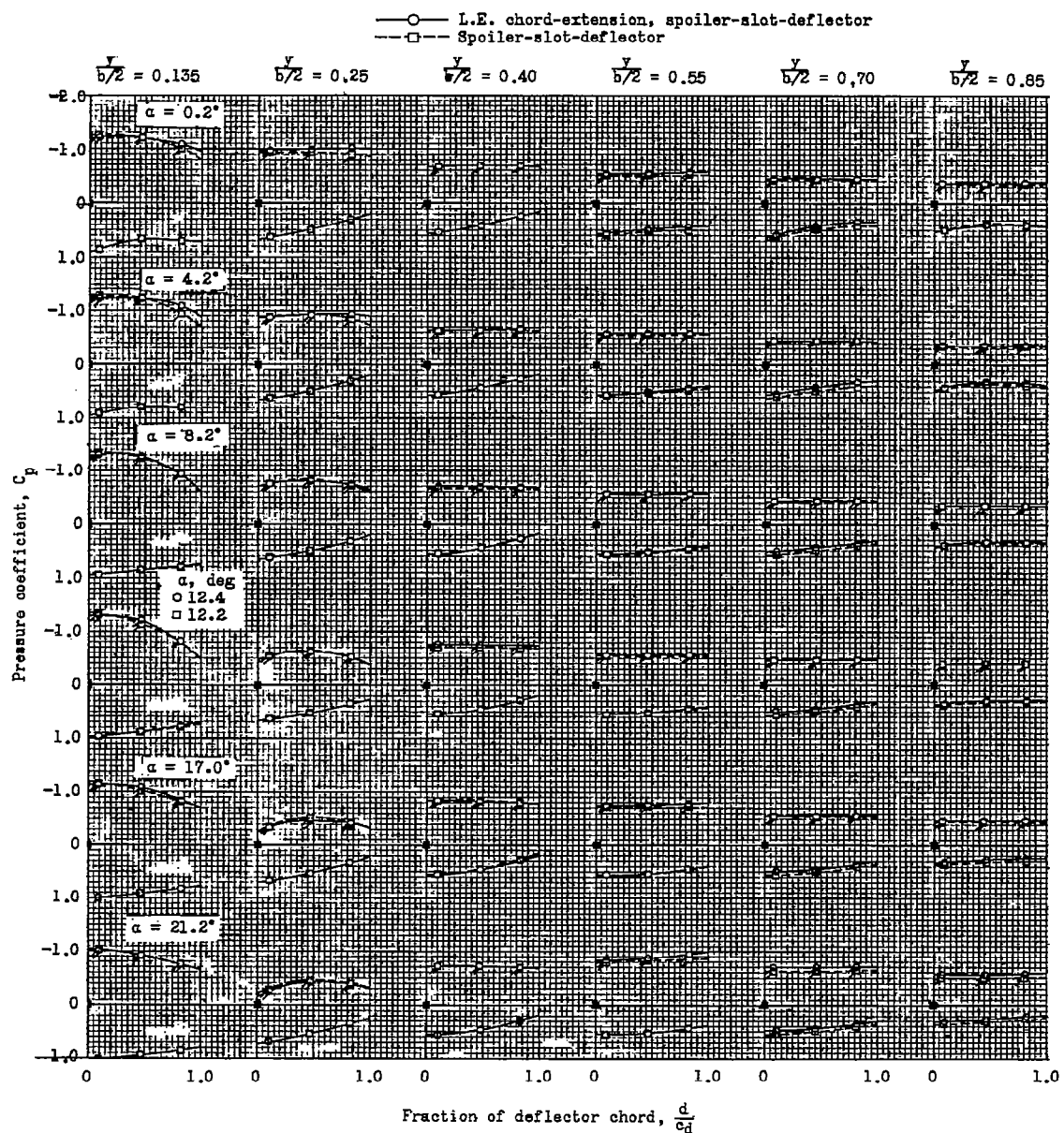
(b)  $M = 0.90$ .

Figure 17.- Continued.

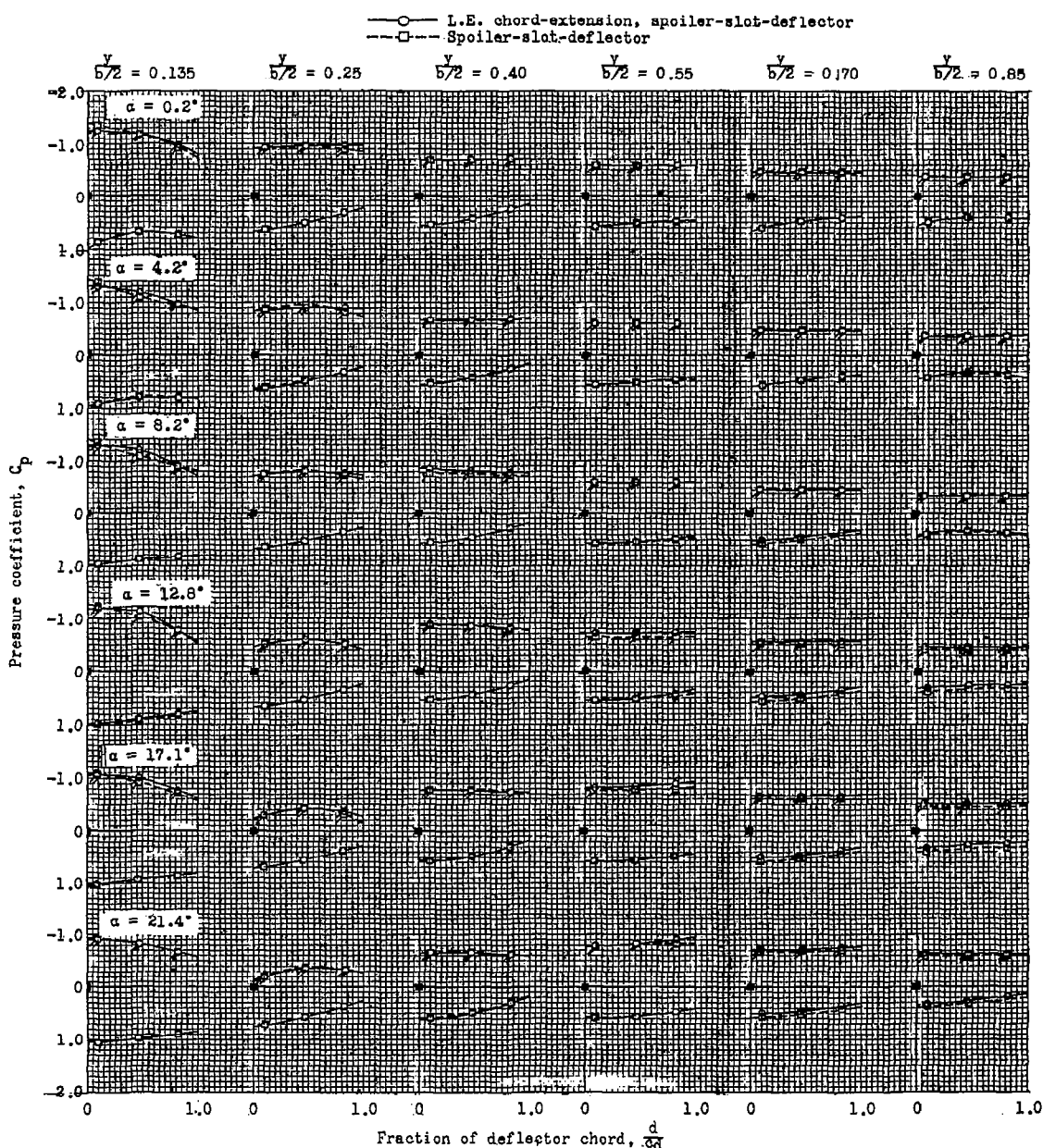
(c)  $M = 0.94$ .

Figure 17.- Continued.

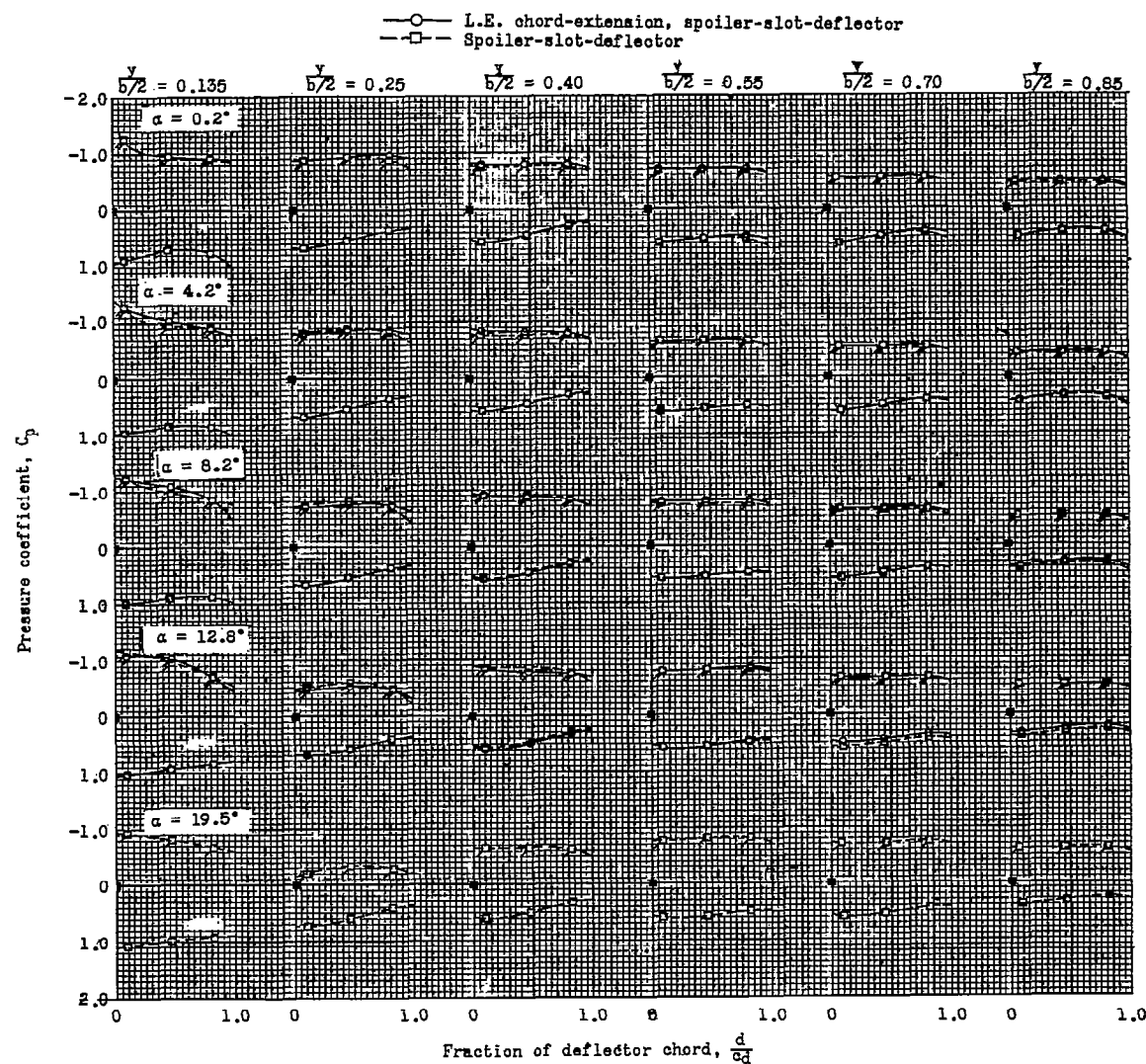
(d)  $M = 0.98$ .

Figure 17.- Continued.

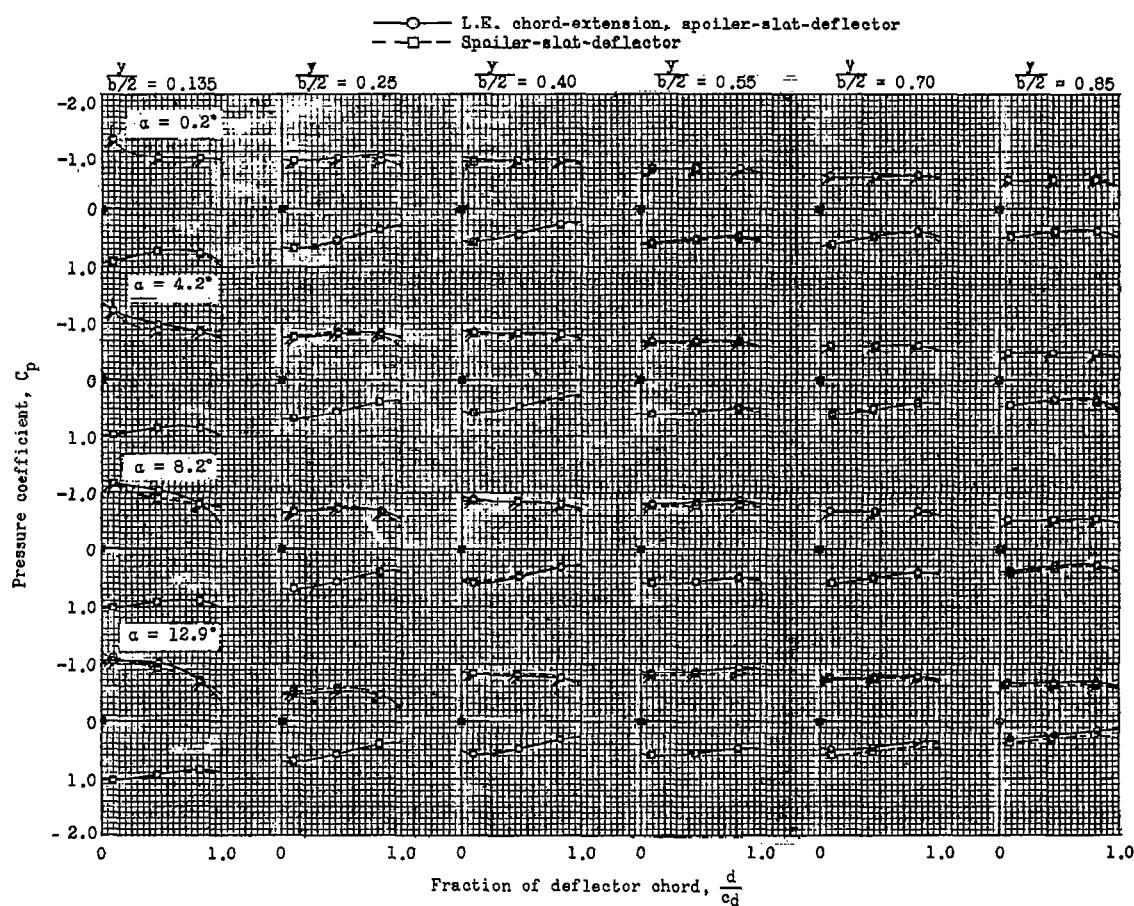
(e)  $M = 1.00$ .

Figure 17.- Concluded.

CONFIDENTIAL

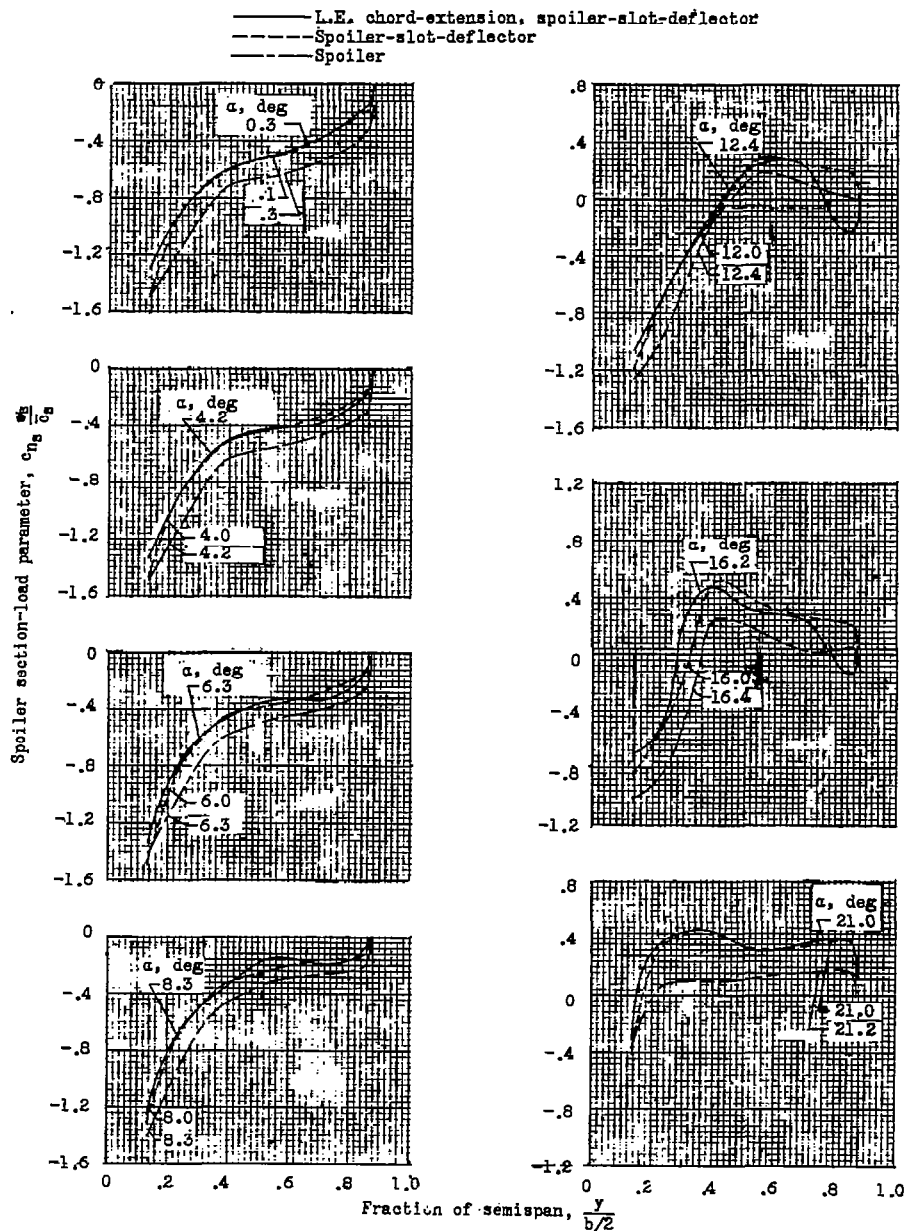
(a)  $M = 0.60$ .

Figure 18.- Span-load distributions for a spoiler aileron and spoilers of the basic and leading-edge chord-extension spoiler-slot-deflector aileron configurations.

CONFIDENTIAL

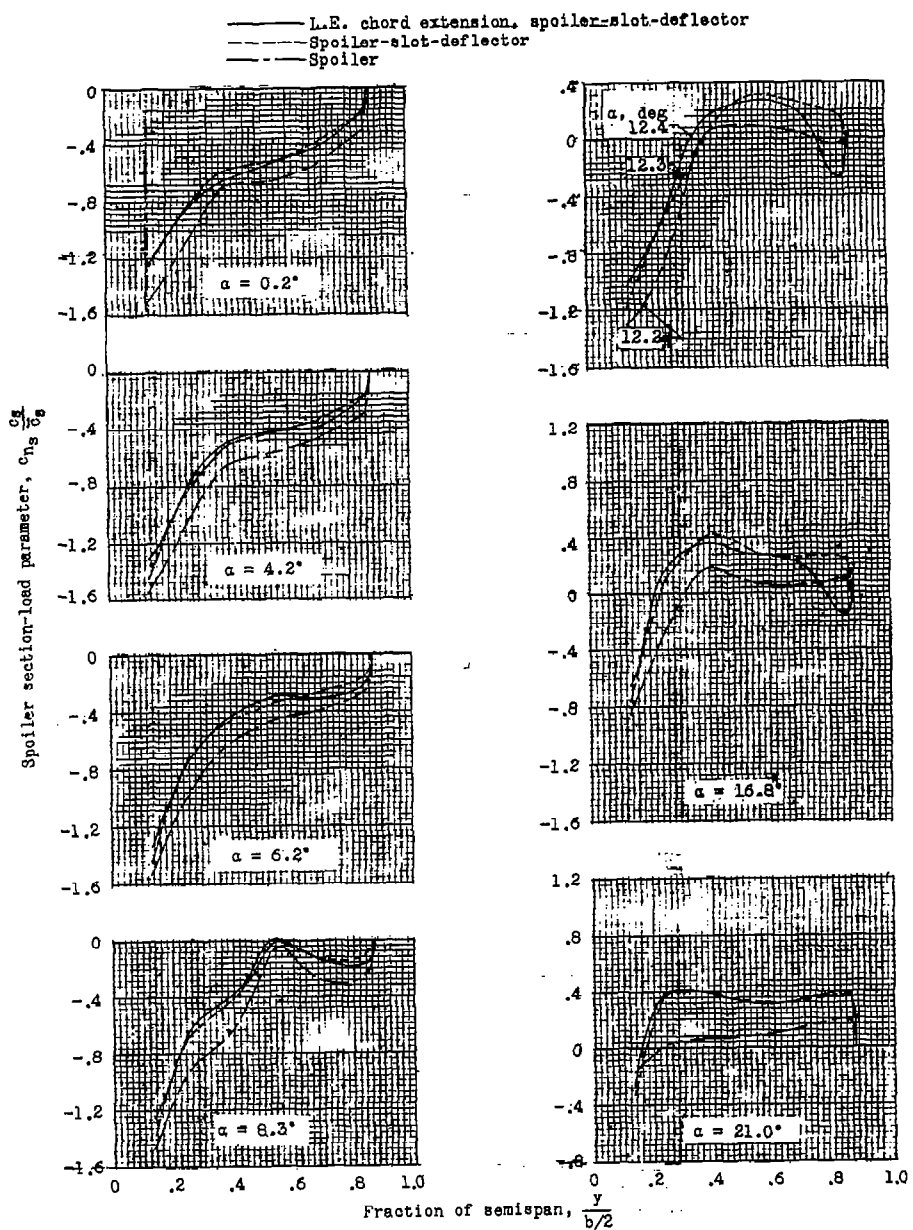
(b)  $M = 0.80$ .

Figure 18.- Continued.

CONFIDENTIAL

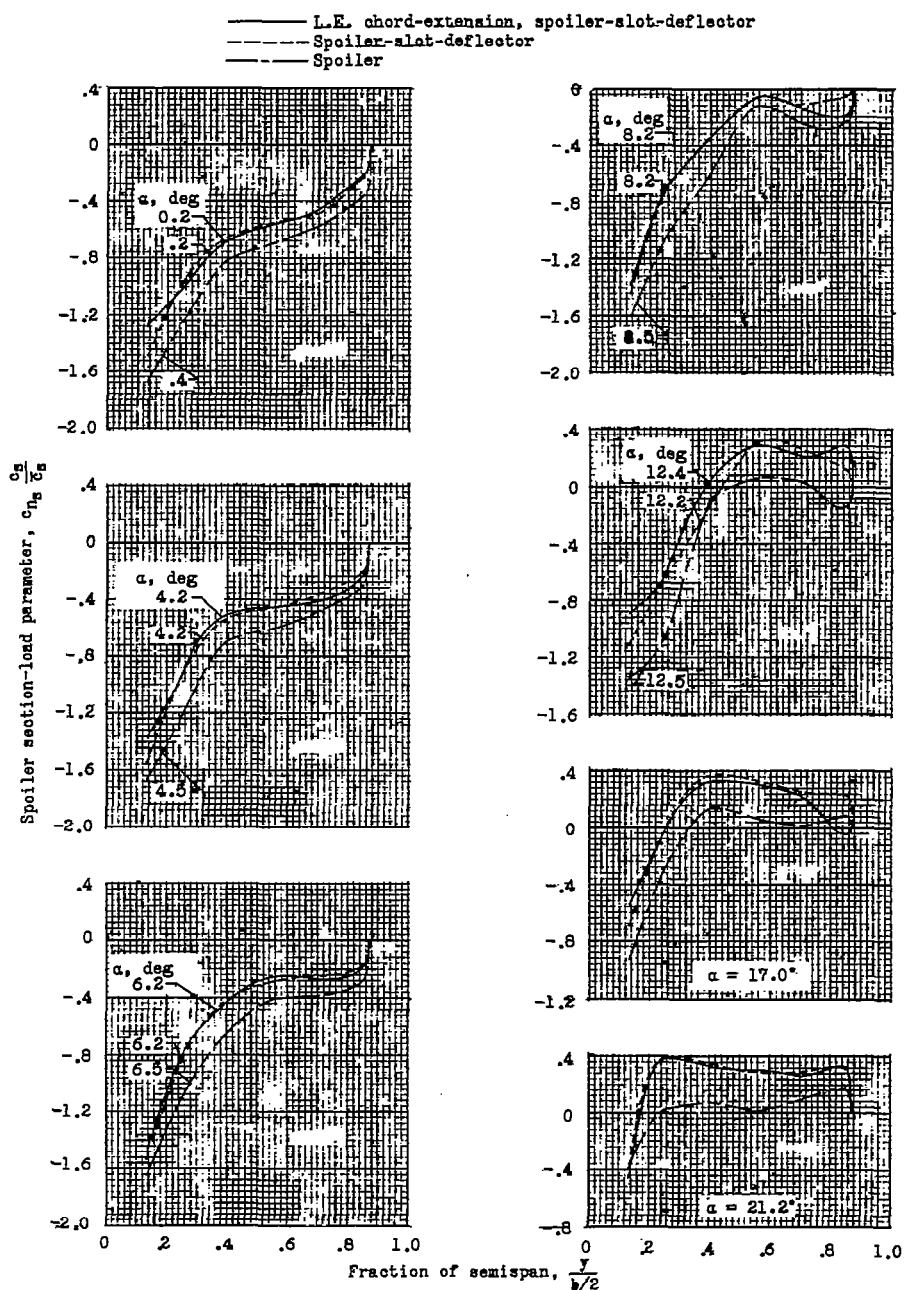
(c)  $M = 0.90$ .

Figure 18.- Continued.

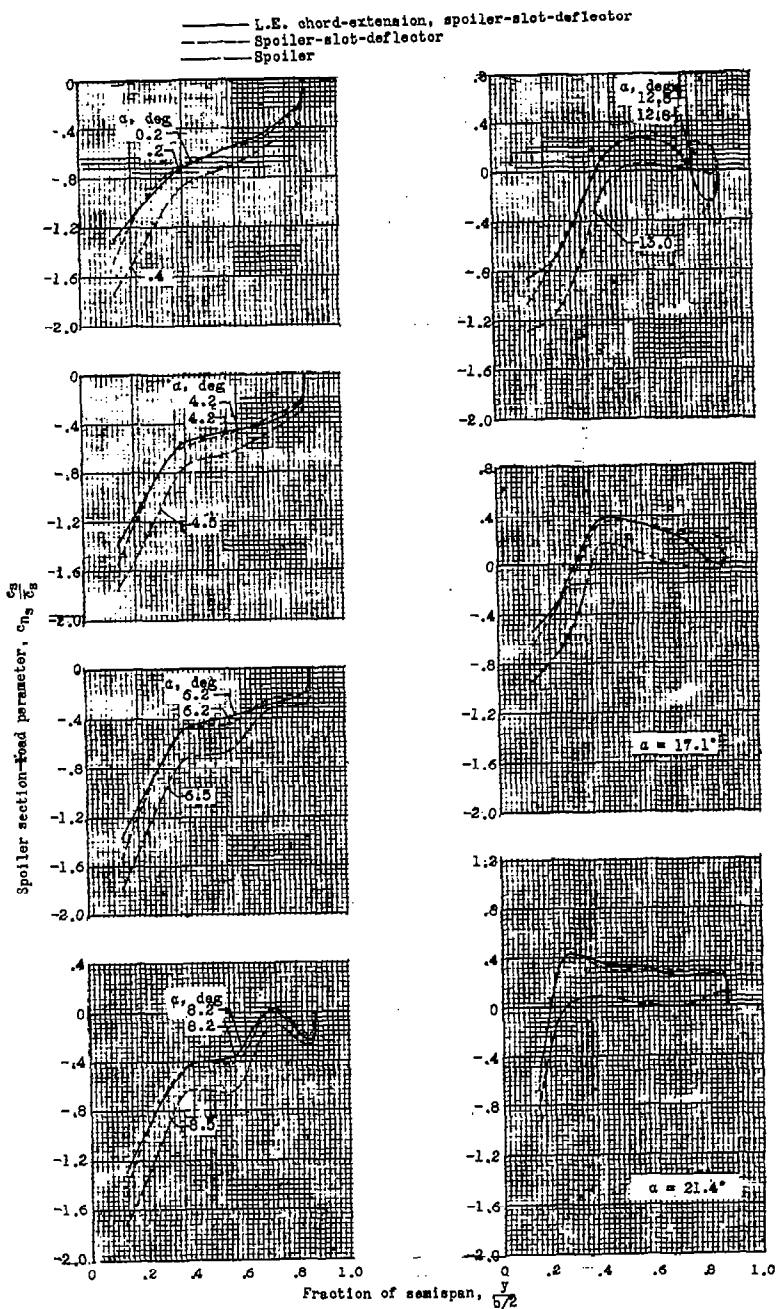
(d)  $M = 0.94$ .

Figure 18.- Continued.

CONFIDENTIAL

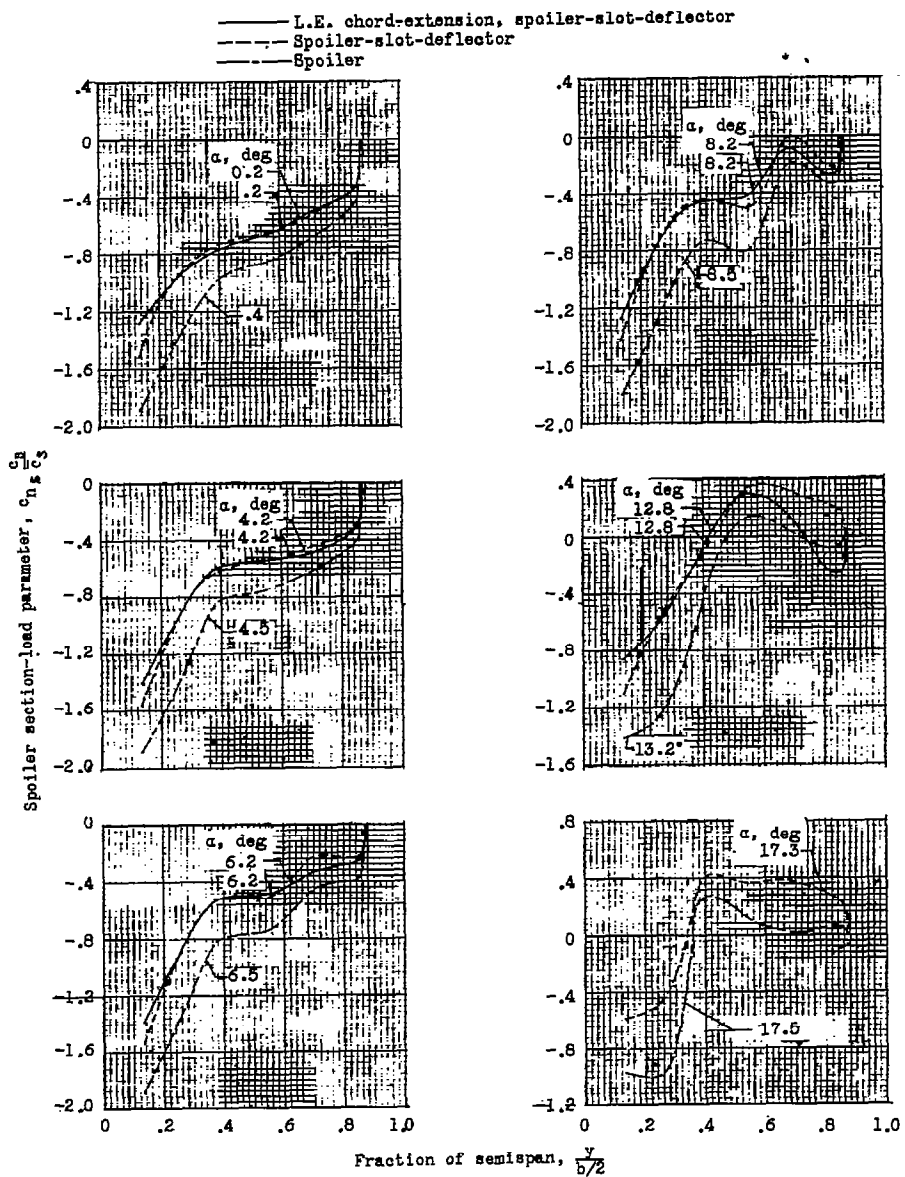
(e)  $M = 0.98$ .

Figure 18.- Continued.

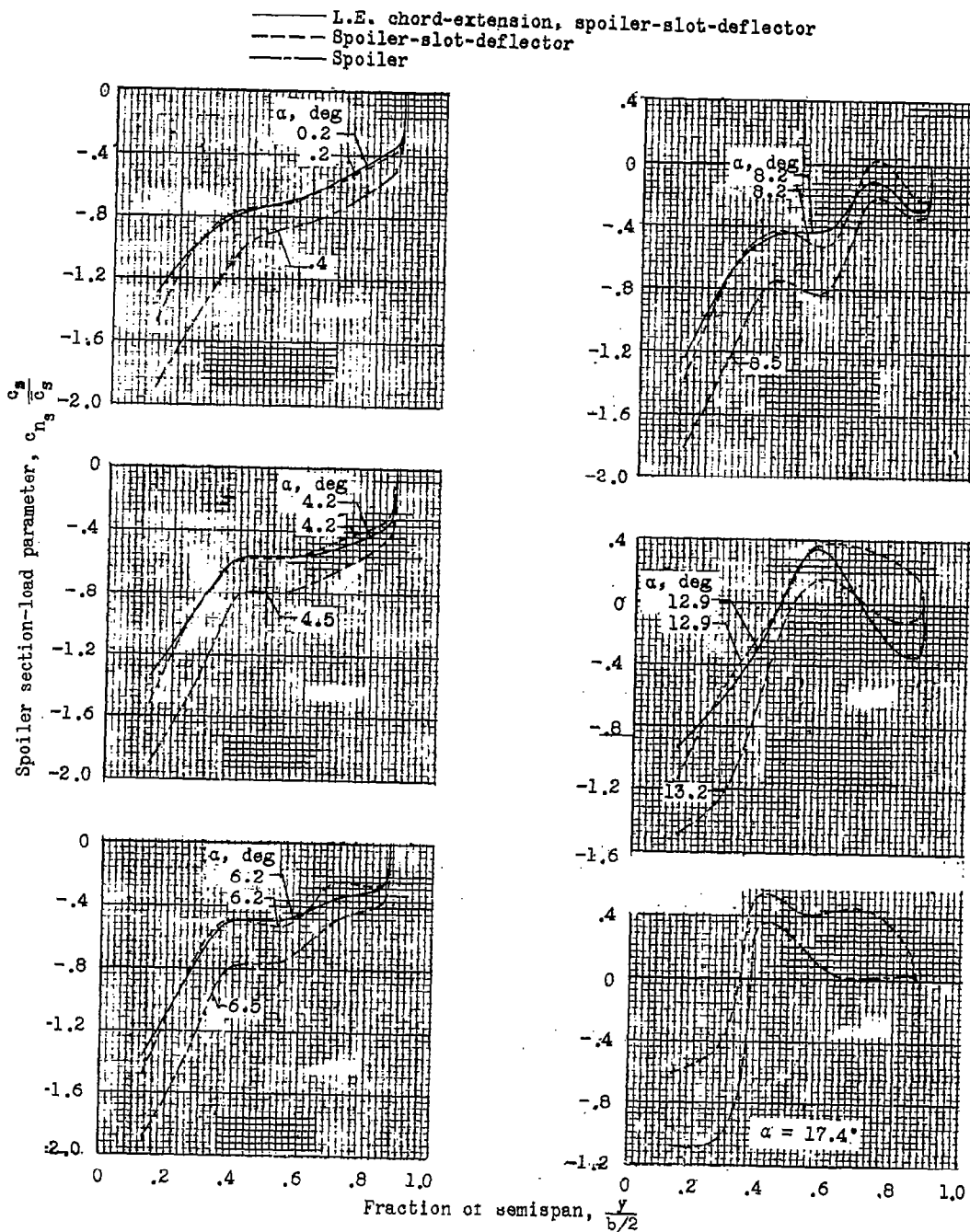
(f)  $M = 1.00$ .

Figure 18.- Continued.

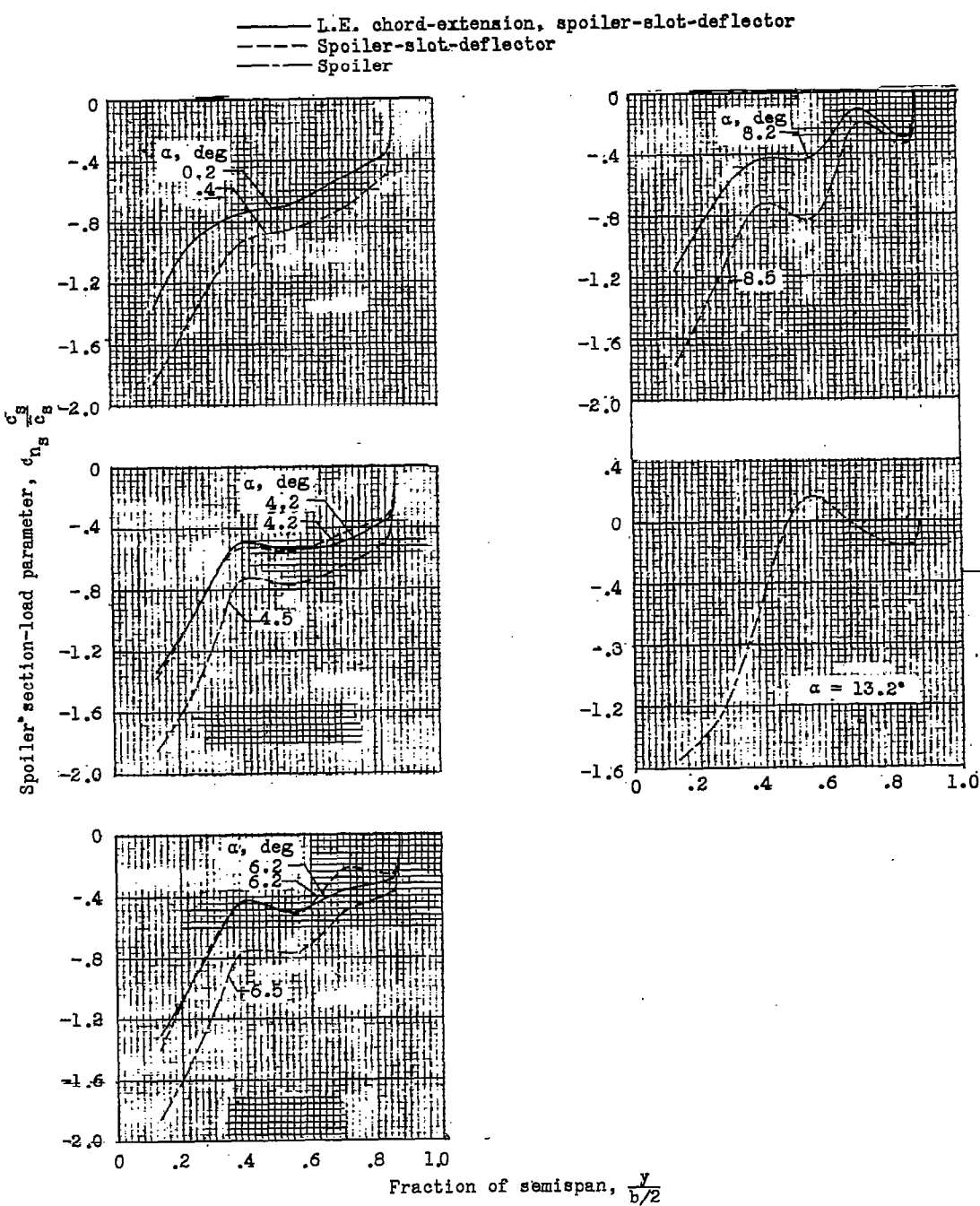
(g)  $M = 1.03$ .

Figure 18.- Concluded.

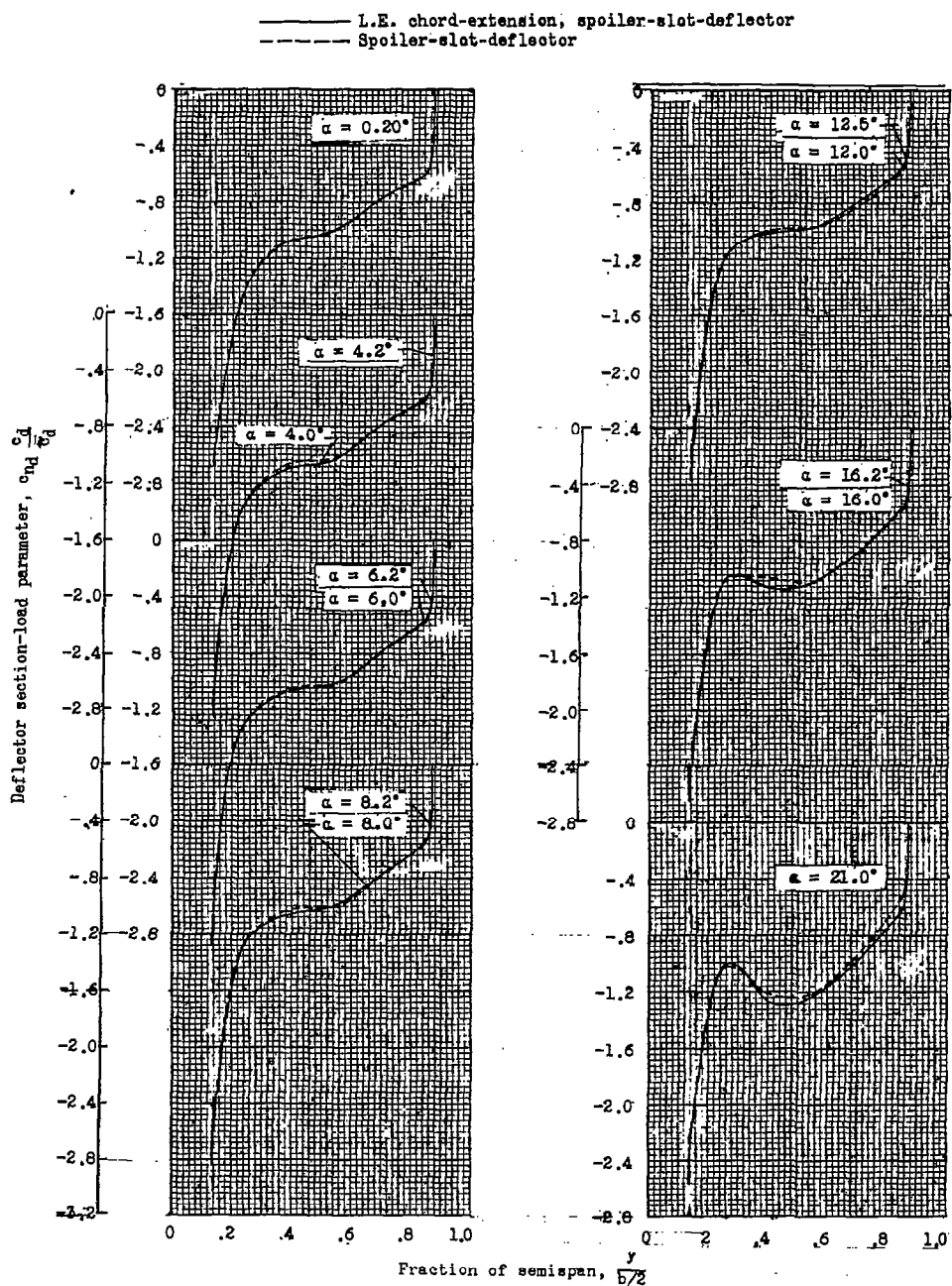


Figure 19.- Span-load distributions for deflectors of basic and leading-edge chord-extension spoiler-slot-deflector aileron configurations.

~~CONFIDENTIAL~~

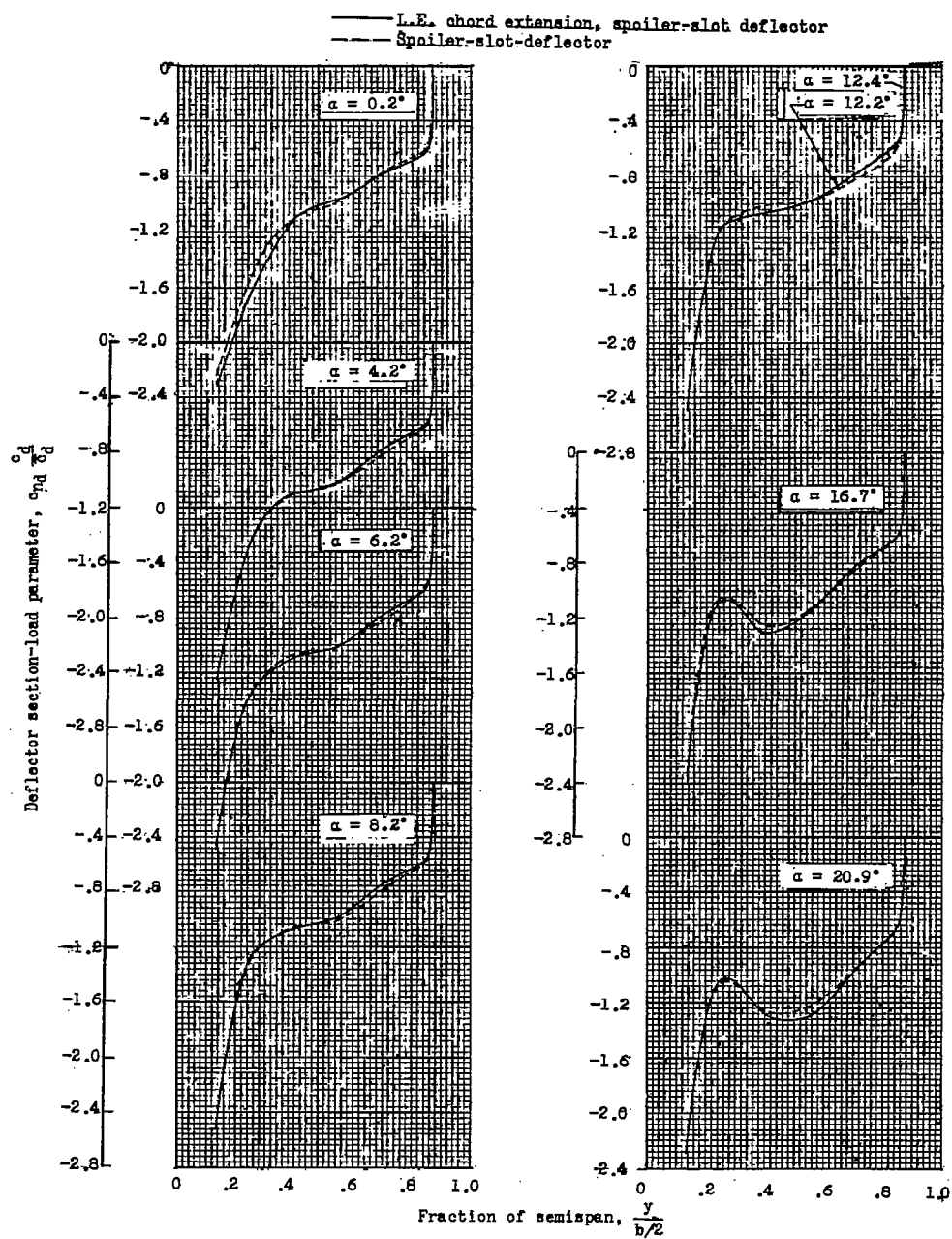


Figure 19.- Continued.

CONFIDENTIAL

CONFIDENTIAL

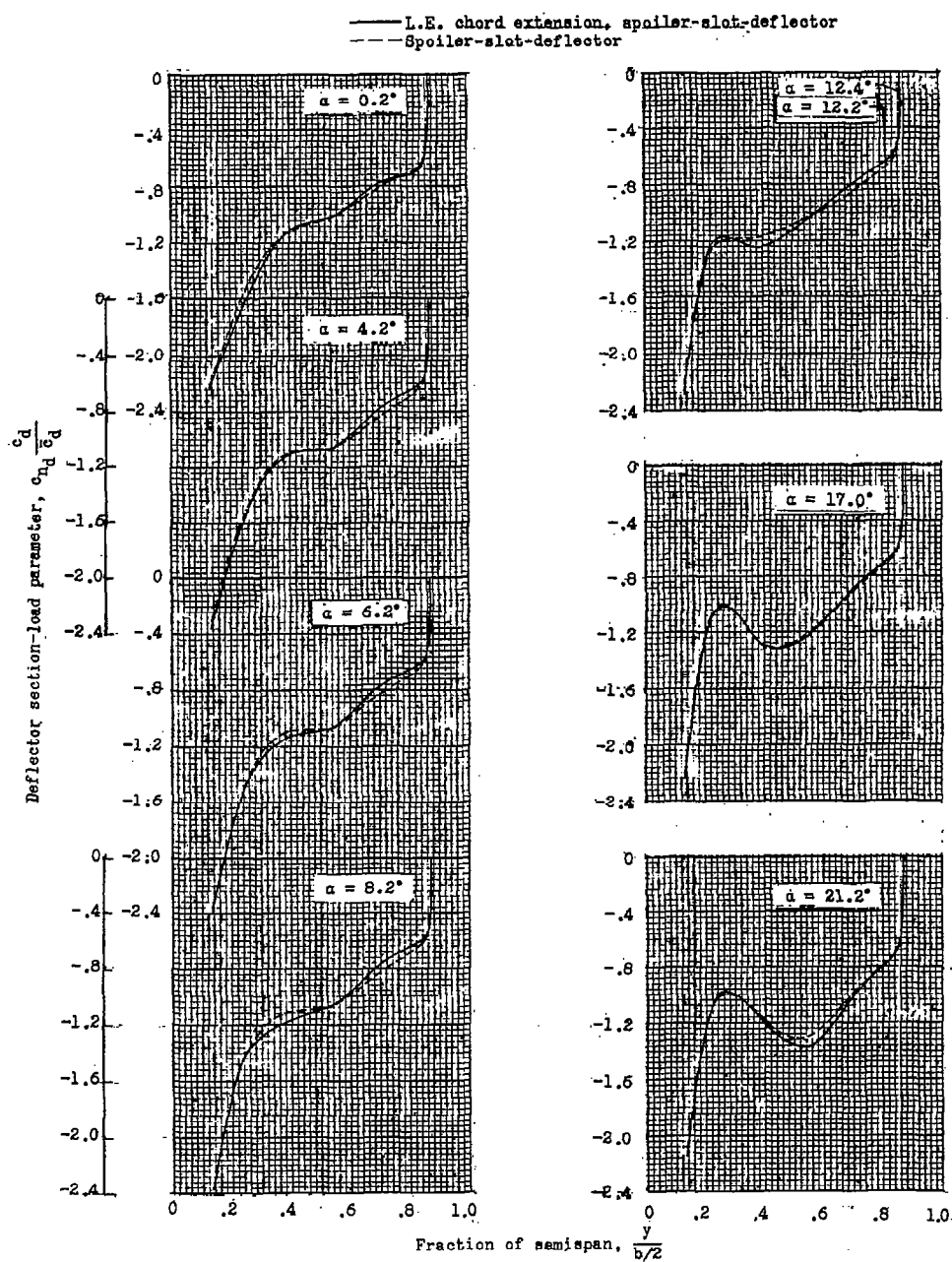
(c)  $M = 0.90$ .

Figure 19.- Continued.

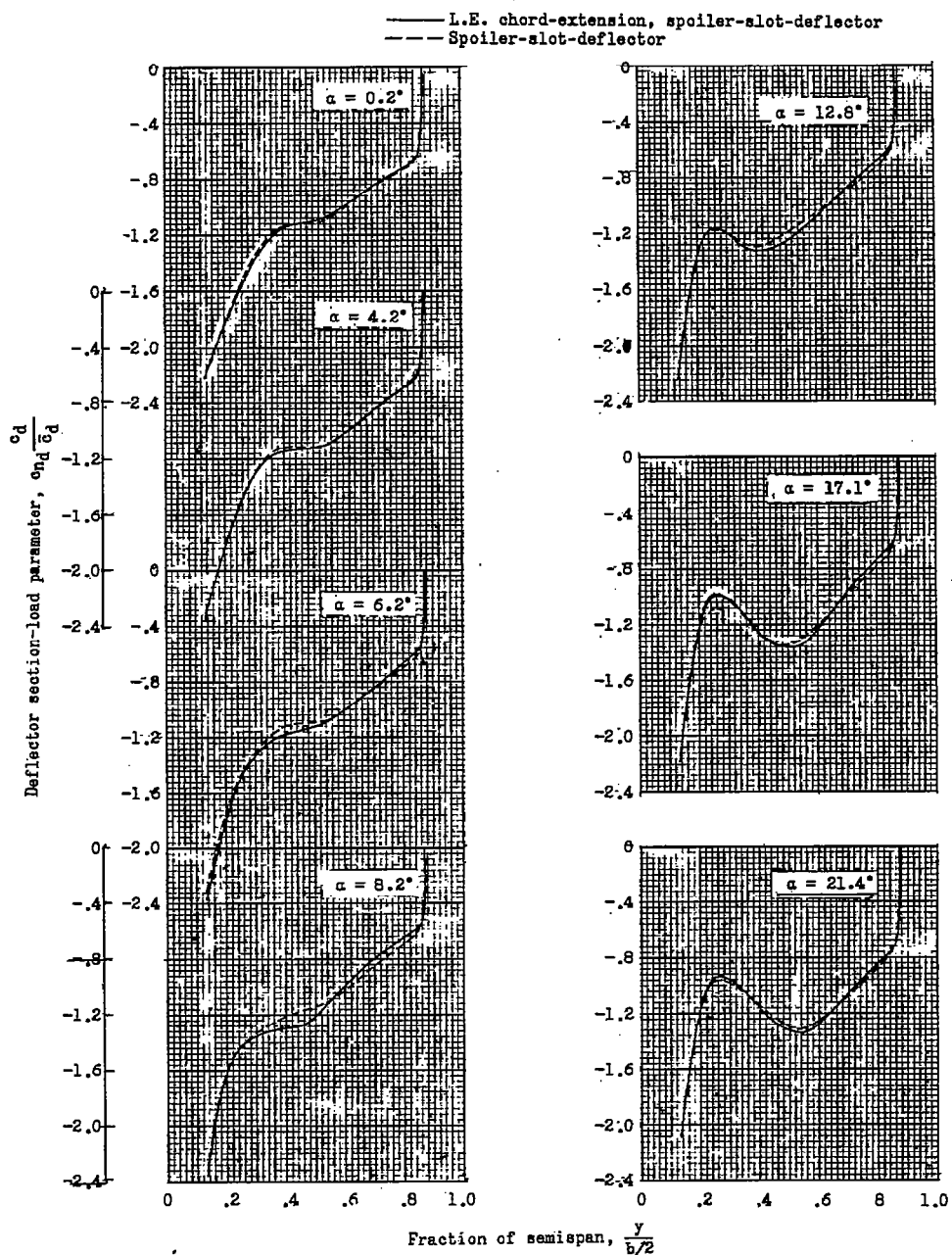
(d)  $M = 0.94$ .

Figure 19.- Continued.

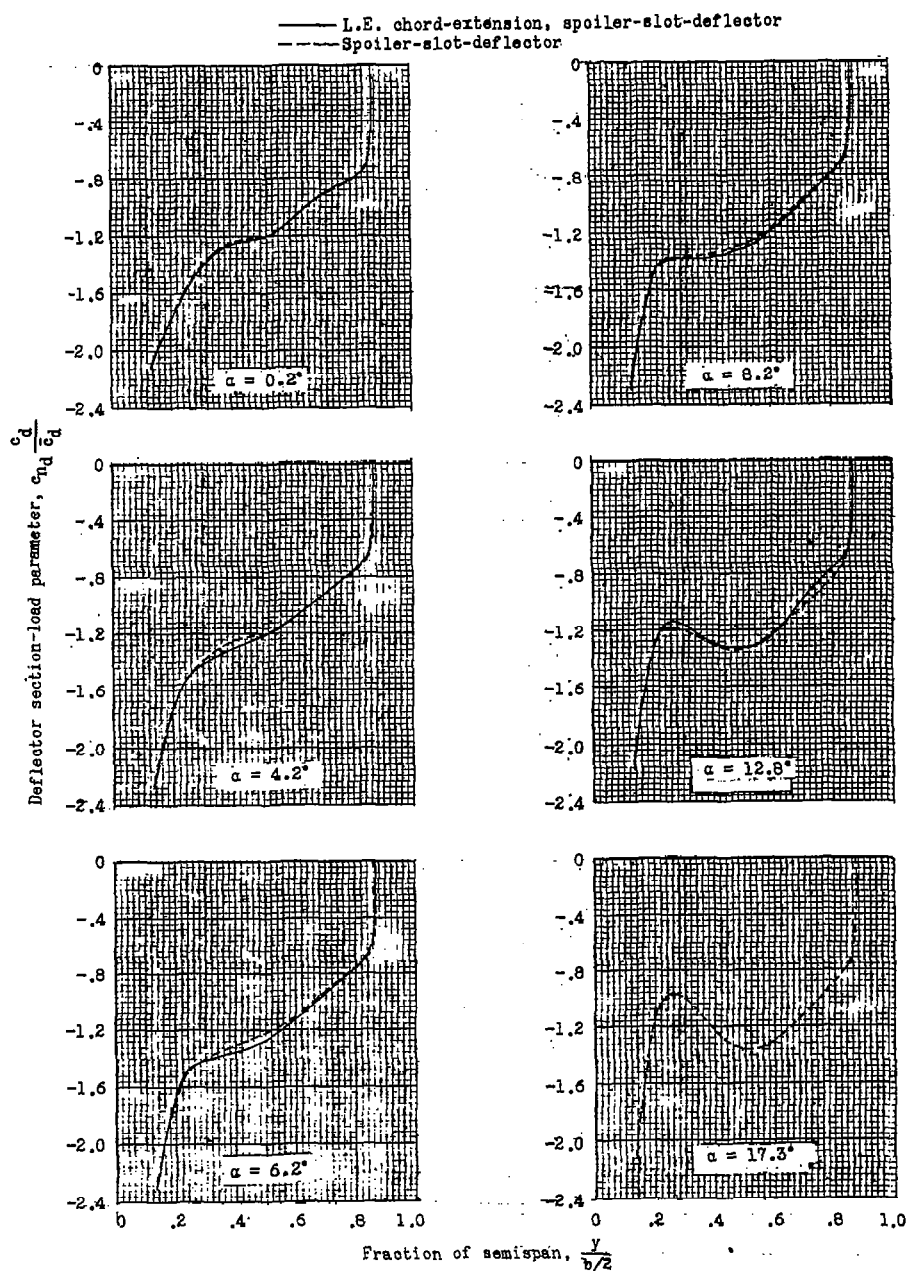
(e)  $M = 0.98.$ 

Figure 19.- Continued.

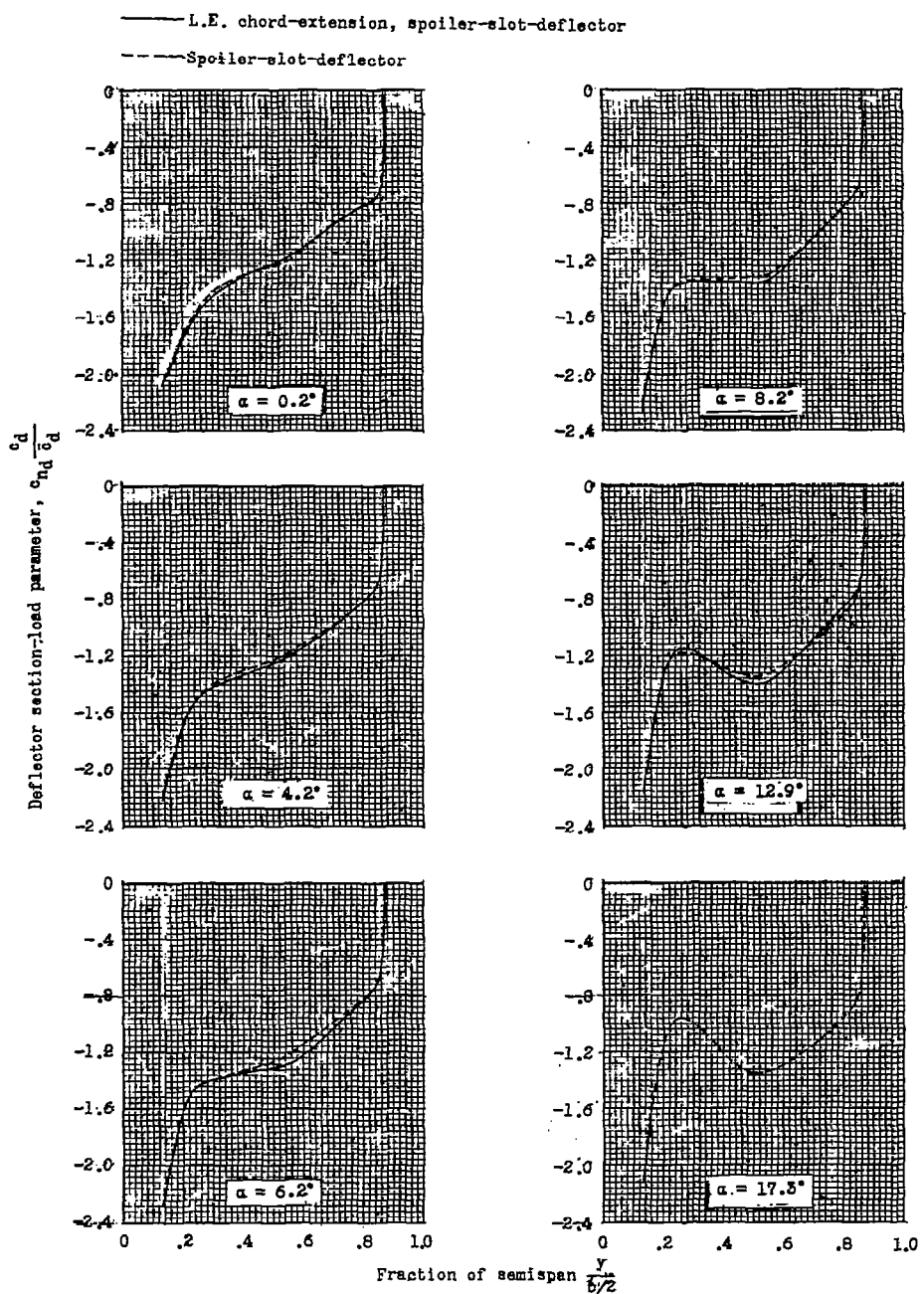
(f)  $M = 1.00$ .

Figure 19.- Continued.

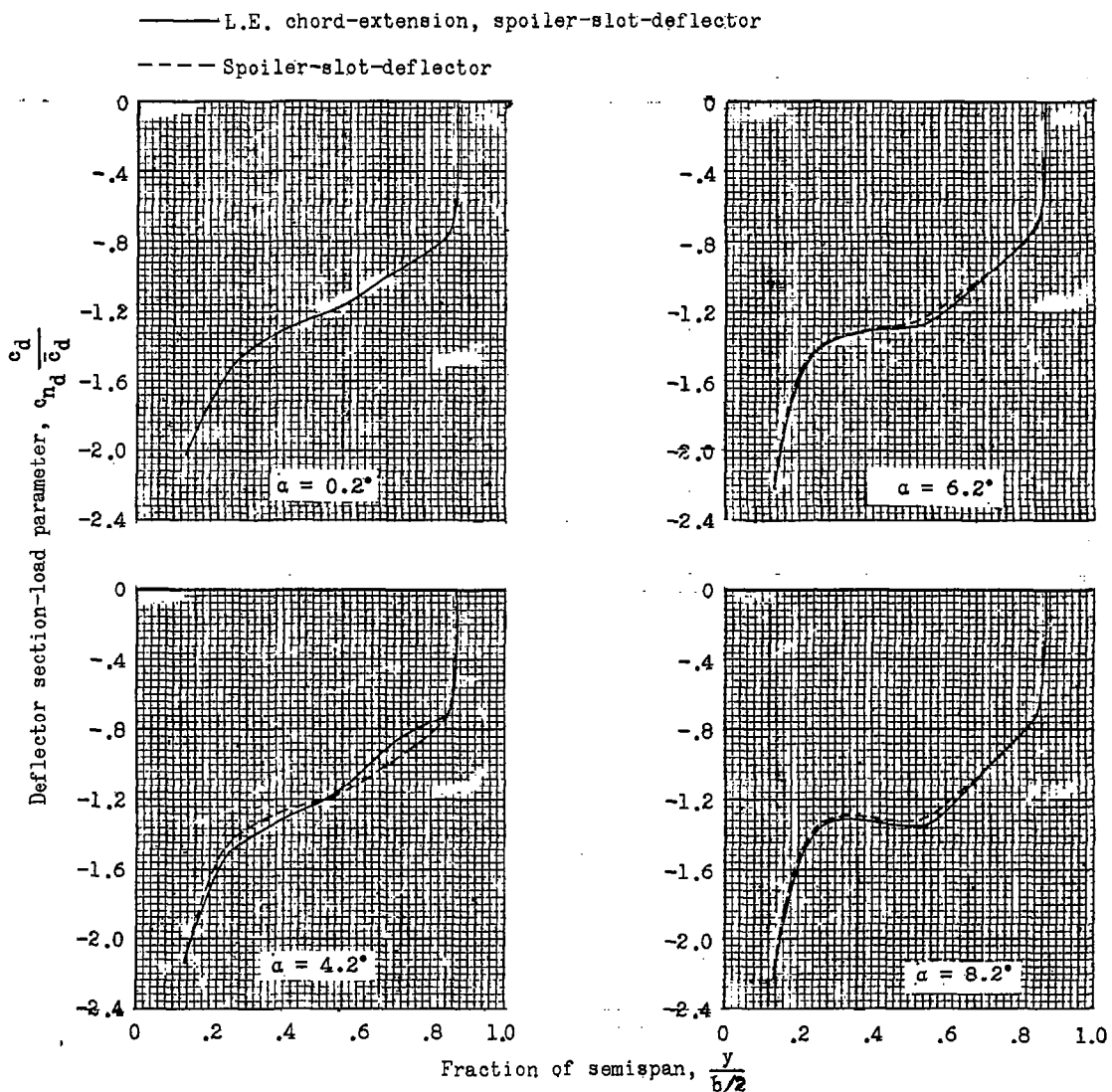
(g)  $M = 1.03$ .

Figure 19.- Concluded.

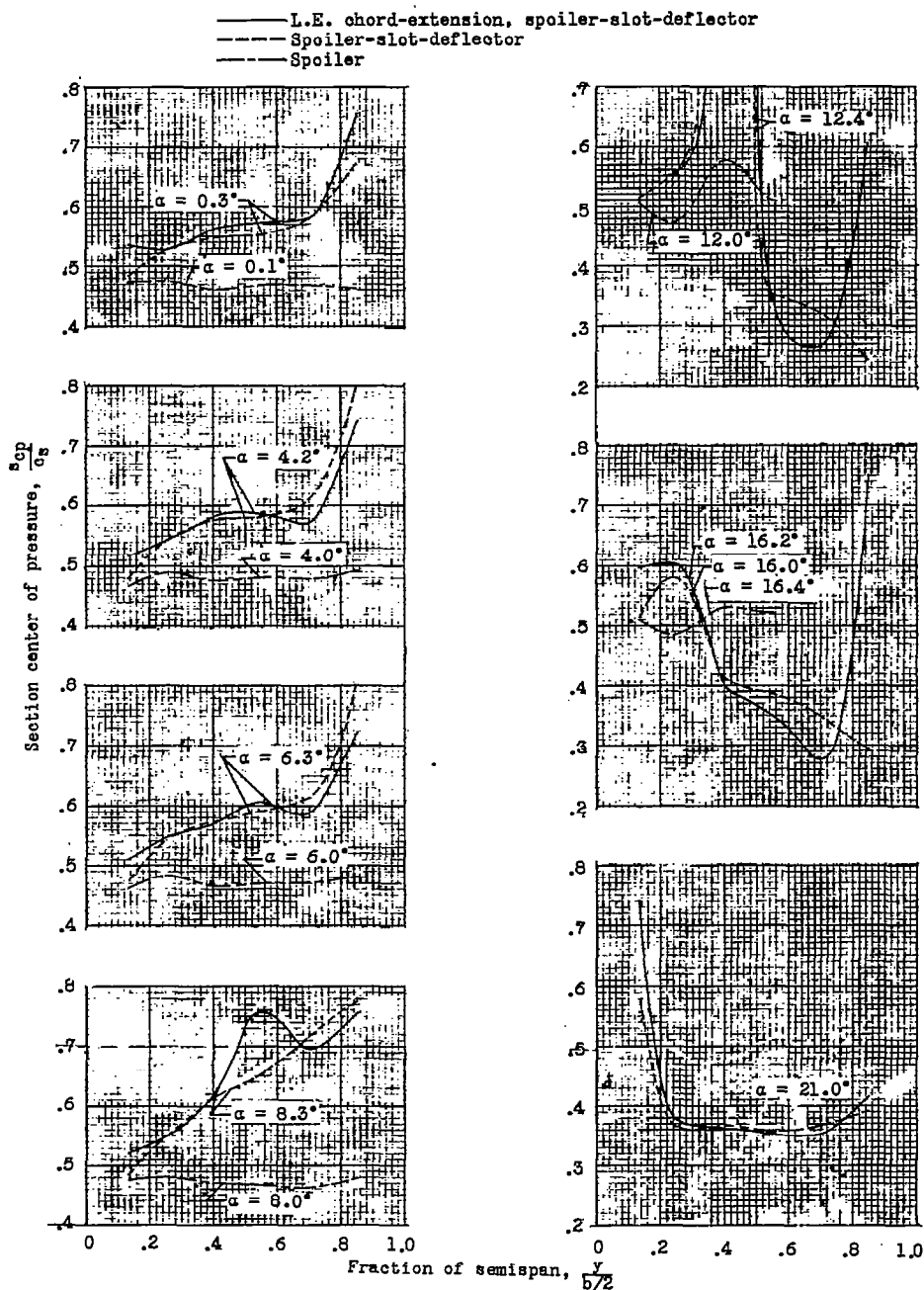
(a)  $M = 0.60.$ 

Figure 20.- Section centers of pressure for a spoiler aileron and spoilers of basic and leading-edge chord-extension spoiler-slot-deflector aileron configurations.

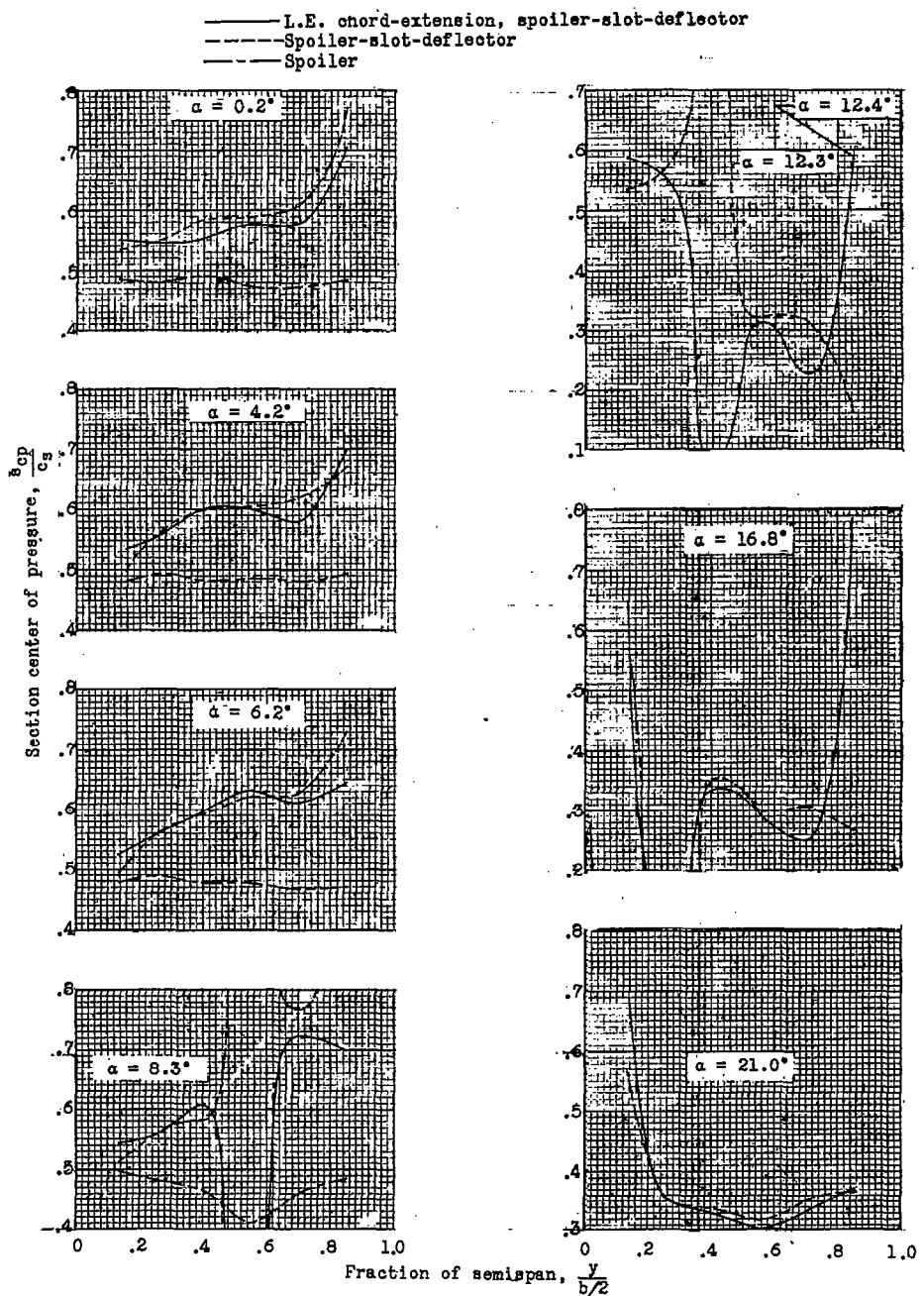
(b)  $M = 0.80$ .

Figure 20.- Continued.

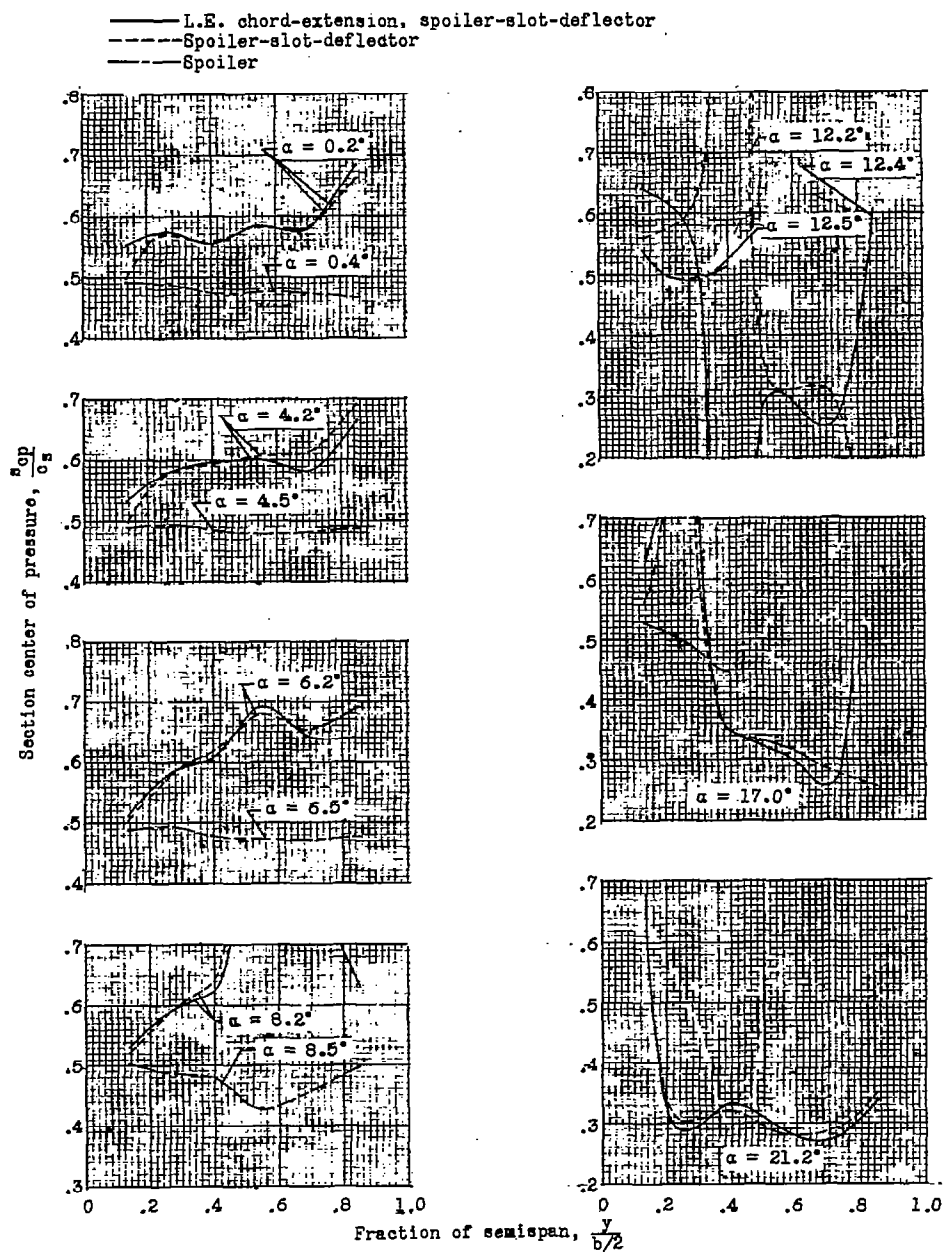
(c)  $M = 0.90$ .

Figure 20.- Continued.

CONFIDENTIAL

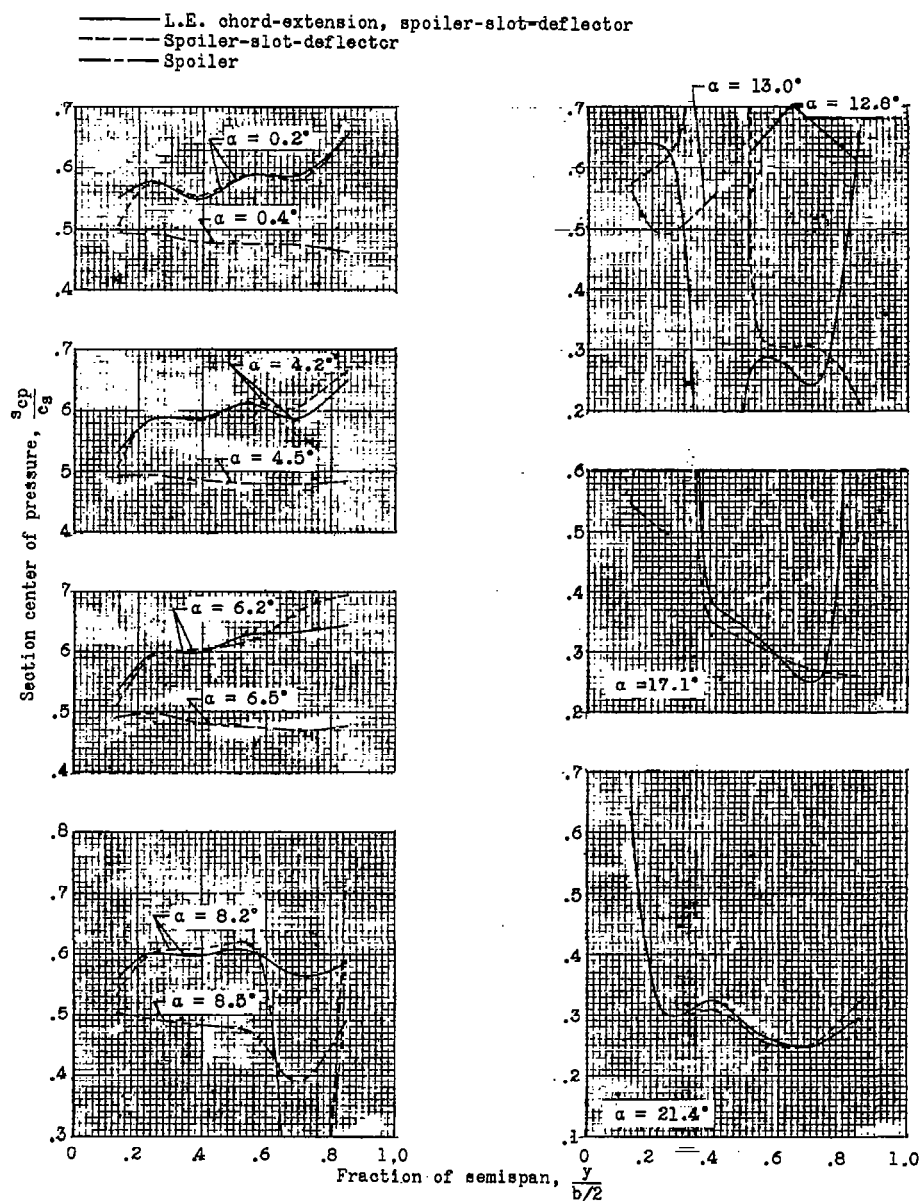
(d)  $M = 0.94$ .

Figure 20.- Continued.

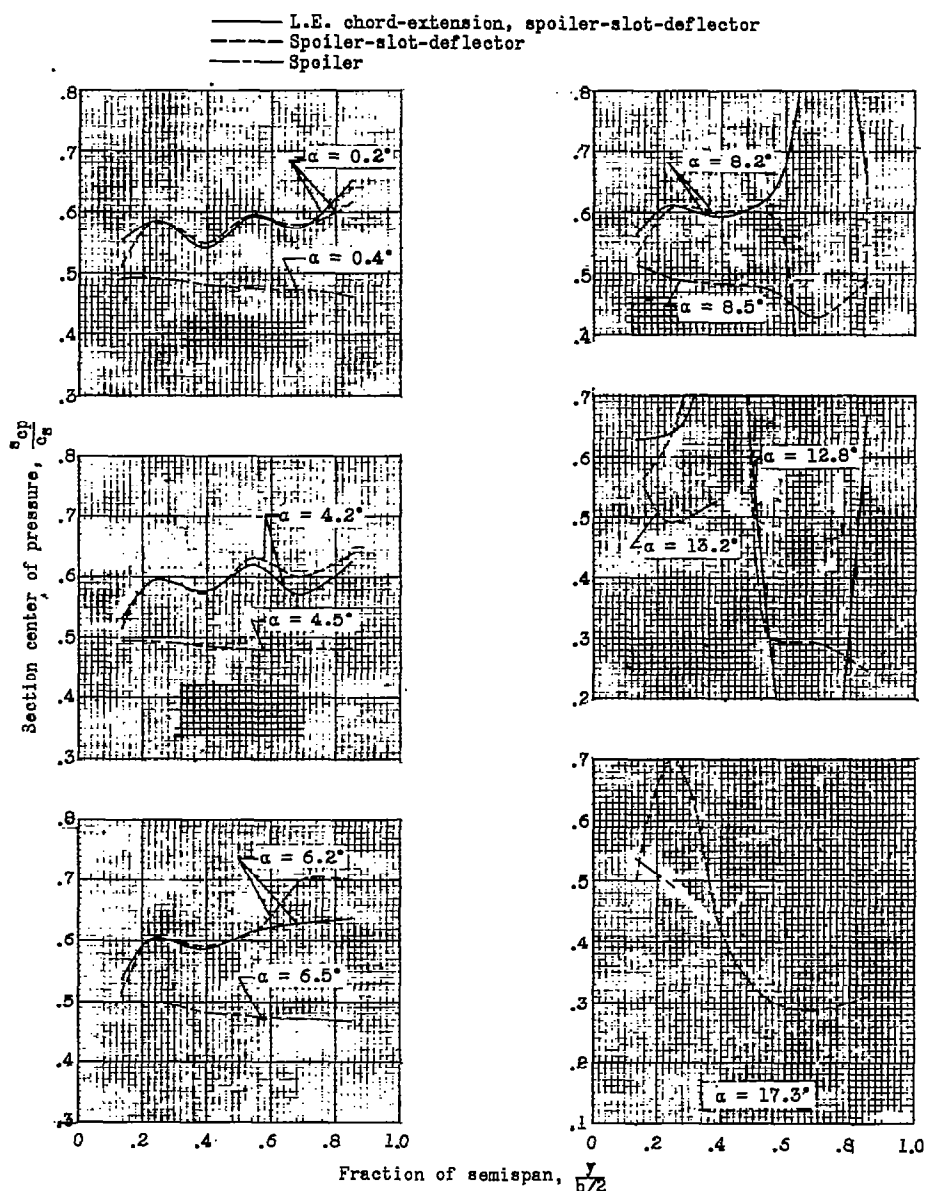
(e)  $M = 0.98.$ 

Figure 20.- Continued.

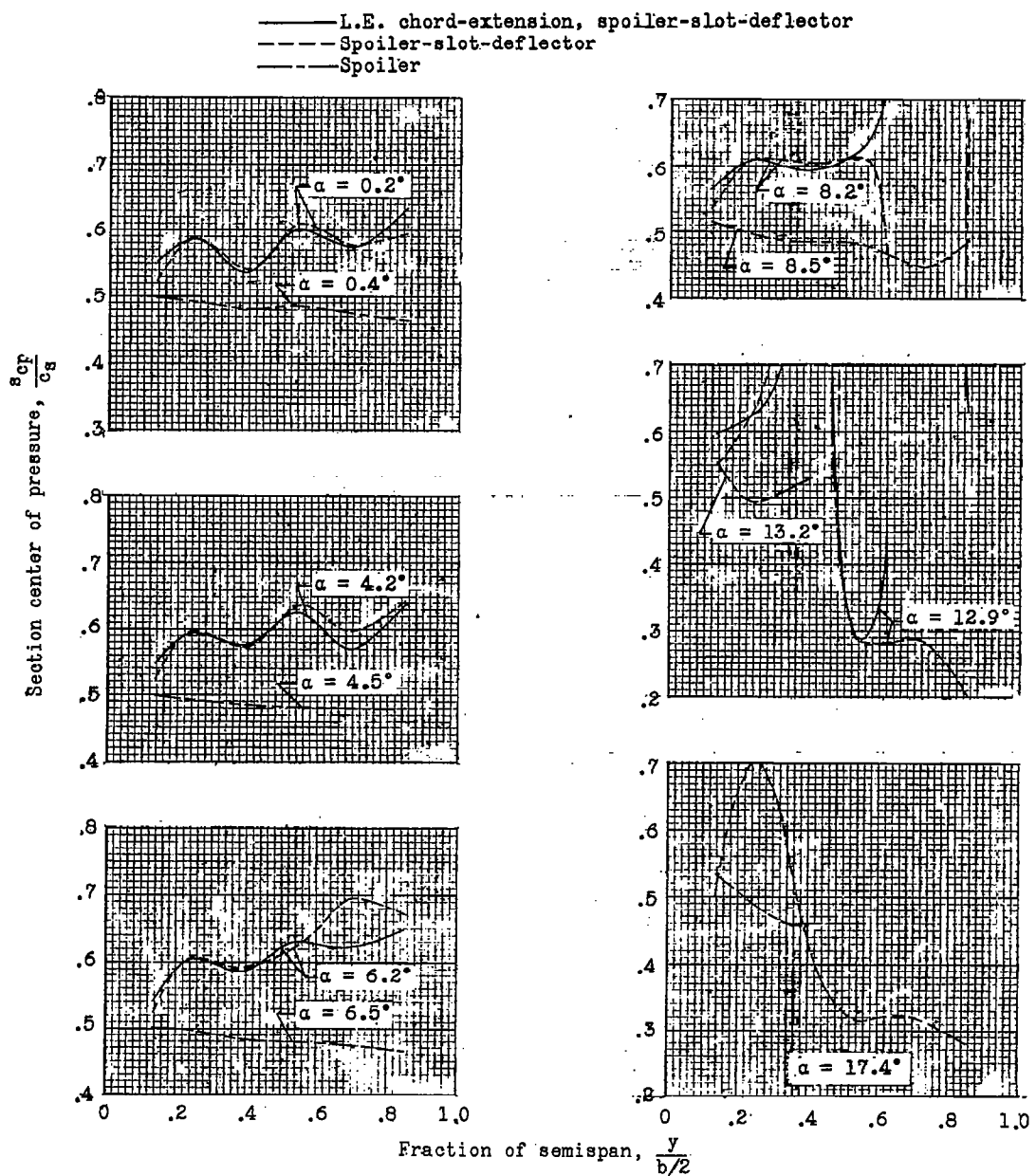
(f)  $M = 1.00$ .

Figure 20.- Continued.

~~CONFIDENTIAL~~

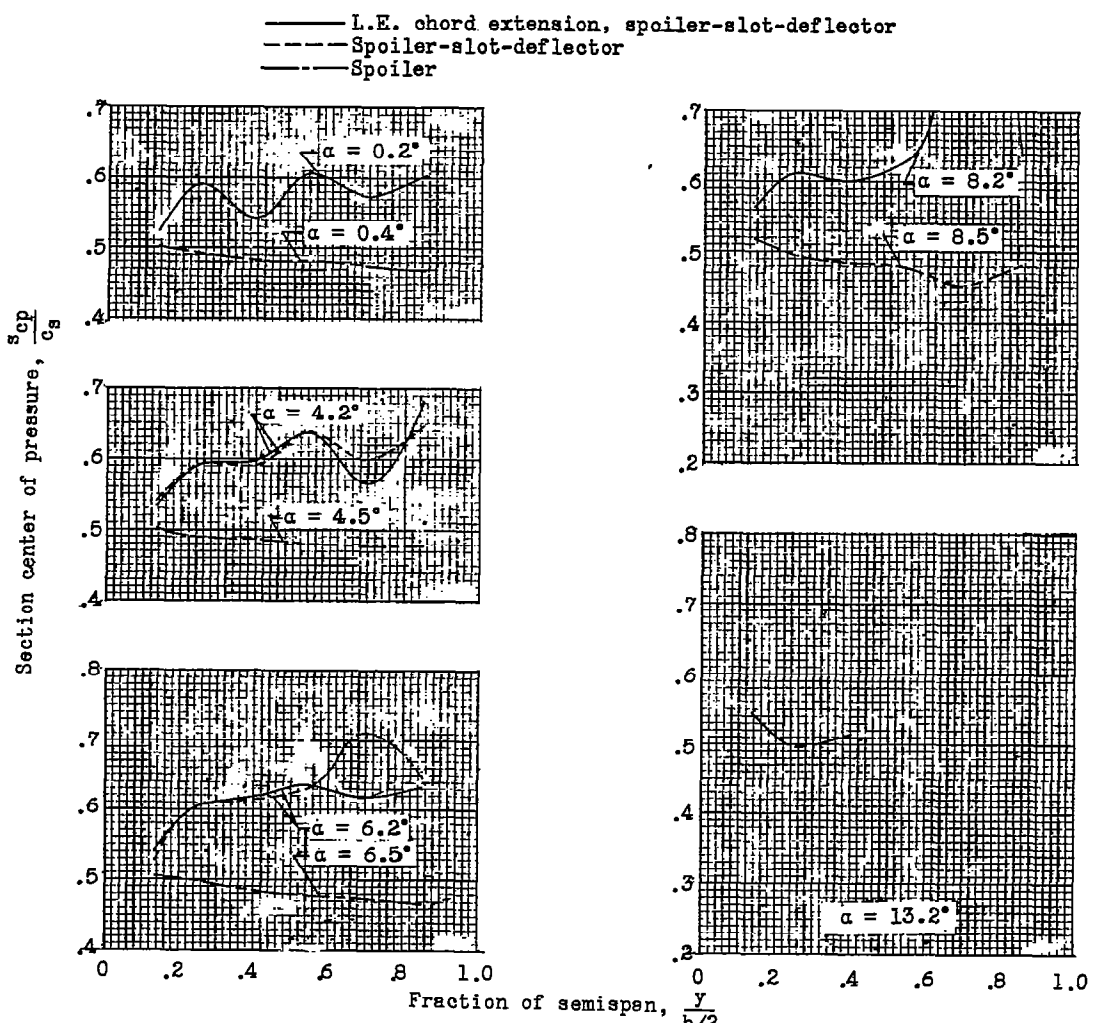
(g)  $M = 1.03$ .

Figure 20.- Concluded.

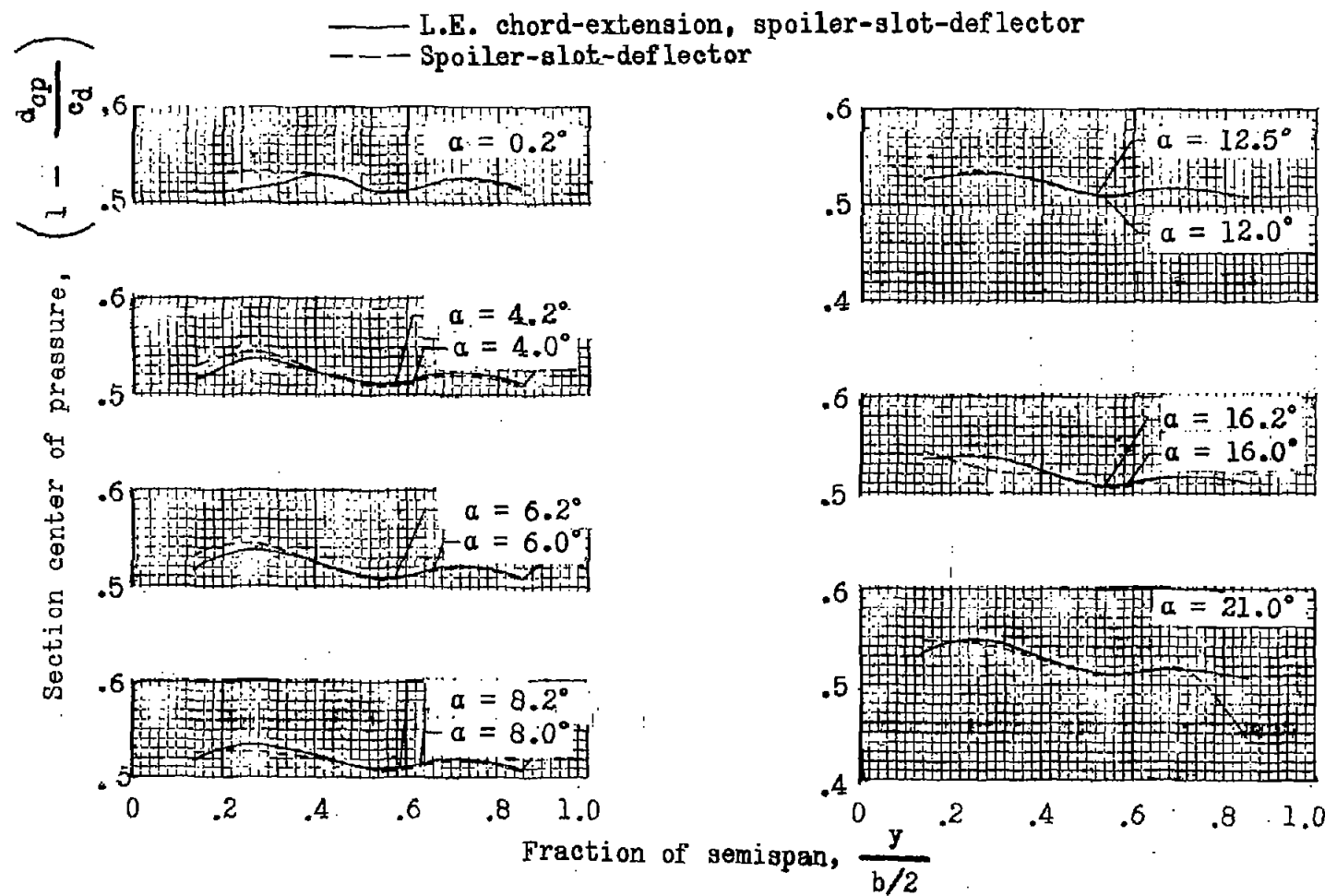
(a)  $M = 0.60.$ 

Figure 21.- Section centers of pressure (measured from hinge line) for deflectors of the basic and leading-edge chord-extension spoiler-slot-deflector aileron configurations.

CONFIDENTIAL

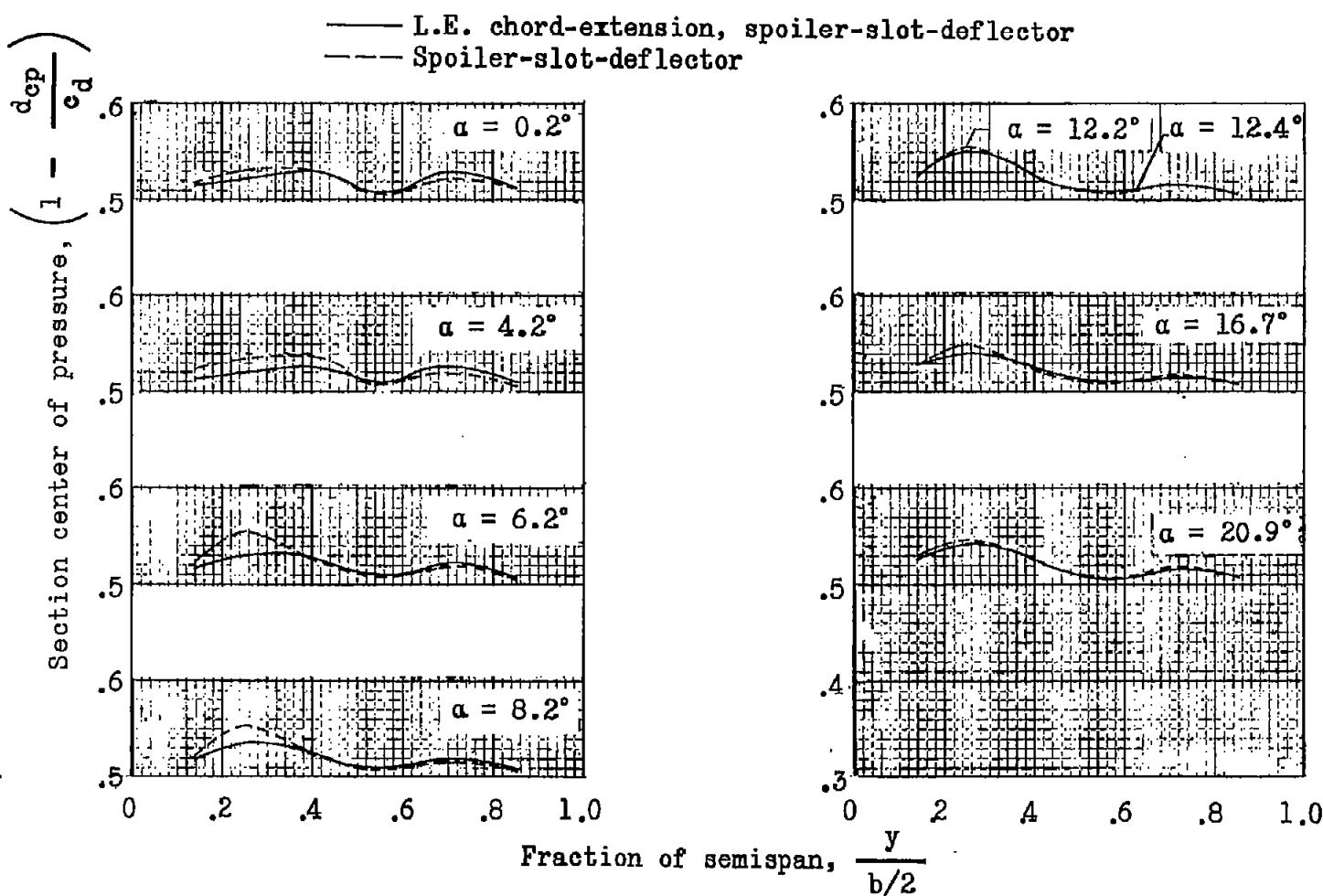
(b)  $M = 0.80$ .

Figure 21.- Continued.

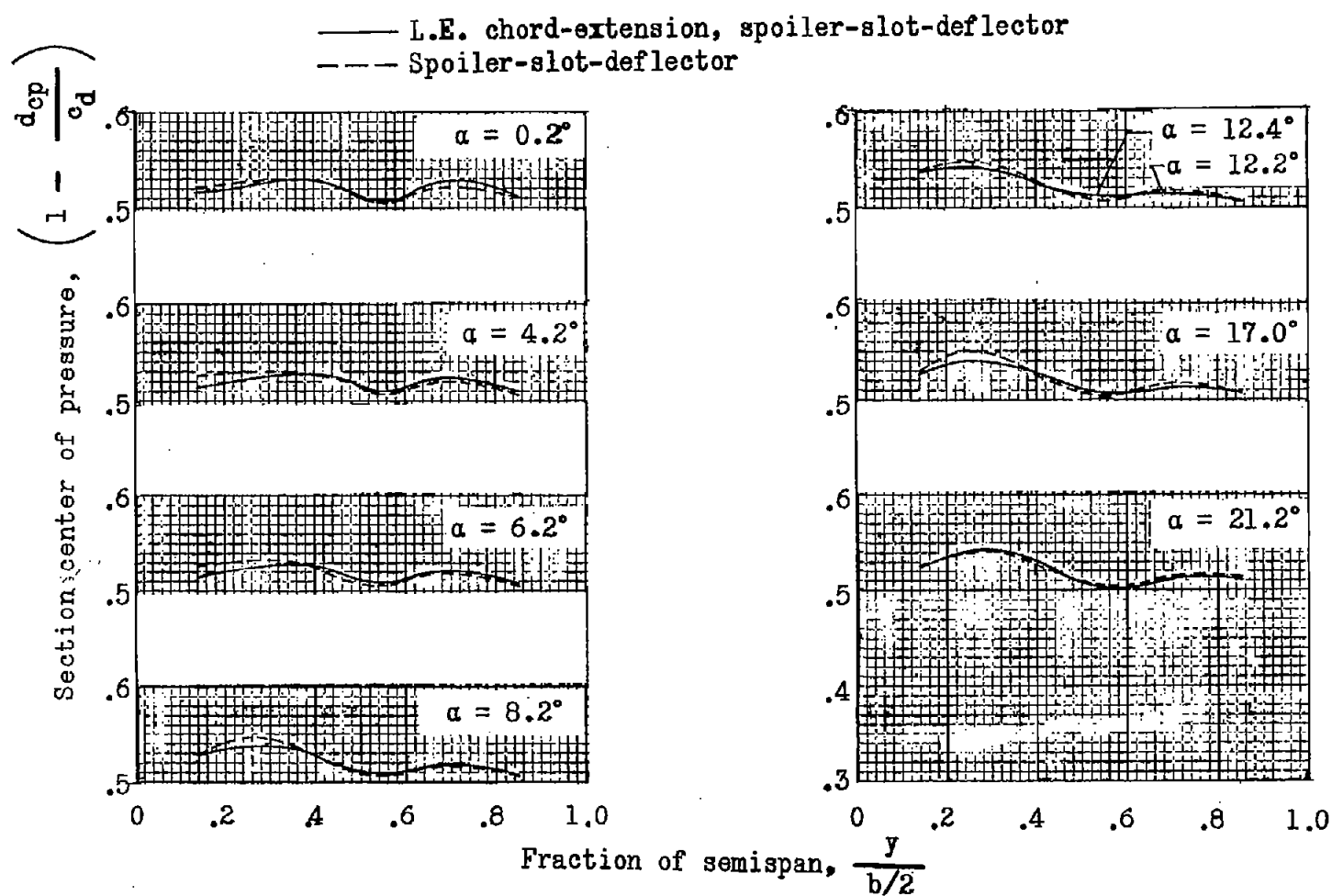
(c)  $M = 0.90$ .

Figure 21c.- Continued.

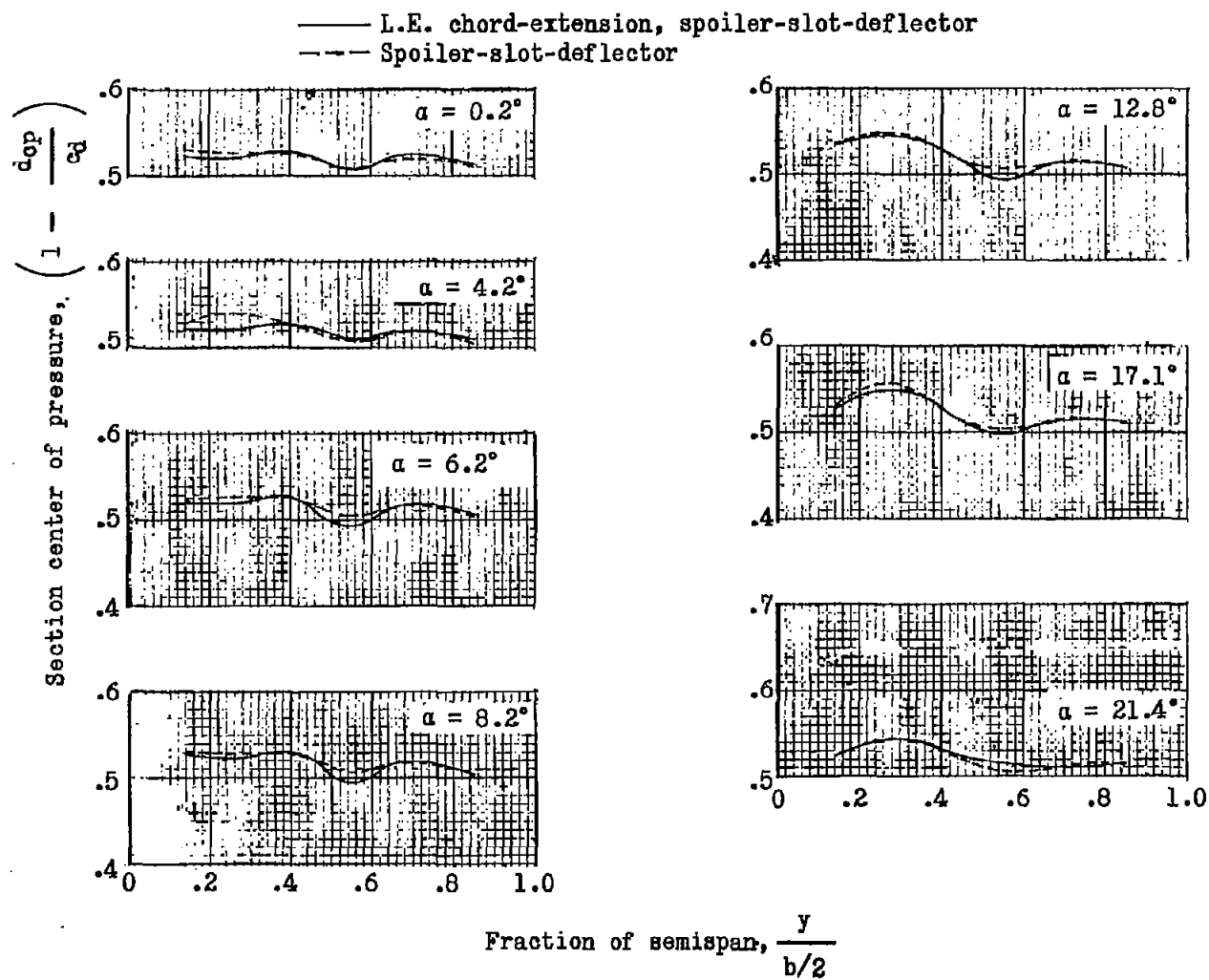
(d)  $M = 0.94$ .

Figure 21.- Continued.

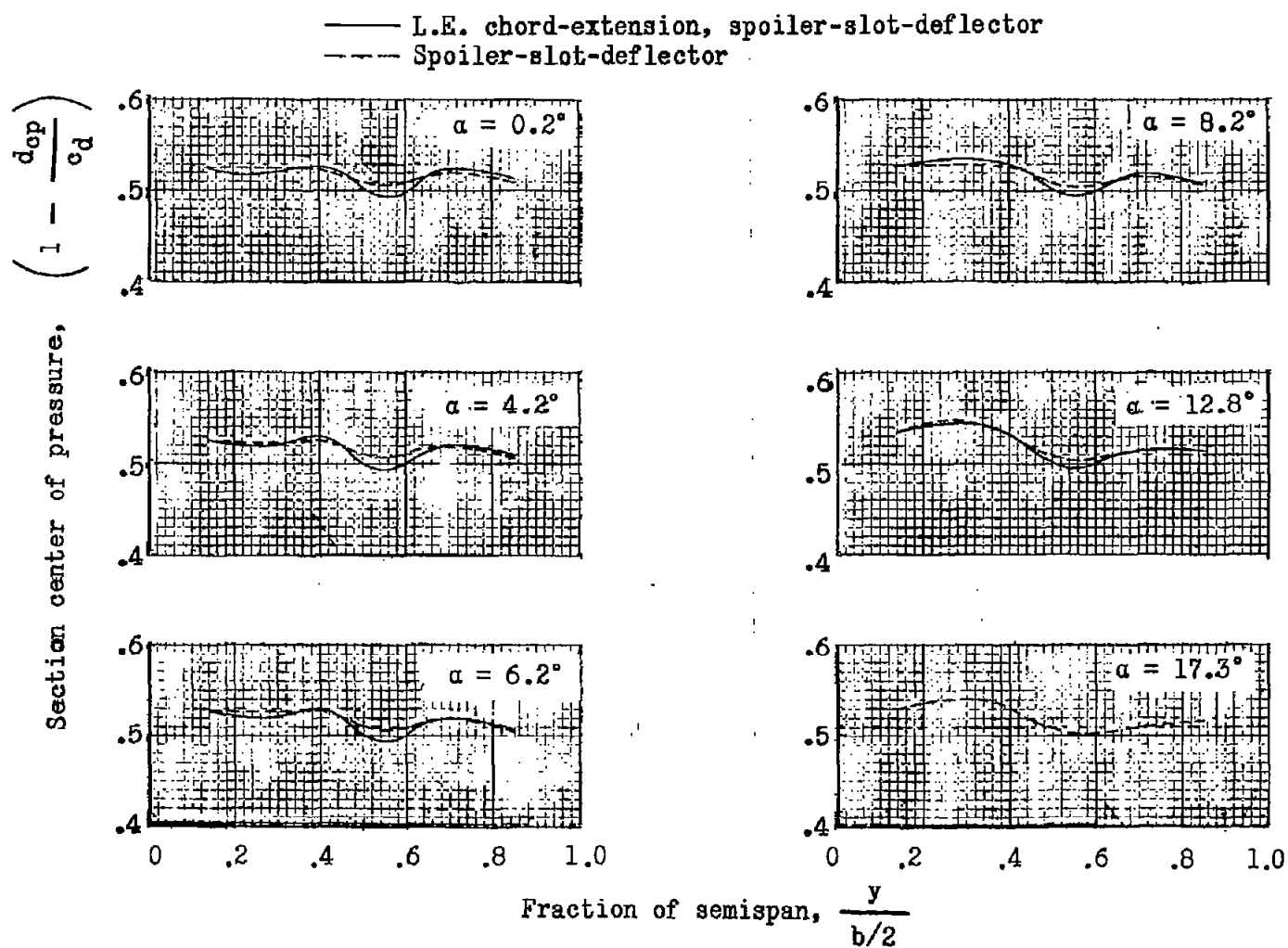
(e)  $M = 0.98$ .

Figure 21.- Continued.

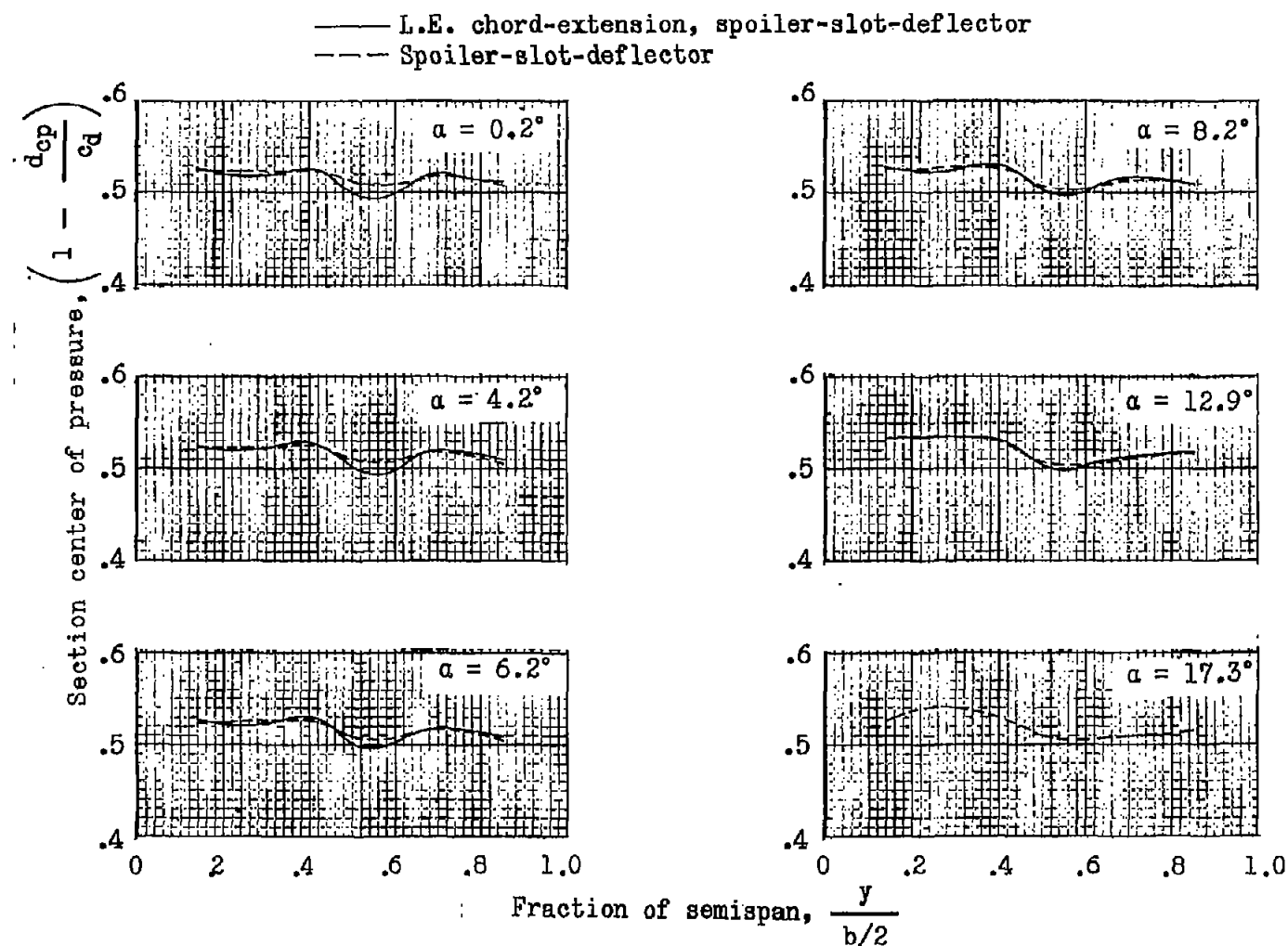
(f)  $M = 1.00$ .

Figure 21.- Continued.

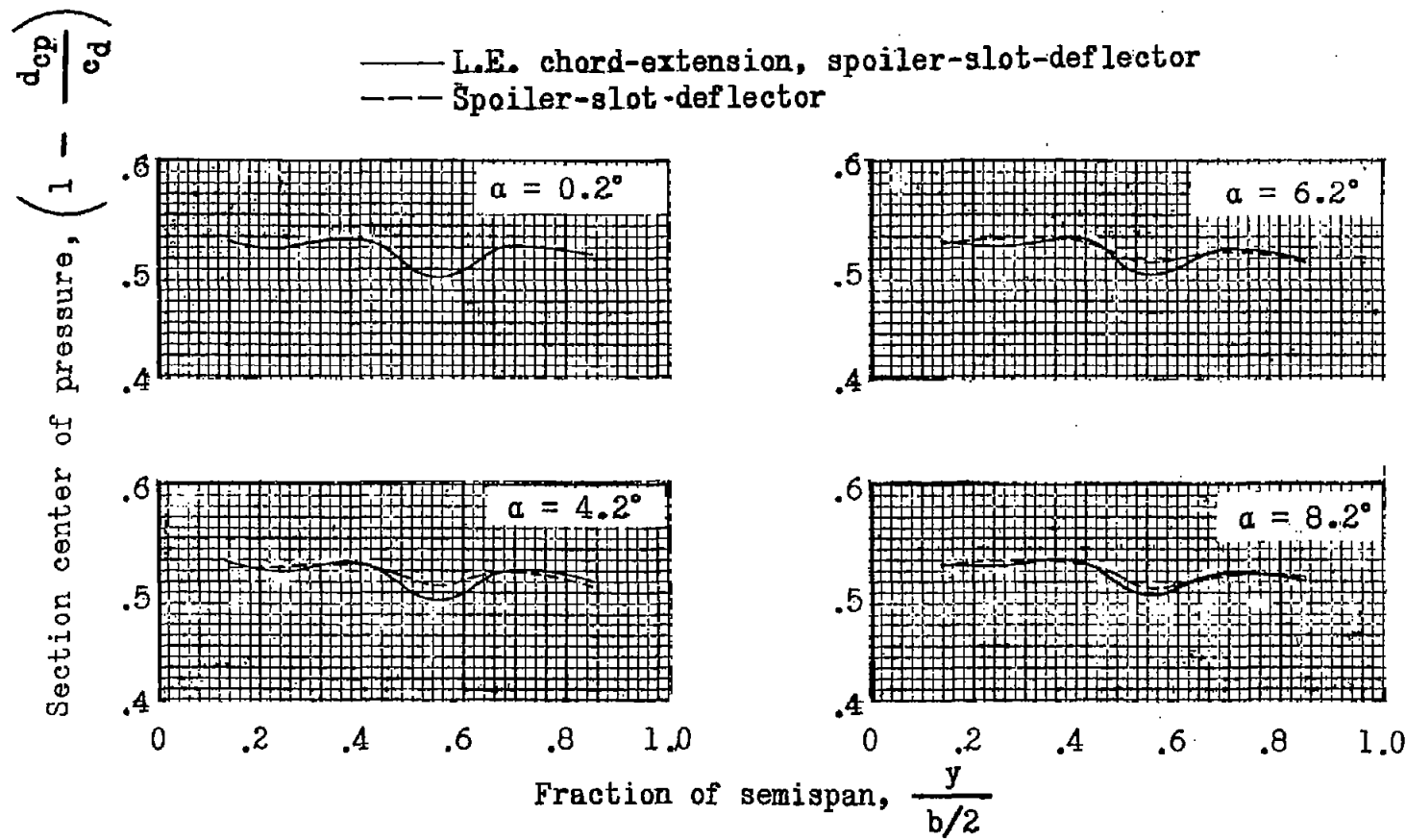
(g)  $M = 1.03$ .

Figure 21.. Concluded.